

GEORGIA INSTITUTE OF TECHNOLOGY
SCHOOL OF MECHANICAL ENGINEERING
ATLANTA, GEORGIA

SPACE RADIATOR SIMULATION
SYSTEM ANALYSIS

Contract NAS9-10415

by

William Z. Black and Wolfgang Wulff

Sponsored by the

Power Generation Branch, Manned Spacecraft Center

NATIONAL AERONAUTICS AND SPACE ADMINISTRATION

Houston, Texas

April 1972

SPACE RADIATOR SIMULATION
SYSTEM ANALYSIS

by

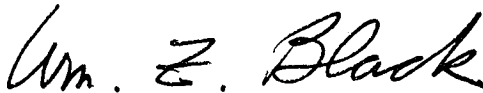
William Z. Black and Wolfgang Wulff

SCHOOL OF MECHANICAL ENGINEERING
GEORGIA INSTITUTE OF TECHNOLOGY
ATLANTA, GEORGIA 30332

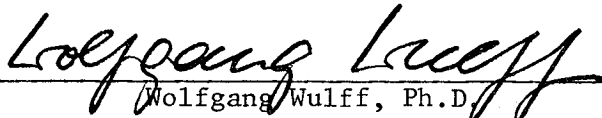
April 1972

Sponsored by

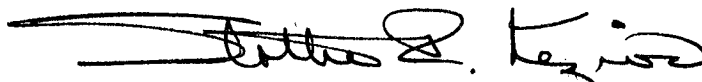
Power Generation Branch, Manned Spacecraft Center
NATIONAL AERONAUTICS AND SPACE ADMINISTRATION
Houston, Texas



William Z. Black, Ph.D.
Associate Professor



Wolfgang Wulff, Ph.D.
Associate Professor



Stothe P. Kezios, Ph.D.
Director, School of Mechanical Engineering

FOREWORD

This report covers the results of one portion of a two year research project carried out by the School of Mechanical Engineering at the Georgia Institute of Technology, Atlanta, Georgia for the NASA Manned Spacecraft Center, Houston, Texas, under Contract No. NAS 9-10415. This report summarizes the results of the radiator simulation analysis. The users manual for the execution of the computer program resulting from the analysis in this report is contained in a separate report. A third report covers the development of a simplified system simulation and the initial phases of a system optimization procedure. The project title is "Study of Design Parameters of Space Base and Space Shuttle Heat Rejection Systems." The work reported here was monitored by Dr. W. E. Simon of the Power Generation Branch of NASA MSC, Houston, Texas, and was carried out by Dr. W. Z. Black and Dr. W. Wulff as Co-Investigators and Mr. S. M. Morcos, Mr. S. L. Yao, and Mr. R. M. Hinson graduate students in the School of Mechanical Engineering under the direction of Dr. S. P. Kezios.

The work carried out by Dr. W. Z. Black is reflected in the analysis of Part II, Chapters 2, 7, 8, 11 and 14. Dr. Wulff is responsible for the analysis of Part II, Chapters 1 and 3 through 6, Chapters 9, 10, 12 and 13 as well as the numerical analysis in Part III. Mr. Morcos completed the property analysis reported in the Appendices A and B. Mr. Yao completed the surface coating property and the shape factor analysis reported in Appendices C and D, respectively.

SUMMARY

A transient heat transfer analysis was carried out on a space radiator heat rejection system exposed to an arbitrarily prescribed combination of aerodynamic heating, solar, albedo and planetary irradiation. A rigorous analysis was carried out for the radiation panel and tubes lying in one plane and an approximate analysis was used to extend the rigorous analysis to the case of a curved panel. For the rigorous analysis the radiator system consists of equally spaced parallel coolant flow channels, all in one plane and connected by plane fin panels of trapezoidal cross-section, symmetric with respect to two normal planes, one passing through the tube axis, the other through the center between adjacent tubes. Investigated was one typical tube-fin element and the result extended over the entire system, on the basis of the above symmetry.

The rigorous analysis was extended, by approximate methods, to include radiator system which do not conform to the above symmetry restrictions. As a result, radiator systems can be treated whose coolant flow channels do not lie in one plane, provided that the radiative interaction between neighboring tube-fin elements is small when compared with the radiant flux densities at the panel. Moreover, radiator systems with non-uniform irradiation, non-uniform coolant inlet conditions and U-shaped coolant channels can be treated, provided that the spacing between channels is small when compared with the channel length.

The analysis permits the consideration of both gaseous and liquid coolant fluids, including liquid metals, under prescribed, time-dependent inlet conditions. The flow channels are covered with the same passive thermal control coating with optically diffuse but wavelength and temperature dependent optical properties.

The major results of the analysis are the prediction of both transient and steady-state, two-dimensional temperature profiles, the local and total heat rejection rates, the coolant flow pressure drop in the flow channel, and the total system weight and the protection layer thickness.

A computer program consisting of 62 program units was coded to execute the numerical solution of the system of differential equations

occurring in the analysis and to predict principal design parameters. The modular program structure readily permits later modifications. A separate final report entitled "Space Radiator Simulation, Manual for Computer Program" has been prepared which describes the computer programs [29].

A simplified analysis was carried out to aid the detailed analysis and to serve as the basis of systematic optimization. This analysis is covered in a companion report, entitled "Simplified Analysis and Optimization of Space Base and Space Shuttle Heat Rejection Systems" [30]. Regarding the heat rejection rates, its results are, for the test cases carried out so far, within 4% in agreement with the results of the detailed analysis. However, this rigorous analysis has greater applicability and detail.

This engineering analysis report is one of three final reports. The other two reports are a user's manual describing the computer code of this extensive, rigorous analysis [29] and the final report covering the simplified radiator system analyses and system optimization which describe both analysis and computer codes [30].

This report is written in two principal parts. The analysis and the governing equations are contained in the first part, Chapter II, titled Analysis. The numerical techniques are covered in Chapter III. Details which the reader may need to expand the program are placed in the appendices.

TABLE OF CONTENTS

	Page
FOREWORD	ii
SUMMARY	iii
LIST OF FIGURES	vii
LIST OF TABLES	viii
NOMENCLATURE	ix
I. OBJECTIVE	1
II. ANALYSIS	3
A. System Description	4
B. Heat Transfer	7
1. Introduction	7
2. The Fin	8
3. The Coolant Fluid	14
4. The Flow Channel	26
5. The Meteoroid Protection Layer	32
6. Radiation	34
7. Aerodynamic Heating	43
C. System Parameters	51
8. The Meteoroid Protection Thickness	52
9. The Mass of the System	62
10. Non-dimensional Parameters	64
D. Extensions of the Analysis to Related Systems	68
11. Non-symmetrical Heating	68
E. Property Fundamentals	78
12. Thermodynamic Properties	80
13. Transport Properties	83
14. Atmospheric Properties	84

TABLE OF CONTENTS (continued)

	Page
III. NUMERICAL TECHNIQUES	92
1. Introduction	92
2. Runge-Kutta-Simpson Integration	93
3. The Evaluation of Polynomials	98
4. Aitken Interpolation	99
5. Numerical Differentiation	100
6. Numerical Integration	101
7. Solutions to Systems of Linear Algebraic Equations	102
IV. RECOMMENDATIONS AND CONCLUSIONS	104
APPENDIX A Structural Material Properties	105
I. Copper	107
II. Aluminum 7075	110
III. Beryllium ($\frac{1}{2}$ -3% BeO)	114
APPENDIX B Coolant Fluid Properties	117
I. Helium	118
II. Silicon Oil	124
III. NaK (78.6% K)	133
IV. FC-75 Inert Fluorochemical Liquid	140
V. FC-43 Inert Fluorochemical Liquid	145
APPENDIX C Optical Properties	150
I. Z-93	151
APPENDIX D Shape Factors	152
I. Tube to Fin Shape Factor	152
II. Tube to Tube Shape Factor	155

LIST OF FIGURES

Figure	Page
1. Fin Element and Coordinate System	6
2. Control Volume for Low-Biot Number Cases	29
3. (a) Fin Segments Inclined at Tube Locations - Geometry for Physical Model	70
(b) Fin Segments Inclined at Location of Adiabatic Planes - Geometry for Mathematical Model	70
4. Fin Geometry for Non-Symmetrical Panel	71
5. View Factor Between Adjacent Tubes	156

LIST OF TABLES

Table	Page
1. Forced Convection Nusselt Number for Orbiter	47
2. Empirical Constants for Meteoroid Protection Layer Thickness	58
3. Ratio of Relative Error in Thickness to Relative Uncertainty in Empirical Constants	60
4. Lapse Rate and Base Temperatures for Atmospheric Model	87

NOMENCLATURE

a	empirical constant used to account for spalling of protection layer (Eq. 8.8)	
a	function of temperature, used to express the isothermal compressibility and the zero-pressure isobaric thermal expansion coefficient, see also b and c (Eq. 12.9)	
a_z	axial fluid flow acceleration	ft/sec ²
A	area	ft ²
A_n	coefficients in polynomial for atmospheric pressure at high altitudes (Eq. 14.8)	-
A_s	surface area	ft ²
A_x	cross-sectional area perpendicular to x coordinate	ft ²
A_z	cross-sectional area perpendicular to z coordinate	ft ²
b	defined in Eq. 12.9 , see also a	
B	fin geometrical parameter (Eq. 2.14)	-
B_N	coefficients in polynomial for atmospheric density at high altitudes (Eq. 14.8)	-
c	atmospheric speed of sound	ft/sec
c	negative slope of fin sides	-
c	defined in Eq. 12.9 , see also a	
c	speed of light	ft/sec
\bar{c}	speed of sound in meteoroid protection material	ft/sec
c_p	specific heat at constant pressure	Btu/(slug R)
c_v	specific heat at constant volume	Btu/(slug R)

c_v	zero-pressure specific heat at constant volume	Btu/(slug R)
d	diameter of meteoroid particle	in
d	tube diameter	ft
D	fin geometrical parameter (Eq. 2.15)	-
E	emissive power	Btu/(hr ft ²)
E	modulus of elasticity	lbf/in ²
E	relative error	-
f	Fanning friction factor	-
F	cumulative meteoroid flux (eq. 8.4)	1/(ft ² day)
F	dimensionless parameter, Eqs. 3.31-34	
g_c	32.174 ft lbm/(lbf sec ²)	
h	Plank's constant, $h = 6.625 \times 10^{-34}$ W s ²	
h	specific enthalpy	Btu/slug
H	geopotential altitude	ft
H	fin height, from root to tip	ft
h_c	convective film coefficient	Btu/(hr ft ² R)
h_i	convective heat transfer coefficient used in reference enthalpy method	lbm/(hr ft ²)
k	Boltzmann constant, $k = 1.380 \times 10^{-23}$ W s/K	
k	thermal conductivity	Btu/(hr ft R)
L	temperature gradient in atmosphere (Table 4)	(K/km)
L	tube (and fin) length	ft
M	Mach number of orbiter	-
M	mass	slug
M	molecular weight	-
M_{ij}	transfer matrix Eq. 6.19	

M_m	inverted M	-
M	defined by Eq. 10.22	
n	constant that describes depth of penetration as a function of angle of incidence (Eq. 8.6)	-
n	number of tubes	
n	refractive index	-
N	cumulative number of meteoroid impacts	-
N_{Bi}	Biot number	-
N_{Fo}	Fourier number	-
N_{Gr}	Grashof number	-
N_{Nc}	Conductance parameter	-
N_{Nu}	Nusselt number	-
N_{Re}	Reynolds number	-
N_{Pr}	Prandtl number	-
p	absolute pressure	lbf/ft ²
P_j	nondimensional exitation vector, Eq. 6.21	-
P_j	excitation vector, Eq. 6.18	
P_o	probability of no damage due to meteoroid impact	-
P_∞	depth of penetration of a meteoroid particle into an infinite target.	in
q"	heat flux	Btu/(hr ft ²)
\tilde{q}	nondimensional heat flux	-
\bar{Q}_o	nondimensional inlet power flux	-
\bar{Q}_{rad}	defined by Eq. 10.21	-
r,z	polar coordinates, see Fig. 1	ft
r	recovery factor	-

R^*	universal gas constant	ft lbf/(lb mole R)
R	outer meteoroid protection layer radius	ft
s	thickness	ft
$s_f = \frac{s_r}{2}$	fin half thickness at root	ft
\bar{s}_f	normalized fin thickness (Eq. 2.13)	-
$\overline{s_i s_j}$	direct exchange area (Eq. 6.1)	ft ²
S	constant in atmospheric viscosity equation (Eq. 3.7)	K
SS	direct exchange "area", partially evaluated	ft
t	time	hr
T	absolute temperature	R
u	specific interval energy	Btu/slug
V	velocity of orbiter	ft/sec
\bar{V}	velocity of meteoroid relative to radiator	ft/sec
w	coolant flow velocity	ft/sec
w_j	nondimensional radiosity, Eq. 6.21	-
W_j	radiosity	Btu/(hr ft ²)
x	distance from orbiter stagnation point to radiator panel	ft
x, z	rect. Cart. coordinates, see Fig. 1	ft
x_{ij}, x_{ijk}	auxiliary parameters, defined by Eqs. 6.10 and 6.11	-
y	overall length of radiator in direction parallel to gravity	ft
y	transverse fin coordinate	ft
z	axial distance	ft
Z	geometric altitude	ft

Greek Symbols

α	experimental meteoroid flux parameter, (Eq. 8.4)	$1/(\text{ft}^2 \text{day gm}^\beta)$
α	thermal diffusivity	ft^2/hr
α_{ij}	total hemispherical absorptance	-
β	constant in atmospheric viscosity equation, (Eq. 3.7)	$\text{kg}/(\text{sec mK}^{1/2})$
β	experimental meteoroid flux parameter, (Eq. 8.4)	-
β	isobaric thermal expansion coefficient, see Eq. 3.5	$1/R$
γ	ratio of specific heats	-
δ	diameter-over-length ratio	-
δ_{ij}	Kronecker delta	-
ϵ	total hemisphere emittance	-
ζ	dimensionless axial distance, Eq. 3.19	-
η	dimensionless radius, Eq. 3.25	-
θ	dimensionless temperature, Eq. 3.21	-
θ	empirical constant (Eq. 8.1)	-
κ	isothermal compressibility, Eq. 3.4	ft^2/lbf
λ	angle between path of meteoroid and normal to protected surface (Eq. 8.6)	deg.
λ	wave length	ft
λ_1	parameter, defined by Eq. 4.11	-
λ_2	parameter, defined by Eq. 4.12	-
μ	dynamic viscosity	$\text{slug}/(\text{ft sec})$
ν	dimensionless density	-
ν	kinematic viscosity	ft^2/sec
ξ	dimensionless x coordinate	-

π	dimensionless pressure, Eq. 3.22	
ρ	density	slug/ft ³
σ	Stefan-Boltzmann constant	Btu/(hr ft ² R ⁴)
τ	dimensionless time, Eq. 3.20	-
τ	time radiator is exposed to meteoroid environment	day
ϕ	angle between surface normal and radiation beam	-
ϕ	dimensionless property Eqs. 3.27-3.30, Eq. 4.4	-
ϕ, ϕ^*	polar angle in Eq. 6.15	-
ϕ_{Nc}	modified conduction parameter, Eq. 5.6	
ϕ	empirical constant (Eq. 8.1)	-
χ	quadrature coefficient	-
ψ	circumferential fraction, defined by Eq. 4.3	-
ψ	residual, see Eqs. 12.1 and 12.2	-
ω	dimensionless velocity Eq. 3.23	-

Subscripts

aw	adiabatic wall
aero	aerodynamic
b	values at the endpoints of straight line segments of atmospheric temperature profile, (Table 4)
c	coolant fluid
c	critical value
c	enclosure
c _p	referring to specific heat at constant pressure

e	outer surface of meteoroid protection layer, (environment)
f	referring to friction factor
f	fin
F	Fourier number
i, j	position index
m	meteoroid protection layer
M	Mach number
net,rad	net radiant
p	meteoroid particle
p	referring to pressure
r	fin root
t	fin tip
t	target material
t	tubes
w	channel wall
w	surface or wall condition
z	axial distance
z	thermal equation of state
o	entrance (reference) conditions
o	sea level values
1	upper fin side
2	lower fin side
∞	free stream condition
ζ	partial differentiation with resp. to ζ
η	partial differentiation with resp. to η
κ	referring to compressibility

λ monochromatic

τ partial differentiation with respect to τ

Superscripts

* evaluated at reference temperature T^*

I. OBJECTIVE

The purpose of the analysis presented here is to develop a radiator system simulation which serves (i) to provide the design parameters necessary for the development of the radiator system, (ii) to predict the transient radiator performance under prescribed environmental and operation conditions, (iii) to predict the system response to conditions which lead to coolant fluid temperatures outside their operational temperature range, and (iv) to use the system performance data to suggest design options for shuttle radiator panel.

The class of system analyzed here is described in the following section. The system parameters produced for design purposes are those which describe coolant fluid flow field and the thermal state of the radiator structures as well as the geometry and the weight of the system components.

The arbitrarily prescribed environmental conditions consist of the specification of ascent and reentry profiles and of solar, planetary and albedo irradiation as a function of time.

The prescribed operating conditions are the coolant fluid inlet properties.

The analysis is designed to accommodate spectral characteristics of surface coatings, specified as functions of temperature. The analysis is, however, restricted to optically diffuse coatings.

Both coolant and structural material properties are accepted as prescribed functions of temperature. Coolant properties are specified as functions of pressure or density as well as temperature.

The analysis serves as the basis for a large-scale computer code in modular form. Material properties, complex mathematical operations and readily identifiable tasks in the computer code are written as subprograms.

The computer code is designed to simulate space radiator heat rejection systems during ascent, reentry and mission phases of the spacecraft and to optimize the radiator system configuration via enumeration of parameter sets.

The Analysis is covered in the following chapter. The numerical techniques employed are discussed in Chapter III, while the preparation for the program units describing material properties is deferred to the Appendices.

The computer code is described in a separate manual [29].

When the contract began over two years ago, the emphasis on radiator design was primarily on the space base heat rejection system. Since that time, the emphasis has shifted so that it is now heavily placed on the shuttle vehicle. Furthermore, the responsibility of developing the heat rejection system has been shifted from the Power Generation Branch and the design philosophy has changed to an integrated system which includes waste heat from sources other than the power generation system which was anticipated as the sole source of waste heat when the contract began. Due to the shift in design philosophy, the report will not recommend detailed design considerations, although once heat loads from other sources are known, the analysis presented here can be used to aid in the design of an integrated radiator system.

II. ANALYSIS

The analysis is presented in three major parts. In the first part are developed the governing equations of transient heat transfer within and from the radiator system; these equations are the basis of the numerical simulation. The second part of the analysis is devoted to the computation of design parameters dictated by operational conditions, while third part covers the development of thermodynamic and transport properties of structural materials, coolant fluids, and the atmosphere.

A. System Description

Two radiator systems are considered in this analysis. The first system considers a flat radiator panel divided by regularly spaced coolant channels all having identical inlet coolant fluid properties. This system is treated rigorously. The second system considers a non-symmetrical radiator panel. The non-symmetrical conditions can be caused by a curvature in the radiator panel or by coolant channels that are parallel but not equally spaced or formed in the shape of a U. This system is treated in an approximate manner. The details of the non-symmetrical analysis are given in Section II D.

For the purposes of system simulation, the radiator system consists of four components:

- (i) the fin
- (ii) the coolant fluid
- (iii) the coolant flow channel
- (iv) the meteoroid protection layer

Two coordinate systems were introduced (see Figure 1), one for the fin and the other for the flow channel and the meteoroid protection layer. The rectangular Cartesian system (x,z) for the fin has its z -axis parallel to the tube axis, starting at the inlet plane, and its x -axis passing through the line of profile symmetry, with $x = 0$ designating the root of the fin. Cylindrical coordinates (r,z) are used for both the tube and the meteoroid protection layer, with the z -axis along the tube.

The radiator system is describable in terms of the following six dependent state variables:

(i) for the fin:

the fin temperature $T_f(t;x,z)$

(ii) for the coolant fluid:

the fluid temperature $T_c(t;z)$

the fluid pressure $p(t;z)$

the fluid velocity $w(t;z)$

(iii) for the fluid flow channel:

the tube wall temperature $T_w(t;r,z)$

(iv) for the meteoroid protection layer

the protection layer temperature $T_m(t;r,z)$

These six dependent variables must satisfy four equations of energy conservation, one for each component of the system, and further, the equations of mass conservation and of momentum balance for the fluid. These conservation equations take on the form of partial differential equations subject to initial and boundary conditions. Finally, the energy conservation equation for the fin involves the net radiant and convective power fluxes leaving the fin.

In the following Sections, II B.2 through II B.5 are discussed, in that order, the six principal governing equations associated with the four system components listed above, the subsidiary equations governing the radiative heat exchange and, lastly, the convective heat transfer between coolant fluid and tube wall and between the fin and the atmosphere during ascent and reentry.

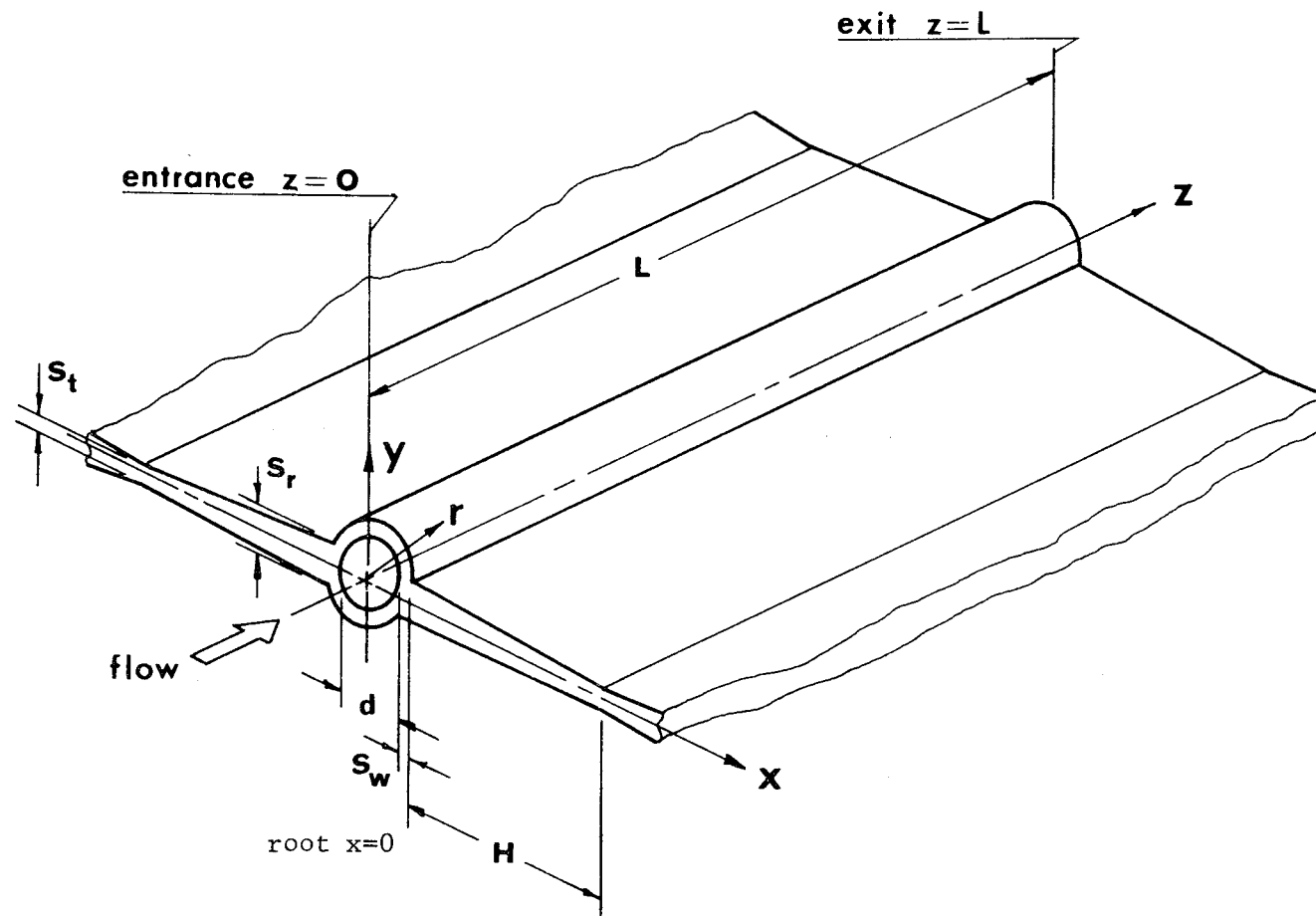


Figure 1 Fin Element and Coordinate System

B. HEAT TRANSFER

1. Introduction

The objective of the radiator simulation is to predict both the transient and the steady state heat transfer characteristics under pre-determined operating conditions, stationary in the latter case and dynamic in the former. Both cases were treated as initial value problems, and the principal governing equations are partial differential equations which are linear in the time-derivatives of first order at most.

Under stationary boundary conditions steady state will be reached, regardless of initial conditions*, as all partial derivatives with respect to time vanish on account of dissipative effects within the system. For the computer simulation of steady state conditions this means that the process of advancing in time can be discontinued as soon as all variables y_i , $i = 1, 2, \dots, N$, have reached their expected asymptotic values $(y_i)_\infty$ with sufficient accuracy, that is when for some chosen ϵ_i

$$\delta_i = |y_i - (y_i)_\infty| \leq \epsilon_i \quad (1.1)$$

has been reached. The expected asymptotic values $(y_i)_\infty$ can be estimated on the basis of the recognition that for large enough values of the time, $t > t_M$

$$y_i \rightarrow (y_i)_\infty \pm ae^{-bt} \quad (1.2)$$

with, $a > 0$, $b > 0$, to be determined; $t > t_M$. The evaluation δ_i during the numerical integration is covered in Chapter III.

*Subject to certain continuity requirements which are discussed in Chapter III.

2. The Fin

The objective of this section is to develop the energy equation for the fin. The derivation is based on the assumptions that the thermal conductivity and specific heat of the fin material are functions of temperature while the fin density is constant. The energy balance for the fin accounts for both radiative and convective fluxes from the fin surfaces. The development of a method to predict the net radiant flux from the fin surfaces can be found in Section II-6. The procedure used for the evaluation of the convective flux from the fin surface is outlined in Section II-7.

The energy balance on a differential volume of the fin can be expressed as

$$\frac{\partial}{\partial x} \left[k_f A_x \frac{\partial T_f}{\partial x} \right] dx + \frac{\partial}{\partial z} \left[k_f A_z \frac{\partial T_f}{\partial z} \right] dz + q''_{\text{net,rad}} A_s + q''_{\text{aero}} A_s = \rho_f V c_{pf} \frac{\partial T_f}{\partial t} \quad (2.1)$$

where T is the fin temperature and the coordinate system is shown in Fig. 1. The areas A_x and A_z represent the cross-sectional areas of the fin perpendicular to the heat flow in the x and z directions, and A_s represents the total non-adiabatic surface area of the fin element. The symbol V is the volume of the fin element. The properties of the fin material are represented by the symbols k_f , ρ_f and c_{pf} which stand for the thermal conductivity, density and specific heat, respectively. The terms $q''_{\text{net,rad}}$ and q''_{aero} appearing in Eq. 2.1 denote the radiative and convective heat gain from the surroundings to the fin surfaces.

The first two terms in Eq. 2.1 constitute the net conduction of energy into the fin element. The third and fourth terms on the left hand side of the equation stand for the net radiation and convection gain, respectively, from the surfaces of the fin element. The term of the right

hand side of the equation represents the storage of internal energy within the fin element.

The appropriate areas and the volume to be substituted into Eq. 2.1 are

$$dA_x = 2[s_f - cx] dz \quad (2.2)$$

$$dA_z = 2[s_f - cx] dx \quad (2.3)$$

$$dA_s = dx dz / [c^2 + 1]^{1/2} \quad (2.4)$$

$$dV = 2[s_f - cx] dx dz \quad (2.5)$$

where s_f is the fin half thickness at its root and c is the negative slope of the fin side surfaces.

Substituting Eqs. 2.2 through 2.5 into Eq. 2.1 and simplifying the resulting equation yields

$$\rho_f c_{pf} \frac{\partial T_f}{\partial t} = k_f \left[\frac{\partial^2 T_f}{\partial x^2} + \frac{\partial^2 T_f}{\partial z^2} \right] + \frac{dk_f}{dT} \left[\left(\frac{\partial T_f}{\partial x} \right)^2 + \left(\frac{\partial T_f}{\partial z} \right)^2 \right] \quad (2.6)$$

$$- \left(\frac{ck_f}{t-cx} \right) \frac{\partial T}{\partial x} + \frac{\sqrt{c^2+1}}{2(t-cx)} [q''_{\text{net,rad}} + q''_{\text{aero}}]$$

The Normalization of Eq. 2.6 is achieved by defining nine dimensionless quantities:

Let

$$\xi = x/H \quad (2.7)$$

$$\zeta = z/L \quad (2.8)$$

represent the nondimensional fin coordinate perpendicular and parallel to the tube, respectively. Then

$$\tau = tw_o/L \quad (2.9)$$

is the dimensionless time. The symbol w_o stands for the velocity of the coolant fluid entering the tube.

The nondimensional fin temperature is defined as

$$\theta_f(\tau, \xi, \zeta) = \frac{T_f(\tau, \xi, \zeta)}{T_o} \quad (2.10)$$

where T_o is the temperature of the coolant fluid entering the tube.

The dimensionless conduction parameter N_{Nc} and the Fourier number are defined as

$$N_{Nc} = H\sigma T_o^3 / k_f \quad (2.11)$$

$$N_{Fo} = \frac{\alpha_f L}{w_o H^2} = \frac{k_f L}{\rho_f c_{pf} w_o H^2} \quad (2.12)$$

and the nondimensional geometrical quantities are defined as

$$\bar{s}_f = s_f / H \quad (2.13)$$

$$B(\xi) = 2(\bar{s}_f - c\xi) \quad (2.14)$$

$$D = (c^2 + 1)^{1/2} \quad (2.15)$$

where c is the negative slope of the fin side surfaces. For a non-tapered fin c is zero.

Both the net radiative and convective flux terms appearing in Eq. 2.6 are normalized by dividing each term by σT_o^4 , or

$$\tilde{q}_{net,rad} = \frac{q''_{net,rad}}{\sigma T_o^4} \quad (2.16)$$

$$\tilde{q}_{aero} = \frac{q''_{aero}}{\sigma T_o^4} \quad (2.17)$$

The energy equation, Eq. 2.6, may now be written in terms of the nondimensional quantities given in Eqs. 2.7 through 2.17. The resulting nondimensional equation is

$$\begin{aligned} \dot{\theta}_f = N_{Fo} \left\{ (\theta_f)_{\xi\xi} + \left(\frac{H}{L}\right)^2 (\theta_f)_{\zeta\zeta} + \frac{T_o}{k_f} \frac{dk_f}{dt} \left[(\theta_f)_{\xi}^2 + \left(\frac{H}{L}\right)^2 (\theta_f)_{\zeta}^2 \right] \right. \\ \left. - 2 \frac{c}{B} (\theta_f)_{\xi} + \frac{D}{B} N_{Nc} [\tilde{q}_{\text{net,rad}} + \tilde{q}_{\text{net,conv}}] \right\} \end{aligned} \quad (2.18)$$

The dot superscript appearing in Eq. 2.18 denotes differentiation with respect to nondimensional time and the subscripts ξ and ζ represent partial differentiation with respect to the dimensionless coordinates indicated.

The normalized energy equation, Eq. 2.18, defines the rate of change of the dimensionless fin temperature θ_f .

The Boundary Conditions for Eq. 2.18 are taken as follows:

- (i) The fin root is at the temperature of the outside of the tube.
- (ii) The fin tip is insulated.
- (iii) The portion of the fin in contact with the inlet manifold is at the outside temperature of the manifold.
- (iv) The portion of the fin in contact with the exit manifold is at the temperature of the outlet manifold.

Written in mathematical terms these four boundary conditions are

$$\theta_f(\tau, 0, \zeta) = \theta_w(\tau, \xi_o, \zeta) \quad (2.19)$$

$$\frac{\partial \theta_f}{\partial \xi}(\tau, 1, \zeta) = 0 \quad (2.20)$$

$$\theta_f(\tau, \xi, 0) = \theta_w(\tau, \xi_o, 0) \quad (2.21)$$

$$\theta_f(\tau, \xi, 1) = \theta_w(\tau, \xi_o, 1) \quad (2.22)$$

Implied in Eqs. 2.21 and 22 is, firstly, that the fluid temperature in the manifolds be equal to the fluid temperature at the tube inlet (inlet manifold) and at the tube exit (exit manifold) and that it remain unaltered along the manifold and vary only in time; secondly, that the temperature drop through the manifold wall be equal to that through the tube wall. The latter assumption is well justified because the temperature drop is exceedingly small.

It may be noted in connection with the boundary conditions that the radiative interactions between manifold and fin as well as between manifold and tube are not taken into consideration at this time.

The Initial Condition for Eq. 2.18 may be any arbitrary relation representing a continuous temperature distribution over the fin, including the boundaries. The selection of the initial fin temperature distribution is left to the user.

3. The Coolant Fluid

The objective is to develop a unified treatment of all possible coolant fluids, that is gases, dielectric fluids and liquid metals. Three principal governing equations are sought which, together with the necessary thermodynamic and transport properties specified for each fluid of interest, define the fluid temperature T_c , the fluid pressure p (and thus the thermodynamic state of the fluid) and the fluid velocity w , all as functions of time t and axial distance z .

The Continuity Equation for one dimensional flow through channels of constant cross-sections reads

$$\frac{\partial \rho}{\partial t} + \frac{\partial}{\partial z} (\rho w) = 0 \quad (3.1)$$

where ρ represents the fluid density. Replacing the density through the thermal equation of state

$$p = p(\rho, T_c) \quad (3.2)$$

renders the continuity equation in terms of derivatives of the primary variables T_c , p and w :

$$\kappa \frac{\partial p}{\partial t} - \beta \frac{\partial T_c}{\partial t} = - \frac{\partial w}{\partial z} + w \left(\beta \frac{\partial T_c}{\partial z} - \kappa \frac{\partial p}{\partial z} \right) \quad (3.3)$$

where κ and β stand for the isothermal compressibility and the isobaric expansion coefficient, respectively

$$\kappa = \frac{1}{\rho} \left(\frac{\partial \rho}{\partial p} \right)_{T_c} \quad (3.4)$$

$$\beta = -\frac{1}{\rho} \left(\frac{\partial \rho}{\partial T_c} \right)_{\rho} \quad (3.5)$$

The Momentum Equation

$$\rho \left(\frac{\partial w}{\partial t} + w \frac{\partial w}{\partial z} \right) = - \frac{\partial p}{\partial z} - \frac{4f}{d} \rho \frac{w^2}{2} + \rho a_z \quad (3.6)$$

constitutes the balance between inertia forces on the left-hand side, pressure forces, wall friction and external field forces (gravity) in axial direction, on the right-hand side of Eq. 3.6. The Fanning friction factor f is a function of the Reynolds-number $N_{Re} = d w / \nu$, where d and ν stand for the tube diameter and the kinematic viscosity, respectively and subscript o designates the fluid inlet conditions. The following relations are used to compute the Fanning friction factor:

for $N_{Re} < 2300$ (laminar flow)

$$4f = \frac{64}{N_{Re}} \quad (3.7)$$

for $2300 \leq N_{Re} \leq 10^6$ (Ref. 1)

$$4f = 0.0054 + 0.396 N_{Re}^{-0.3} \quad (3.8)$$

for $N_{Re} > 10^6$ (Ref. 2)

$$4f = 0.0032 + 0.221 N_{Re}^{-0.237} \quad (3.9)$$

Equations 3.8 and 3.9 could be replaced by a single equation (Ref.3)

$$4f = \left[0.86859 \ln \frac{N_{Re}}{1.964 \ln N_{Re}} - 3.8215 \right]^{-2} \quad (3.10)$$

which, however, requires more computational effort.

The Energy Equation. Let u , h , \bar{h}_c and $T_w = T_w(t; r_i, k)$ represent, respectively the internal energy and the enthalpy of the fluid, the convective film coefficient and the tube wall temperature at the fluid-wall interface. For one-dimensional flow through channels of constant cross-section and with heating or cooling from the wall, conservation of energy requires that, with respect to a stationary reference frame

$$\begin{aligned} \frac{\partial}{\partial t} \left[\rho \left(u + \frac{w^2}{2} \right) \right] + \frac{\partial}{\partial z} \left[\rho w \left(h + \frac{w^2}{2} - a_z z \right) \right] &= \frac{4}{d} \bar{h}_c (T_w - T_c) \\ + \frac{\partial}{\partial z} \left(k_c \frac{\partial T}{\partial z} \right) & \end{aligned} \quad (3.11)$$

The first term constitutes the storage of thermal and kinetic energies; the storage of potential energy, being negligibly small for expected accelerations, is ignored. The second term on the left-hand side stands for the convection of thermal, kinetic and potential energies as well as the power associated with the pressure. The right-hand side contains, firstly, the convective heat transfer from the channel wall to the fluid and, secondly, the axial heat conduction term which will later be shown to be negligibly small for all fluids. The factor $4/d$ in front of the convective heat transfer term results from the ratio of the channel circumference to the cross-sectional area, evaluated for a circular tube. The symbol k_c represents the thermal conductivity of the coolant.

Given a caloric equation of state

$$u = u(\rho, T_c) \quad (3.12)$$

or an equivalent expression for the specific heat, c_p , one can write, with the aid of Eqs. 3.2, 4 and 5

$$dh = c_p dT_c + \frac{1}{\rho} (1 - \beta T_c) dp \quad (3.13)$$

$$du = (c_p - \frac{p\beta}{\rho}) dT_c + \frac{1}{\rho} (kp - \beta T) dp \quad (3.14)$$

and then recast Eq. 3.11 in terms of the derivatives of the principal variables T_c , p and w :

$$\begin{aligned} \rho c_p \frac{\partial T_c}{\partial t} - \beta T_c \frac{\partial p}{\partial t} + \rho w \frac{\partial w}{\partial t} &= \frac{4}{d} \bar{h}_c (T_w - T_c) \\ &+ \frac{\partial}{\partial z} (k_c \frac{\partial T_c}{\partial z}) - \rho w [c_p \frac{\partial T_c}{\partial z} + \\ &\frac{1}{\rho} (1 - \beta T) \frac{\partial p}{\partial z} + w \frac{\partial w}{\partial z} - a_z] \end{aligned} \quad (3.15)$$

Thus, three governing equations, Eqs. 3.3, 3.6 and 3.15, have been established which define the three principal variables T_c , p and w , provided the initial and boundary conditions are properly specified and the convective film coefficient can be predicted. Since the normalization of these equations, followed by an order-of-magnitude comparison will indicate that the conductive term in Eq. 3.15 is negligible so as to simplify the boundary conditions, the discussion of the initial and boundary conditions is deferred until after the normalization.

The convective film coefficient is computed from the following relationships between the Nusselt number $N_{Nu} = \bar{h}_c d/k_c$, the Reynolds number

N_{Re} and the Prandtl number $N_{Pr} = \mu c_p / k_c$ where μ represents the dynamic viscosity:

For $N_{Pr} < 0.1$ (liquid metals)

$$N_{Nu} = 6.5 + 0.025 (N_{Re} N_{Pr})^{0.8} \quad (3.16)$$

which produces Nusselt numbers between those appropriate for uniform heat flux (Martinelli) and for uniform wall temperature (Seban and Shimazaki) (Ref. 4).

For $N_{Pr} > 0.1$ and

for $N_{Re} < 2300$ (laminar flow, Ref. 5)

$$N_{Nu} = 3.65 + \frac{0.0668 (N_{Re} N_{Pr} \delta)}{1 + 0.045 (N_{Re} N_{Pr} \delta)} \quad (3.17)$$

for $N_{Re} \geq 2300$ (turbulent flow, Ref. 5)

$$N_{Nu} = 0.116 (N_{Re}^{0.667} - 125) N_{Pr}^{0.333} (1 + \delta) \quad (3.18)$$

where $\delta = d/L$ stands for the tube diameter-over-length ratio.

The Normalization of Eqs. 3.3, 6 and 15 is carried out for the purpose of scaling and performing an order-of-magnitude comparison. The computational effort is also reduced in the process.

Let

$$\zeta = z/L \quad (3.19)$$

$$\tau = tw_o/L \quad (3.20)$$

represent the nondimensional axial distance and the nondimensional time, respectively, and let the dimensionless state variables be defined as

$$\theta_c(\tau, \zeta) = \frac{T_c(t, z)}{T_o} \quad (3.21)$$

$$\pi(\tau, \zeta) = \frac{p(t, z)}{p_o} \quad (3.22)$$

$$\omega(\tau, \zeta) = \frac{w(t, z)}{w_o} \quad (3.23)$$

and to represent the nondimensional temperature, pressure and velocity of the fluid, that is, the principal dependent fluid flow variables. The subscript "o" designates the constant reference state of the fluid at the tube entrance. Introduce next the nondimensional density

$$v(\tau, \zeta) = \frac{\rho(t, z)}{\rho_o}, \quad (3.24)$$

the nondimensional radial distance from the channel axis

$$\eta = \frac{2r}{d}, \quad (3.25)$$

and the nondimensional tube wall temperature

$$\theta_w(\tau; \eta, \zeta) = \frac{T_w(t; r, z)}{T_o} \quad (3.26)$$

Notice, that all dependent variables lie between zero and unity, except v and ω whose product ($v\omega$) remains essentially equal to unity with neither v nor ω departing far from unity. The reference temperature T_o is, under normal operating conditions, the highest temperature in the system.

Furthermore, consider the following ϕ -values to vary along the channel axis:

$$\phi_{\beta} = T_o \beta \quad (3.27)$$

$$\phi_k = p_o \kappa \quad (3.28)$$

$$\phi_{cp} = \frac{c_p}{c_p (\rho_o, T_o)} = \frac{c_p}{c_{p,o}} \quad (3.29)$$

$$\phi_k = \frac{k}{k (\rho_o, T_o)} = \frac{k}{k_o} \quad (3.30)$$

and finally, the following constant F-parameters:

$$F_p = \frac{p_o}{\rho_o w_o^2} \quad (3.31)$$

$$F_f = 4f \frac{L}{d} = \frac{4f}{\delta} \quad (3.32)$$

$$F_z = \frac{p_o}{\rho_o c_{p,o} T_o} \quad (3.33)$$

$$F_M = F_z / F_p = \frac{w_o^2}{C_{p,o} T_o} \quad (3.34)$$

Let the dot above a variable designate partial differential with respect to the nondimensional time τ and the subscript ζ partial differentiation with respect to the dimensionless axial coordinate ζ . Then the principal conservation equations, Eqs. 3.3, 3.6 and 3.15 read, respectively and in nondimensional form:

$$\phi_\beta [\dot{\theta}_c + \omega(\theta_c)_\zeta] = \omega_\zeta + \phi_\kappa (\dot{\pi} + \omega\pi_\zeta) \quad (3.35)$$

$$\dot{\omega} + \omega \omega_\zeta = -\frac{F_p}{v} \pi_\zeta - F_f \frac{\omega^2}{2} \quad (3.36)$$

$$\begin{aligned} \dot{\theta}_c - F_z \frac{\phi_\beta}{\phi_{cp}} \frac{\theta_c}{v} + F_M \frac{1}{\phi_{cp}} \omega \omega_\zeta &= \delta \frac{4N_{Nu}}{N_{Re} N_{Pr}} \cdot \frac{1}{v \phi_{cp}} (\theta_\omega - \theta_c) + \frac{\delta^2}{4N_{Nu}} \\ &\times [\phi_\kappa (\theta_c)_\zeta]_\zeta - \omega(\theta_c)_\zeta + \\ &F_z \frac{1-\theta_{cb}}{\phi_{cp}} \cdot \frac{1}{v} \pi_\zeta + F_M \frac{1}{\phi_{cp}} \omega \omega_\zeta \end{aligned} \quad (3.37)$$

These are the three equations which define the three time rates of change, $\dot{\theta}_c$, $\dot{\pi}$ and $\dot{\omega}$. It can be seen from Eq. 3.37 that the axial conduction is always small, of an order less than δ^2 (since $N_{Nu} > 3$), when compared with the convective term, unless the fluid should reach the wall temperature within the very first small fraction of the tube length. Axial conduction is hence ignored as $\delta^2 \approx 10^{-6}$, and the order of differentiation of Eq. 3.37 is reduced to one.

$$\dot{\theta}_c - F_z \frac{\phi_\beta}{\phi_{cp}} \frac{\theta_c}{v} \dot{\pi} + F_M \frac{1}{\phi_{cp}} \dot{\omega} = \frac{4N_{Nu}}{\delta N_{Re} N_{Pr}} \frac{\theta_w - \theta_c}{v \phi_{cp}} - \omega \left\{ \left(\theta_c \right)_\zeta + F_z x \right. \\ \left. \frac{1 - \theta_c \phi_\beta}{v \phi_{cp}} \pi_\zeta + \frac{F_M}{\phi_{cp}} \omega \omega_\zeta \right\} \quad (3.38)$$

The Boundary Conditions to be imposed on Eqs. 3.35, 3.36 and 3.38 are chosen, at the channel entrance, to be

- (i) mass flow rate \dot{m} , prescribed as a function of time
- (ii) constant inlet pressure P_o .
- (iii) continuous transition, of the inlet fluid temperature, from an initial temperature $\theta = \theta_i$ to the constant operational temperature $\theta(t,0) = 1$, or an arbitrarily prescribed inlet fluid temperature that is a continuous function of time

These boundary conditions accommodate the calculation of the steady state conditions as well as of the most likely start-up operation toward stationary operating conditions. Notice that there are no step changes implied in any of the dependent variables which is essential for the numerical integration. Writing these boundary conditions more specifically, one gets at $\zeta = 0$

$$\theta(\tau, 0) = 1 - (1 - \theta_i) e^{-7\tau} \quad (3.39)$$

$$\pi(\tau, 0) = 1 \quad (3.40)$$

$$\omega(\tau, 0) = \frac{1}{v(\pi, \theta)} \quad (3.41)$$

Here, the time constant was chosen arbitrarily so as to have the fluid reach, within 0.1%, its steady inlet temperature at the inlet during the

time interval that it takes a fluid particle to pass through the channel. Equation 3.41 is given through the thermal equation of state, Eq. 3.2.

The Initial Conditions appropriate to the system of Eqs. 3.35, 3.36 and 3.38 are derived from the requirement that the flow should initially be at steady state with the fluid inlet temperature equal to the uniform channel wall temperature. Setting the time derivatives equal to zero in Eqs. 3.35, 3.36 and 3.38 results in a system of three ordinary differential equations which are linear in $d\pi/d\zeta$, $d\theta_c/d\zeta$ and $d\omega/d\zeta$:

$$F_p \frac{d\pi}{d\zeta} + \frac{d\omega}{d\zeta} = -F_f v \frac{\omega^2}{2} \quad (3.42)$$

$$F_z \frac{\phi_\beta}{v} \frac{d\pi}{d\zeta} + \frac{d\theta_c}{d\zeta} + \frac{F_M}{\phi_{cp}} \omega \frac{d\omega}{d\zeta} = \frac{4N_{Nu}}{\delta N_{Rc} N_{Pr}} (\theta_w - \theta_c) \quad (3.43)$$

$$\phi_\kappa \frac{d\pi}{d\zeta} - \phi_\beta \frac{d\theta_c}{d\zeta} + \frac{1}{\omega} \frac{d\omega}{d\zeta} = 0 \quad (3.44)$$

These equations can be solved subject to the boundary conditions at $\zeta = 0$

$$\left. \begin{aligned} \pi &= 1 \\ \theta_c &= \theta_i \\ \omega &= \frac{1}{v(\pi, \theta_c)} \end{aligned} \right\} \quad (3.45)$$

provided the function $\theta_w = \theta_w(0; 1, \zeta)$ prescribing the initial channel wall temperature is specified. For the present analysis θ_w was set equal to θ_i . Equations 3.42 through 3.45 define the initial flow field.

Quasi-Steady Flow. It may be recognized that the momentum transport takes place at a much smaller time scale than the transport of thermal energy in that the pressure and the velocity fields adjust virtually

instantaneously to a change in flow inlet conditions while the response of the temperature field to a change in channel wall temperature takes considerably longer, the reason being that the pressure perturbations propagate along the channel with the speed of sound. Unless one is specifically interested in the motion of sound waves one may consider the dynamics of the flow field, that is the pressure and velocity distributions, as part of the boundary conditions and imposed instantly and adiabatically by the flow inlet conditions.

The fluid temperature remains stationary during the dynamic adjustment and the time rate of change of both pressure and temperature remain small since ordinarily the pressure gradient remains balanced by the wall shear (and by the convective acceleration in the case of a gaseous coolant medium). Consequently, Eqs. 3.42 and 3.44 may serve to establish the pressure and velocity fields at all times, subject to boundary conditions given by Eqs. 3.40 and 3.41 while the temperature field remains defined by Eqs. 3.35, 36, 38 and the initial conditions discussed above. Particularly, solving Eqs. 3.35, 36 and 38 for $\dot{\theta}_c$ gives the differential equation which governs the temperature field:

$$\dot{\theta}_c = \frac{1}{1 - \frac{F_z}{\phi_{cp}} \frac{\phi_\beta^2}{\phi_\kappa} \frac{\theta}{v}} \left\{ \frac{4N_{Nu}}{\delta N_{Re} N_{Pr}} (\theta_w - \theta_c) \right. \\ \left. + F_z \frac{\phi_\beta}{\phi_{cp} \phi_\kappa} \times \left[\phi_\beta \omega(\theta_c)_\zeta - \frac{\theta_c}{v} \omega_\zeta \right] \right. \\ \left. - \omega[(\theta_c)_\zeta + F_M F_f \frac{1}{\phi_{cp}} \frac{\omega^2}{2}] \right\} \quad (3.46)$$

This completes the discussion of the development of the governing differential equations for the coolant fluid. All equations are solved numerically as discussed in Chapter III. The thermodynamic properties c_p , β , and κ are derived from the thermal equation of state, Eq. 3.2 and from the zero-pressure specific heat or other available properties. All thermodynamic functions as well as the transport properties κ and μ are considered, in general, as functions of two state variables, that is, of ρ and T or of p and T , as discussed in Section E of Chapter II.

4. The Flow Channel

The flow channel is treated as a circular tube with inner radius $r_i = d/2$ and outer radius $r_o = r_i + s_t$. The tube wall temperature $T_w(t; r, z)$ is defined through the familiar equation of energy conservation, written for the case of circular symmetry:

$$\frac{\partial T_w}{\partial t} = \alpha_w \left[\frac{1}{r} \frac{\partial}{\partial r} \left(r \frac{\partial T_w}{\partial r} \right) + \frac{\partial^2 T_w}{\partial z^2} \right] + \frac{1}{(\rho c)_w} \frac{dk_w}{dT} \left[\left(\frac{\partial T_w}{\partial r} \right)^2 + \left(\frac{\partial T_w}{\partial z} \right)^2 \right], \quad (4.1)$$

where α_w represents the thermal diffusivity of the wall material and $(\rho c)_w$ its volumetric heat capacity. The boundary conditions are

at $r = r_i$

$$\bar{h}_c (T_w - T_c) = k_w \frac{\partial T_w}{\partial r} \quad (4.2)$$

at $r = r_o$

$$k_w \frac{\partial T_w}{\partial r} - \psi k_f \frac{\partial T_f}{\partial x} - (2\pi - \psi) k_m \frac{\partial T_m}{\partial r} = 0 \quad (4.3)$$

Here

\bar{h}_c is the convective film coefficient,

T_c the fluid temperature,

k the thermal conductivity,

ψ the portion of outer tube circumference in contact with fins, expressed in radians,

and the subscripts w, f and m designate, respectively, tube wall, fin and meteoroid protection layer. Equations 4.2 and 3 constitute the continuity of the heat flux at the fluid-wall interface and at the wall-fin and wall-protection layer interfaces. Circumferential temperature variations are ignored.

After introducing

$$\eta = \frac{r}{r_i}, \quad \zeta = \frac{x}{H}; \quad \tau = \frac{tw_o}{L}; \quad \theta_w = \frac{T_w}{T_o},$$

$$\phi_c = \frac{k_c}{k_w}, \quad \phi_f = \frac{k_f}{k_w} \frac{r_i}{H},$$

$$\phi_m = \frac{k_m}{k_w} \quad N_{Bi} = \frac{\bar{h}_c d}{k_w}, \quad (4.4)$$

$$\delta = \frac{d}{L}, \quad \phi_{kw} = \frac{T_o}{k_w} \frac{dk_w}{dT}, \quad \phi_{Fo,w} = \frac{\alpha_w L}{w_o r_i^2}$$

with H representing the fin height, that is, the distance between the fin root and fin tip, one may recast Eqs. 4.1, 2 and 3 to read

$$\begin{aligned} \dot{\theta}_w = \phi_{Fo,w} \left\{ \frac{1}{\eta} \frac{\partial}{\partial \eta} \left(\eta \frac{\partial \theta_w}{\partial \eta} \right) + \left(\frac{\delta}{2} \right)^2 \frac{\partial^2 \theta_w}{\partial \zeta^2} \right. \\ \left. + \phi_{kw} \left[\left(\frac{\partial \theta_w}{\partial \eta} \right)^2 + \left(\frac{\delta}{2} \right)^2 \left(\frac{\partial \theta_w}{\partial \zeta} \right)^2 \right] \right\} \end{aligned} \quad (4.5)$$

at $\eta = 1$

$$\frac{1}{2} N_{Bi} (\theta_w - \theta_c) = \frac{\partial \theta_w}{\partial \eta} \quad (4.6)$$

at $\eta = \eta_0$

$$\frac{\partial \theta_w}{\partial \eta} - \psi \phi_f \frac{\partial \theta_f}{\partial \xi} - (2\pi - \psi) \phi_m \frac{\partial \theta_m}{\partial \eta} = 0 \quad (4.7)$$

The superscript dot represents partial differentiation with respect to nondimensional time τ . As before in the treatment of the coolant fluid one recognizes that, with $\delta^2 \approx 10^{-6}$, axial conduction remains insignificant. Thus, Eq. 4.5 takes on this final form

$$\dot{\theta}_w = \phi_{Fo,w} \left\{ \frac{1}{\eta} \frac{\partial}{\partial \eta} \left(\eta \frac{\partial \theta_w}{\partial \eta} \right) + \phi_{kw} \left(\frac{\partial \theta_w}{\partial \eta} \right)^2 \right\} \quad (4.8)$$

Equations 4.6, 7 and 8 define the tube wall temperature, provided Eqs. 4.6 and 7 hold at some initial time and the initial temperature $\theta_w(0; \eta, \zeta)$ is prescribed as a sufficiently smooth function of η and ζ .

Low Biot Number. When one compares possible heat fluxes at the fluid-wall interface with the possible radiant fluxes from the outer surface of the meteoroid protection layer covering the tube, one concludes that the maximum fluxes occur at the inner tube wall and that the Biot number N_{Bi} in Eq. 4.6 is the largest ratio to be expected of external to internal thermal conductances. Thus, if N_{Bi} is small, say less than 0.05 (Ref. 6), then the temperature variation inside the tube wall is too small for experimental detection and a computation of the detailed temperature distribution on the basis of Eq. 4.8 cannot be justified as the associated computational effort is considerable.

In cases where the equivalent Biot number, representing the total thermal resistance within the channel wall and the protection layer, is small, the tube, the protection layer and a representative portion of the fin root are combined into a single control volume as depicted in Fig. 2. The equivalent Biot number \bar{N}_{Bi} and the chosen limit are

$$\bar{N}_{Bi} = N_{Nu} \frac{k}{d} \left(\frac{s_w}{k_w} + \frac{s_m}{k_m} \right) < 0.05 \quad (4.9)$$

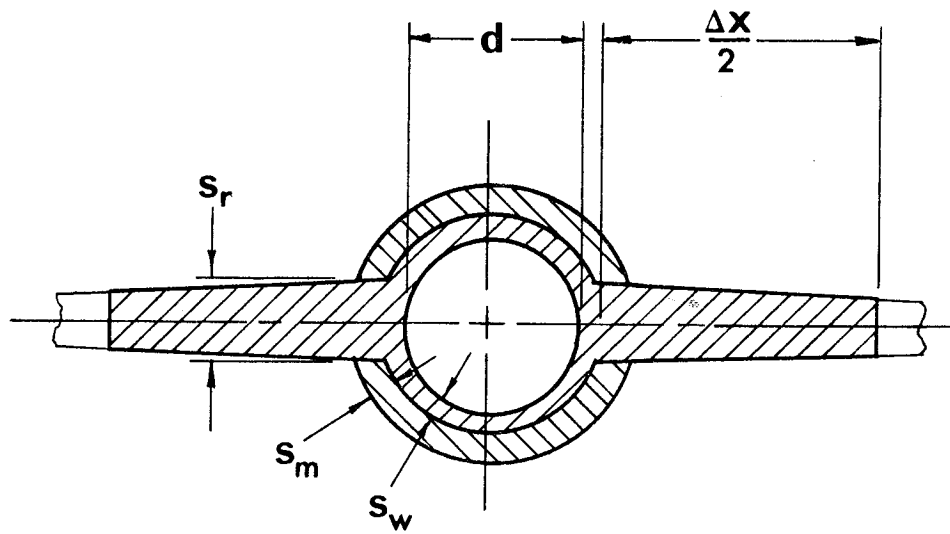


Figure 2. Control Volume for Low-Biot Number Cases

where s_w and s_m stand for, respectively, the tube wall and the protection layer thicknesses. The combined volumetric heat capacity per unit of axial distance for the control volume consists of three parts, the first one for the tube wall, the second for the protection layer and the third for the first half fin element:

$$\pi d (\rho cs)_w \left\{ \left(1 + \frac{s_w}{d}\right) + \left(1 + 2 \frac{s_w}{d} + \frac{s_m}{d}\right) \frac{(\rho cs)_m}{(\rho cs)_w} + \frac{\Delta x}{\pi d} \frac{s_r}{s_w} \times \right. \\ \left. \left[1 - \frac{\Delta \xi}{4} \left(1 - \frac{s_t}{s_r}\right)\right] \frac{(\rho c)_f}{(\rho c)_w} \right\} = \lambda_1 \pi d (\rho cs)_w \quad (4.10)$$

where the subscripts w, m, f, r and t designate, respectively, parameters of the tube wall, the meteoroid protection layer, the fin, the fin root and the fin tip and where

d is the tube diameter,

ρ the density,

s the thickness,

Δx the node spacing on the fin, and

$\Delta \xi = \Delta x/H$, the nondimensional node spacing

Heat enters the control volume, per units of time and axial distance, by convection from the fluid

$$\pi d \bar{h}_c (T_w - T_c),$$

and by convection and/or radiation from outside

$$(2\pi - \psi) \left(\frac{d}{2} + s_w + s_m\right) q''_m + \Delta x (q''_1 + q''_2)_f$$

where the subscripts 1 and 2 designate upper and lower fin sides, respectively, and where q'' represents the sum of the convective and of the net radiant fluxes entering the outer surfaces. In the case of q''_m , the average over upper and lower portions of the outer circumference is to be taken.

Heat leaves the control volume through the fin by conduction, again per units of time and axial distance

$$2 \left(s \frac{\partial T}{\partial x} \right)_f$$

evaluated at $x = \Delta x/2$.

Combining the last four expressions into the energy balance leads to this expression

$$\lambda_1 \pi d (\rho c s)_w \frac{\partial T_w}{\partial t} = \pi d \bar{h}_c (T_w - T_c) + \pi d \lambda_2 q''_m + \Delta x (q''_1 + q''_2)_f + 2 \left(s \frac{dT_f}{dx} \right) \Big|_{\frac{\Delta x}{2}} \quad (4.11)$$

where λ_1 is defined by Eq. 4.10 and

$$\lambda_2 = \left(2 - \frac{\psi}{\pi} \right) \left(\frac{1}{2} + \frac{s_w + s_m}{d} \right) \quad (4.12)$$

Equation 4.11 replaces Eqs. 4.6, 7 and 8 as well as Eqs. 5.3, and 5 governing the temperature distribution in the meteroid protection layer and, lastly, Eq. 2.19 which constitutes one of the boundary conditions for the differential equation governing the fin temperature distribution. The only condition under which all the above equations may be replaced by the single equation, Eq. 4.11, is given by Eq. 4.9. Finally, it may be noted that Eq. 4.11 could also be normalized but since no new dimensionless groups result from such normalization it is omitted here.

5. The Meteoroid Protection Layer

The differential equation governing the temperature distribution within the meteoroid protection layer which covers the flow channel, is identical to that for the channel wall, Eq. 4.8, except for the two dimensionless parameters, the Fourier coefficient ϕ_{Fo} and the conductivity temperature coefficient ϕ_k which now must be evaluated for the protection layer material:

$$\phi_{Fo,m} = \frac{\alpha_m}{\alpha_w} \phi_{Fo,w} \quad (5.1)$$

$$\phi_{k,m} = \frac{T_o}{k_m} \frac{dk_m}{dT} \quad (5.2)$$

After ignoring the axial conduction for the reasons stated in Section 4 one obtains as the nondimensional energy conservation equation

$$\dot{\theta}_m = \phi_{Fo,m} \left\{ \frac{1}{\eta} \frac{\partial}{\partial \eta} \left(\eta \frac{\partial \theta_m}{\partial \eta} \right) + \phi_{k,m} \left(\frac{\partial \theta_m}{\partial \eta} \right)^2 \right\} \quad (5.3)$$

Two boundary conditions are required, one of which is given by Eq. 4.7 while the other one is dictated by the heat flux continuity at the outer boundary:

at $r = r_e$

$$k_m \frac{\partial T_m}{\partial r} = q'' \quad (5.4)$$

where q'' is defined as the net flux entering both by radiation and/or aerodynamic heating. Equation 5.4 reads in nondimensional form at $\eta = \eta_e$

$$\frac{\partial \theta_m}{\partial \eta} = \phi_{Nc} (\tilde{q}_{net,rad} + \tilde{q}_{aero}) \quad (5.5)$$

with ϕ_{Nc} representing a local conductance parameter

$$\phi_{Nc} = \frac{\sigma d T_o^3}{2k_m} \quad (5.6)$$

and

$$\tilde{q}_{net,rad} = \frac{q''_{net,rad}}{\sigma T_o^4} \quad (5.7)$$

$$\tilde{q}_{aero} = \frac{q''_{aero}}{\sigma T_o^4} \quad (5.8)$$

Here, σ represents the Stefan-Boltzmann constant, and $q''_{net,rad}$ and q''_{aero} the net radiant incident heat flux and the convective heat flux, respectively.

If the initial temperature distribution is given, and if Eqs. 4.7 and 5.5 hold initially, then the protection layer temperature θ_m is completely defined as a function of time and location by Eqs. 5.3, 5 and 4.7, provided the incident radiation and the aerodynamic heating are prescribed as functions of time. The prediction of these incident heat fluxes is discussed in Section 6 and 7 of this Chapter.

In the case of low Biot numbers at the coolant fluid-tube wall interface the meteoroid protection layer is lumped together with the tube wall as discussed in Section 4 of Chapter II.

6. Radiation

The objective of this section is to develop a procedure to predict the net radiant heat flux incident on fin and tube surfaces which are exposed to any combination so solar, albedo and planetary irradiation. Included into the assessment of radiative transfer is the radiative energy exchange between fin panel and flow channel or its protective coating as well as the effect of structural panels in the vicinity of the fin system; however, not included is any possible gas radiation as could conceivably be encountered during reentry.

In seeking the proper mathematical model it is recognized, firstly, that the prevailing thermal radiant energy lies in either the visible (solar irradiation) or the infrared portion of the spectrum, and, secondly, that the fin system is coated, for the purpose of optical optimization, with a dielectric paint. Consequently, spectrally dependent optical properties must be dealt with, but, for the latter reason, the transfer matrix of radiative exchange can be expected to remain temperature insensitive over some range of operational conditions, a fact which is very much appreciated from the computational view point.

For the analysis, the fin surface A_f , the outer surface on the flow channel A_n , and the structural surface(s) A_n , are all considered as parts of an enclosure C which is completed by a set of arbitrarily concave, non-reflecting imaginary surfaces A_e which connect A_m , A_f and A_n and along which is specified the emerging net radiant heat flux representing solar, albedo and planetary irradiation. The sum $A_m + A_f + A_n + A_e$ is the inner surface A_c of the enclosure.

Three steps are necessary for the prediction of the incident net radiant heat flux $q''_{\text{net,rad}}$. Firstly, the elemental exchange areas*

$$\frac{\partial^2 \overline{s_i s_j}}{\partial A_i \partial A_j} = \frac{\cos \phi_i \cos \phi_j}{\pi r^2} \quad (6.1)$$

*For terminology and notations consult Ref. 7, Chapter 2.

need to be computed on the basis of the geometric relation between fin panels and flow channels. Here, the symbol r designates the distance between two area elements dA_i and dA_j which are visible from each other, and ϕ_i and ϕ_j represent the respective angles between r and the surface normals on dA_i and dA_j . The next step is to compute, from its definition, the radiosity or leaving radiant flux density, W_j :

$$W_j = \int_0^\infty W_{j,\lambda} d\lambda = \int_0^\infty \epsilon_{j,\lambda} E_{j,\lambda} d\lambda + \quad (6.2)$$

$$\int_{A_c} \frac{\partial^2 \overline{s_i s_j}}{\partial A_i \partial A_j} \int_0^\infty (1 - \epsilon_{j,\lambda}) W_{i,\lambda} d\lambda dA_i$$

where $W_{j,\lambda}$, $E_{j,\lambda}$ and $\epsilon_{j,\lambda}$ stand for the monochromatic radiosity, the monochromatic black body emissive power

$$E_{j,\lambda} = \frac{2 hc^2 n^2}{\lambda^5} \frac{1}{e^{(hc)/(\lambda T_j)} - 1} \quad (6.3)$$

and the monochromatic hemispherical emittance, respectively; the subscripts i and j designate two discrete points on A_c , and λ represents the wavelength. The Eq. 6.3 constitutes Planck's law of monochromatic emissive power intensity; h , c and k stand for, respectively, Planck's constant, the speed of light in vacuo and the Boltzmann constant. The third and last step is to calculate, on the basis of local energy balance, the net incident heat flux

$$(q''_{\text{net,rad}})_j = \int_0^\infty q''_{j,\lambda} d\lambda = \int_{A_c} (W_i - W_j) \frac{\partial^2 \overline{s_i s_j}}{\partial A_i \partial A_j} dA_i \quad (6.4)$$

It should be obvious that Eqs. 6.1, 2 and 4 contain all the necessary fundamental principles but their evaluation will introduce a number of simplifications and modifications, each selected for the particular system of interest. Specifically, Eq. 6.4 will have to supplement Eq. 6.2 for portions of A_c where the heat flux is specified. More importantly, however, there is a choice to be made in view of the computational process regarding particularly Eq. 6.2. One may either solve the monochromatic version of Eq. 6.2 n times for the n significant spectral intervals encountered and thus face the ultimate task of solving $n \times N$ simultaneous linear algebraic equations when N discrete points on A_c need to be considered (possibly at several time steps during the calculation process) and then integrate the resulting total interchange areas over the spectrum (see Ch. 5.6 of Ref. 7). Or, one may force the non-gray surface analysis into a gray surface analysis by placing the burden of complexity on the evaluation of appropriate optical properties. Both techniques afford any desirable accuracy of allowing for the spectral differences in surface properties, limited only by available calculation time; but the latter technique was chosen because, as a result of this choice, the complexity remains at peripheral parts of the computer code which are more accessible for later modifications toward greater sophistication, also the complexity may turn out, in almost all cases, to reduce partly to simple hand calculations.

After introducing

$$\epsilon_i = \frac{\int_0^\infty \epsilon_{i,\lambda} E_{i,\lambda} d\lambda}{\int_0^\infty E_{i,\lambda} d\lambda} = \frac{1}{E_i} \int_0^\infty \epsilon_{i,\lambda} E_{i,\lambda} d\lambda \quad (6.5)$$

$$\alpha_{ij} = \frac{\int_0^\infty \epsilon_{i,\lambda} W_{j,\lambda} d\lambda}{\int_0^\infty W_{j,\lambda} d\lambda} \quad (6.6)$$

Equation 6.2 simplifies to

$$W_j = \epsilon_j E_j + \int_{A_c} \frac{\partial^2 \overline{s_i s_j}}{\partial A_i \partial A_j} (1 - \alpha_{ij}) W_i dA_i \quad (6.7)$$

which reduces to the gray-surface radiosity equation whenever Eq. 6.6 reduces to $\alpha_{ij} = \epsilon_i$. The difficulty now lies in evaluating Eq. 6.6 even though the radiosity $W_{j,\lambda}$ is as yet unknown.

By successively substituting the right-hand side of Eq. 6.2, in its monochromatic form, for $W_{i,\lambda}$ on the right-hand side of that equation, one obtains first (Ref. 8)

$$W_{j,\lambda} = \epsilon_{j,\lambda} E_{j,\lambda} + (1 - \epsilon_{j,\lambda}) \left\{ \int_{A_c} \frac{\partial^2 \overline{s_i s_j}}{\partial A_i \partial A_j} \left[\epsilon_{i,\lambda} E_{i,\lambda} + (1 - \epsilon_{i,\lambda}) \int_{A_c} \frac{\partial^2 \overline{s_i s_m}}{\partial A_i \partial A_m} \epsilon_{m,\lambda} E_{m,\lambda} + \dots \right] dA_i \right\} \quad (6.8)$$

and subsequently α_{ij} as the quotient of two infinite series. Since the enclosure radiation is dominated by the fin-sun and fin-sky interaction and since Eq. 6.8 contributes significantly only to the fin-flow channel interaction, the infinite series in Eq. 6.8 may be terminated after two terms (two reflections; the resulting error is less than the uncertainty in ϵ_λ), and Eq. 6.6 becomes:

$$\alpha_{ij} = \frac{X_{ij} E_j + \int_{A_c} \frac{\partial^2 \overline{s_j s_k}}{\partial A_j \partial A_k} E_k (X_{ik} - X_{ijk}) dA_k}{\epsilon_j E_j + \int_{A_c} \frac{\partial^2 \overline{s_j s_k}}{\partial A_j \partial A_k} E_k (\epsilon_k - X_{jk}) dA_k} \quad (6.9)$$

where

$$X_{ij} = \int_0^\infty E_{j,\lambda} \epsilon_{j,\lambda} \epsilon_{i,\lambda} d\lambda / E_j \quad (6.10)$$

$$X_{ijk} = \int_0^\infty E_{k,\lambda} \epsilon_{k,\lambda} \epsilon_{j,\lambda} \epsilon_{i,\lambda} d\lambda / E_k \quad (6.11)$$

In cases where the net radiant flux is specified over portions of A , the emissive power E is to be replaced by the net radiant flux q'' in Eqs. 6.9, 10 and 12, which results in one additional term each in the numerator and the denominator of Eq. 6.9.

In summary, the incident net radiant heat flux for the diffuse, non-gray enclosure is calculated on the basis of an approximate gray-surface analysis in accordance with Eqs. 6.4, 7 and 9 through 11. The spectral differences of the surfaces are accounted for in Eqs. 9 through 11. The remainder of this section is devoted to the solution of the radiosity equation, Eq. 6.7.

Recalling that A_c is the sum $A_m + A_n + A_f + A_e$ of the outer channel surface A_m , the possibly present, nearby structural surfaces A_n , the fin surface A_f , and the remainder of the enclosure A_e , one recognizes that the integrals over A_c in Eqs. 6.4, 7 and 9 need to be evaluated twice for each of the four parts, namely once with $j = 1$ representing the fin area and then with $j = 2$ for the exposed channel area. Since the incident solar, albedo and planetary radiant flux intensities are uniform over the fin area and averaged over the circumference of the channel area

$$\int_{A_e} \frac{\partial^2 \overline{s_1 s_1}}{\partial A_i \partial A_1} (1 - \alpha_{i1}) W_i dA_i = (1 - \alpha_{e1}) q''_{e1} \quad (6.12)$$

$$\int_{A_e} \frac{\partial^2 \overline{s_1 s_2}}{\partial A_1 \partial A_2} (1 - \alpha_{12}) W_i dA_i = (1 - \alpha_{e2}) q''_{e2} \quad (6.13)$$

where q'' designates incident solar, albedo and planetary heat fluxes, appropriately averaged over a chosen area element. Should any structural surfaces obstruct the incident radiant fluxes ($A_n \neq 0$) then the right-hand sides of Eqs. 6.12 and 13 would have to be modified and reduced in the shaded portions of A_1 and A_2 ; and, if there are m such surfaces,

$$\int_{A_n} \frac{\partial^2 \overline{s_i s_j}}{\partial A_i \partial A_j} (1 - \alpha_{ij}) W_i dA_i = \sum_{k=1}^m \frac{\partial \overline{s_k s_j}}{\partial A_j} (1 - \alpha_{kj}) W_k, \quad (6.14)$$

$$j = 1, 2, \dots, m + 2.$$

Obviously, the radiosity and the temperature are assumed to be uniform over each structural component. No such structural components were included in the analysis reported here, and Eq. 6.14 is taken to be zero.

This leaves only the integrals over A_m and A_f to be discussed. Moreover, since Eq. 6.1 is symmetric with respect to its subscripts i and j , the elemental exchange area is to be evaluated only once.

Considering first the fin, that is $j = 1$ and $i = 2$, and the fact that over the channel surface the radiosity and the temperature are considered to be functions of axial distance only

$$\int_{A_2} \frac{\partial^2 \overline{s_1 s_i}}{\partial A_1 \partial A_i} (1 - \alpha_{1i}) W_i dA_i =$$

$$\int_{z=0}^{z=L} [1 - \alpha_{1i}(z)] W_i(z) \int_{\phi=0}^{\phi^*} \frac{\partial}{\partial A_1} \left(\frac{s_1 s_i}{\Delta A_1} \right) R d\phi dz = \quad (6.15)$$

$$\int_{z=0}^{z=L} [1 - \alpha_{1i}(z)] W_i(z) SS(z; x_f, z_f) dz$$

where L designates the tube length; R and ϕ are the polar coordinates of A_2 , with origin on the tube axis, with $\phi = 0$ and $\phi = \phi^*$ representing, respectively, the root of the fin and the contact line between the tube and its tangent plane through the center of ΔA_1 on the fin. The first step in Eq. 6.15 was obtained by integrating over ΔA_1 and subsequently applying the mean-value theorem of integral calculus, while the second step simply defines the exchange function for every point (x_f, z_f) on the fin which was integrated in closed form for the right-circular flow channel. The result is shown in Appendix D.

The exchange function of the tube with respect to the fin is obtained by dividing SS in Eq. 6.15 by $(R\phi^*)$. Thus

$$\int_{A_1} \frac{\partial^2 \frac{s_2 s_i}{\Delta A_2 \Delta A_i}}{\partial A_2 \partial A_i} (1 - \alpha_{2i}) W_i dA_i = \frac{1}{R\phi^*} \int_{z=0}^L \int_{x=0}^H [1 - \alpha(z, x_f, z_f)] W(x_f, z_f) SS(z, x_f, z_f) dx_f dz_f \quad (6.16)$$

For the numerical evaluation of the integrals a suitable quadrature such as the trapezoidal rule is chosen so as to render Eq. 6.7 in this form

$$P_j = \sum_i M_{ji} W_i \quad (6.17)$$

$$i, j = 1, 2, \dots, N$$

which is a system of N linear algebraic equations for the $N = (n_x + 1)(n_z + 2)$ unknown values of the radiosity W_i . Here, n_x and n_z are the numbers of subdivisions chosen in the x - and the z -directions, respectively. The vector P on the left-hand side of Eq. 6.17 is called the excitation vector

$$P_j = -\epsilon_j E_j - (1 - \alpha_{ej}) q''_{ej} \quad (6.18)$$

on the right-hand side, the transfer matrix M_{ji} is given by

$$\delta_{ji} - \chi_i [1 - \alpha_{ji}] SS_{ji} = M_{ji} \quad (6.19)$$

where

$$\delta_{ji} = \begin{matrix} 0 & i \neq j \\ \text{for} & \\ 1 & i = j \end{matrix}$$

is the Kronecker delta, χ_i is a suitable quadrature coefficient and SS_{ji} is given either by Eq. 6.15 or by Eq. 6.16 depending on whether j refers to the fin or to the channel, respectively. There is no matrix multiplication implied in Eq. 6.19, hence the underscores.

In the present program phase, Eq. 6.17 is solved at every time step only when the transfer matrix is sufficiently temperature sensitive, otherwise the transfer matrix is completely inverted only once to yield the unknown

radiosity at any time.

$$W_i = \sum_j (M_{ij})^{-1} P_j \quad (6.20)$$

through a simple matrix multiplication. It may be noted that the most significant temperature dependence of optical properties is contained in the excitation vector P_j .

All radiant heat fluxes are normalized with respect to σT_o^4 where T_o designates the reference temperature, that is the fluid inlet temperature. Exchange factors are nondimensional and need not be normalized.

$$w_j = \frac{W_j}{\sigma T_o^4}, \quad \tilde{q}_j = \frac{q_j}{\sigma T_o^4}, \quad p_j = \frac{P_j}{\sigma T_o^4} \quad (6.21)$$

The nondimensional forms of Eqs. 6.4 and 6.20 are used to compute $\tilde{q}_{\text{net,rad}}$ in Eqs. 2.17, 4.11 and 5.5.

7. Aerodynamic Heating

The aerodynamic heating model used to evaluate the convective flux from the radiator surface on the orbiter vehicle is subdivided into three major regimes. The first regime encompasses low speed flow for which the heat transfer coefficients are determined from expressions appearing in standard heat transfer texts for flow over a flat plate. The second regime consists of a model for high speed flow in which the convective heat transfer coefficient is evaluated from an experimental correlation for flow over the upper surface of the shuttle orbiter vehicle (Ref. 9). The third section of the model encompasses a low to high speed transitional flow regime. Within this regime the heat transfer coefficient is an interpolated value that lies between the values obtained in the low and high speed regimes. Calculations for the convective heat flux for all three regimes are based on Eckert's reference enthalpy method (Ref. 10).

Within each of the three regimes the heat transfer coefficient is calculated for cases where the flow is laminar, transitional or fully turbulent. In addition to the evaluation of the heat flux when the flow is forced, the procedure accounts for heat transfer by free convection at times when the shuttle vehicle is stationary or moving with a relatively low velocity.

The program for the evaluation of the aerodynamic heating rate is divided into six sub-tasks each of which is written as a separate subprogram. This procedure allows for changes in the periphery of the program without affecting the program foundation. The basic calculations are carried out in and controlled from the SUBROUTINE CONVEC. Atmospheric temperature and speed of sound are evaluated within the SUBROUTINE ATMOS. Atmospheric properties evaluated at the reference temperature are calculated within the SUBROUTINE REFP. The orbiter velocity and altitude are evaluated in the FUNCTION subprogram ALTVEL. The SUBROUTINE NUS evaluates the Nusselt number for the radiator system.

It should be noted that the analysis does not account for the effects of shock wave interaction or interference heating caused by flow interference between the orbiter, booster or any supporting structure.

The analysis for the determination of the aerodynamic heating first requires the evaluation of a reference temperature which is used for the determination of all air properties. The reference temperature is a function of the Prandtl number and recovery factor of the air, as well as the vehicle Mach number.

The Mach number in turn is a function of the altitude and velocity of the orbiter at any instant time. Altitude and velocity profiles for the orbiter are contained in data arrays supplied by the user (see Part A-3c of the Users Manual. If the value of the Integer I is used to specify either ascent or reentry phase, then the N paired data points which define the velocity V and elevation Z as a function of time t may be expressed functionally as

$$V_i = V_i(I, t_i) \quad i = 1, 2, \dots, N \quad (7.1)$$

$$Z_i = Z_i(I, t_i) \quad i = 1, 2, \dots, N \quad (7.2)$$

Once the orbiter velocity and altitude are known as a function of time, the vehicle Mach number M may be calculated from the equation

$$M = \frac{V}{c} \quad (7.3)$$

The speed of sound c is an atmospheric property that is a function only of the altitude.

The reference temperature is a function of the recovery factor r which for laminar flow is

$$r = \sqrt{N_{Pr}}$$

and for turbulent flow (Ref. 11) is

$$r = N_{Pr} \frac{(8 + 0.528M^2/(22 + M^2))}{(7.4)}$$

where the Prandtl number N_{Pr} is an atmospheric property. To avoid a discontinuity in the value of the recovery factor between the laminar and turbulent flow models, Eq. 7.4 was used as the expression for the recovery factor for both flow models. The resulting error in the reference temperature was found to be approximately 5 R in an extreme case.

All of the properties for the atmosphere used in the evaluation of the heat transfer coefficient are evaluated at the high speed reference temperature. Eckert (Ref. 10) recommends the expression

$$i^* = 0.5 (i_\infty + i_w) + 0.11 r (\gamma - 1) M^2 i_\infty \quad (7.5)$$

for the reference enthalpy i^* which can be converted to the reference temperature T^* once the relationship

$$T^* = T^*(i^*) \quad (7.6)$$

between the atmospheric enthalpy and temperature is known. The subscripts " ∞ " and " w " in Eq. 7.5 refer to the enthalpy of the air evaluated at the free stream and surface temperature, respectively, and γ is the ratio of the specific heats for air.

It should be mentioned that when velocities are low ($M \rightarrow 0$) Eqs. 7.5 and 6 yield a reference temperature that approaches the film temperature $(T_\infty + T_w)/2$. As a result Eqs. 7.5 and 6 were used to evaluate the reference temperature for all three flow regimes, i.e., low speed, high speed and the transitional regimes.

The convective flux is the product of the convective heat transfer coefficient and the difference between the air enthalpy evaluated at the surface temperature and at the adiabatic wall temperature. The adiabatic wall

enthalpy i_{aw} is related to the free stream enthalpy, recovery factor and vehicle velocity by the relationship

$$i_{aw} = i_{\infty} + \frac{rV^2}{2g_c} \quad (7.7)$$

The convective heat transfer coefficient h_i used in the reference enthalpy method may be expressed in terms of the Nusselt number N_{Nu}

$$N_{Nu} = \frac{h_{i,xc}^* p^*}{k^*} \quad (7.8)$$

where c_p^* and k^* denote the atmospheric specific heat and thermal conductivity evaluated at the reference temperature T^* . The symbol x denotes a characteristic length of the radiator system which for forced convection is the distance from the stagnation point on the shuttle to the center of the radiator panel.

The expressions for the orbiter Nusselt number selected for the low speed and high speed regime and for laminar, transitional and turbulent flow are summarized in Table 1. Values for the Nusselt number for conditions lying between the low and high speed regimes were obtained by interpolation so that the convective heat flux from the shuttle varies continually from one regime to the other. The symbols N_{Re} and N_{Nu} appearing in the table denote the Reynolds number and Prandtl number, respectively, where

$$N_{Re} = \frac{\rho^* V x}{\mu^*}$$

$$N_{Pr} = \frac{\mu^* c_p^*}{k^*}$$

The "*" superscript on each property indicates that the property is evaluated at the temperature T^* .

TABLE 1

FORCED CONVECTION NUSSELT NUMBER FOR ORBITER

	LOW SPEED REGIME $M \leq 0.5$	HIGH SPEED REGIME $M \geq 1.0$
LAMINAR FLOW $Re < 1.0 \times 10^5$	$N_{Nu} = 0.332 N_{Re}^{1/2} N_{Pr}^{1/3}$	$N_{Nu} = 0.375 N_{Re}^{0.5014} N_{Pr}$
TRANSITIONAL FLOW $1 \times 10^5 \leq Re \leq 1 \times 10^6$	$N_{Nu} = 6.78 \times 10^{-5} N_{Re}^{1.238} N_{Pr}^{1/3}$	$N_{Nu} = 3.339 \times 10^{-4} N_{Re}^{1.111} N_{Pr}$
TURBULENT FLOW $Re > 1 \times 10^6$	$N_{Nu} = 0.0288 N_{Re}^{0.8} N_{Pr}^{1/3}$	$N_{Nu} = 0.0346 N_{Re}^{0.7746} N_{Pr}$

For the low speed regime the expressions for the Nusselt number are those for laminar transitional and turbulent flow over a flat plate (Ref. 6^{*}). Nusselt number relationships for high speed flow regime are taken from Ref. 9 where experimental wind tunnel data are presented for a delta space shuttle orbiter. The data are for leeward surface heat transfer at angles of attack between 10° and 30° and Mach numbers of 8 and 16. The Nusselt number is shown to be relatively independent of angle of attack so that the high speed correlation may be applied to both the ascent phase for which the angle of attack is approximately zero and the reentry phase when the angle of attack may approach 60°. The scatter in the data of Ref. 9 from the selected Nusselt relationships is on the order of 100%.

The leeward surface correlation was selected because the aerodynamic heating rates in this region of the shuttle are relatively low when compared to heating rates for the lower body or windward surface. Estimates place the peak reentry temperature of the lower surface stagnation line around 2100 F while the peak leeward temperature is estimated to be about 600 F (Ref. 12). Therefore, placing the radiator on the upper surface of the orbiter not only will result in a more efficient operation upon reentry, but also will minimize the need for reservicing of the surface coating on the radiator panels.

The aerodynamic heating analysis includes free convection from the radiator surface during pre-launch operation and when the shuttle vehicle is moving with a relatively low velocity. The expression for the free convection Nusselt number is a function of the Grashof Prandtl product where the Grashof number N_{Gr} is given by

$$N_{Gr} = g\beta \left(\frac{\rho}{\mu}\right)^2 y^3 (T_w - T_\infty)$$

where g represents the acceleration of gravity, ρ , μ and T_∞ are the atmospheric density, dynamic viscosity and temperature, respectively and T_w denotes the radiator surface temperature. The symbol y denotes the overall dimension of the radiator panel in the direction parallel to the acceleration of gravity. Since the atmosphere is assumed to be an ideal gas, the

* pp. 296 and 313

coefficient of thermal expansion β is simply the reciprocal of the average absolute temperature of the air

$$\beta = \frac{2}{T_w + T_\infty} \quad .$$

The free convection Nusselt numbers N_{Nu_f} and their applicable ranges of Grashof Prandtl product used for this analysis are

$$N_{Nu_f} = 1.585 (N_{Gr} N_{Pr})^{0.195} \quad (10^{-1} < N_{Gr} N_{Pr} < 10^4) \quad (7.9a)$$

$$N_{Nu_f} = 0.590 (N_{Gr} N_{Pr})^{0.250} \quad (10^4 \leq N_{Gr} N_{Pr} \leq 10^9) \quad (7.9b)$$

$$N_{Nu_f} = 0.130 (N_{Gr} N_{Pr})^{0.333} \quad (N_{Gr} N_{Pr} > 10^9) \quad . \quad (7.9c)$$

The values for the free convection Nusselt number given in Eq. 7.9 were multiplied by the ratio (x/y) and then added to the forced convection Nusselt number to obtain a value that accounts for combined free and forced convection in the low speed regime.

Equations 7.1 through 7.8 combined with the appropriate Nusselt number relationship from Table 1 for forced convection and Eq. 7.9 for free convection are sufficient to determine the convective heat flux into the radiator surface which is given by

$$q''_{aero} = h_i (i_\infty - i_{aw}) \quad . \quad (7.10)$$

The convective flux may be normalized by dividing by the heat flux σT_o^4 or

$$\dot{q}_{\text{aero}} = \frac{h_i (i_{\infty} - i_{\text{aw}})}{\sigma T_o^4} \quad (7.11)$$

where T_o is the fluid temperature at the inlet plane to the flow channel. The normalized convective heat flux given by Eq. 7.11 is used in the energy equation for both the fin (Eq. 2.18) and the meteoroid protection layer (Eq. 5.5).

C. DESIGN PARAMETERS

Certain design parameters are necessary for the design specification, for the selection of the optimum radiator system and even the system definition as required for the heat transfer analysis. In the following are discussed, in that order, the prediction of the meteoroid protection layer thickness, the system weight and a collection of nondimensional groups which define the radiator system, the operational conditions, and the performance characteristics.

8. Meteoroid Protection Thickness

In this section an engineering equation is developed to predict the thickness of a meteoroid protection layer required to cover all radiator surfaces that might be damaged by the impact of a meteoroid. Several assumptions have been made during the derivation. They are:

1. The meteoroid particle is spherical.
2. The meteoroid flux is isotropic.
3. Poissons distribution law describes the probability of an impact of a meteoroid.

It should be mentioned that any equation used to predict meteoroid protection thickness is only as accurate as the experimental data used in that equation. Even though much information has been published in recent years concerning protection theories, there is still considerable question as to the density, velocity and mass distribution of meteoroid particles in outer space. In addition to these uncertainties, two basic models for penetration theory have been proposed within the last decade and there appears to be no close agreement between the two. Experimental verification of either model has been hampered by the fact that particle velocities used in experimental tests have only recently approached the meteoroid velocity range. In short, an extremely reliable theory for the prediction of protection layer thickness does not presently exist.

Structural materials that can be used in this study as a protection layer are copper, aluminum and beryllium. While both copper and aluminum were selected primarily as fin and tube materials due to their superior heat transfer characteristics, beryllium was chosen for its protection capabilities. The penetration theory predicts a protection layer thickness that decreases as the modulus of elasticity increases. Therefore, beryllium becomes an attractive protection material due to its high modulus of elasticity and its relatively low density. In fact studies (Refs. 13 and 14) have shown that beryllium can significantly reduce protection layer weight.

The basic equation (Ref. 15) for the depth of penetration of a meteoroid particle into a target of infinite depth is

$$P_{\infty} = \gamma d \left(\frac{\rho_p}{\rho_t} \right)^{\phi} \left(\frac{\bar{V}}{\bar{c}} \right)^{\theta} \quad (8.1)$$

where

γ empirical constant generally accepted to be in the range of 1.5 to 2.5

ρ_p density of the meteoroid particle

ρ_t density of the target material

\bar{V} velocity of the meteoroid particle

\bar{c} velocity of sound in the target material

d diameter of the meteoroid particle

ϕ constant between 1/3 and 2/3

θ constant between 1/3 and 2/3

The ratio of the meteoroid velocity and the velocity of sound in the target represents a target Mach number. The velocity of sound in the target can be expressed in terms of the modulus of elasticity

$$\bar{c} = \sqrt{E_t g_c / \rho_t} \quad (8.2)$$

where

E_t modulus of elasticity of the target material

g_c proportionality constant relating mass units to force units

ρ_t target density

If the meteoroid particle is assumed to be spherical, the diameter may be written in terms of its mass

$$d = \left(\frac{6M_p}{\pi \rho_p} \right)^{1/3} \quad (8.3)$$

where

M_p meteoroid mass

ρ_p meteoroid density

The probability that an exposed surface will be struck by a meteoroid during a period of time can only be determined after the distribution of meteoroids of a given mass is known. This information is usually given in the form of an equation such as

$$F = \alpha M_p^{-\beta} \quad (8.4)$$

where

F cumulative number of impacts of particles with mass M or larger per unit area per unit time

M_p mass of the meteoroid particle.

The symbols α and β represent experimentally determined constants. Published (Ref. 16) values of α and β vary over a considerable range, but they lie within the limiting values,

$$\begin{aligned} 1.3 \times 10^{-15} < \alpha < 2.54 \times 10^{-9} & \quad [\text{ft}^2 \text{ day gm}^{-\beta}]^{-1} \\ 1.11 < \beta < 1.34 & \quad [\text{Dimensionless}] \end{aligned}$$

The cumulative number of impacts on a surface with a vulnerable area of A during a mission time of τ by a meteoroid of mass M_p or larger is then

$$N = FA\tau = A\tau \alpha M_p^{-\beta}$$

It is generally assumed (Ref. 17) that meteoroids are randomly distributed in outer space and that each collision can be described by Poisson's probability law. From the Poisson distribution function, the probability of zero events occurring P_o when the average number of events is N is

$$P_o = e^{-N}$$

or

$$\ln P_o = -N$$

Substituting the value for N gives the probability that no meteoroid of mass M or larger will impact on the surface of area A during time τ of

$$\ln P_o = A\tau\alpha M_p^{-\beta}$$

or

$$M_p = \frac{\alpha A\tau}{-\ln P_o}^{1/\beta} \quad (8.5)$$

To account for the fact that all meteoroids do not strike the protection layer normally, the meteoroid velocity \bar{V} may be replaced by a critical velocity \bar{V}_c where

$$\bar{V}_c = \bar{V}(\cos \lambda)^n \quad (8.6)$$

λ angle between the direction of \bar{V} and the normal to the protection surface

n an experimentally determined constant.

If n is selected to be unity the damage to the protection layer caused by an oblique collision is based on the meteoroid's normal component of velocity. A more conservative approach would be to set $n = 0$ in which case all particles are considered to impact normally.

If the meteoroid flux is assumed to be isotropic the angle dependence may be replaced by

$$(\cos \lambda)^n = \left(\frac{2}{3n\theta\beta+2} \right)^{1/3\beta} \quad (8.7)$$

Finally account must be taken for the fact that the meteoroid will not impact on an infinite target, but one with a finite thickness. As a result even though the meteoroid may not penetrate the protection layer, spalling may damage the radiator panel. To account for spalling the thickness of meteoroid protection t used should be larger than the predicted penetration into an infinite target or

$$t = aP_{\infty} \quad (8.8)$$

Accepted values of a lie between 1.5 and 2.0.

Equations 8.1 through 8.7 may now be substituted into Eq. 8.8 to give an expression for the meteoroid protection layer thickness. The result is

$$t = a\gamma \left(\frac{6}{\pi} \right)^{1/3} \left(\frac{\alpha A_T}{-\ln P_{\alpha}} \right)^{1/3\beta} \rho_P^{-1/3} \left(\frac{\rho_P}{\rho_t} \right)^{\phi} \left(\frac{V}{12(E_t g_c / \rho_t)^{1/2}} \right)^{\theta} \left(\frac{2}{3n\theta\beta+2} \right)^{1/3\beta} \quad (8.9)$$

where

- t - thickness of protection layer (inches)
- a - experimental constant (dimensionless)
- γ - experimental constant (dimensionless)
- α - experimental constant that relates meteoroid flux to mass
($\text{gm}/(\text{day ft}^2)$)
- β - experimental constant that relates meteoroid flux to mass
(dimensionless)

- A - vulnerable area requiring protection (ft^2)
 τ - mission time (days)
 P_o - probability of no damage caused by impact of meteoroid (dimensionless)
 ρ_p - density of meteoroid particle (gm/cm^3)
 ρ_t - density of protection layer (lb_m/ft^3)
 \bar{V} - velocity of meteoroid (ft/sec)
 E_t - modulus of elasticity of protection material (lb_f/in^2)
 g - $32.174 \text{ lb}_m \text{ ft} / \text{lb}_f \text{ sec}^2$
 θ - experimental constant (dimensionless)
 ϕ - experimental constant (dimensionless)
 n - experimental constant that describes penetration depth as a function of angle of incident (dimensionless).

Selection of Values for Experimental Constants

Values for the experimental constant ρ , β , ρ_p and \bar{V} used in Eq. 8.9 were selected from the Manned Spacecraft Center publication for meteoroid environment criterion (Ref. 18).

The values for α and β for meteoroids having a mass between 1 gm 10^{-6} gm used in Eq. 8.4 are

$$\alpha = 1.888 \times 10^{-10} \text{ gm}^\beta / (\text{ft}^2 \text{ day}) \quad (8.10)$$

$$\beta = 1.213 \quad (8.11)$$

The average meteoroid density is

$$\rho_p = 0.5 \text{ gm}/\text{cm}^3 \quad (8.12)$$

and the average meteoroid velocity is

$$\bar{V} = 20 \text{ km/sec.}$$

(8.13)

Values chosen for the remaining constants appearing in Eq. 8.9 are summarized in Table 2. Values of these constants are also listed in the table that will yield optimistic (minimum) and pessimistic (maximum) thicknesses for the meteoroid protection layer.

	Recommended Value	Pessimistic Value	Optimistic Value
a	1.75	2.0	1.5
γ	1.50	2.5	1.5
ϕ	1/2	1/3	2/3
θ	2/3	2/3	1/3
n	1.0	0	1.0

TABLE 2. Empirical Constants for Meteoroid Protection Layer Thickness

The following is an analysis of the sensitivity that the meteoroid protection layer thickness has to the uncertainty in the values of the five parameters listed in Table 2. This information will enable the user to judge his selection of these constants from within the recommended ranges.

An expression for the error in the meteoroid protection thickness may be obtained by taking the logarithm of Eq. 8.9 followed by differentiating the resulting equation. This process yields the equation

$$\frac{dt}{t} = \frac{da}{a} + \frac{d\gamma}{\gamma} + \phi \left(\frac{\rho_p}{\rho_t} \right) \frac{d\phi}{\phi} + \left[\theta \ln \left(\frac{V}{c} \right) - \frac{n\theta}{3n\theta\beta+2} \right] \frac{d\theta}{\theta} - \left[\frac{n\theta}{3n\theta\beta+2} \right] \frac{dn}{n} \quad (8.14)$$

If the symbol E_a is selected to represent the relative error in the meteoroid

protection thickness resulting from a relative uncertainty in the value for the parameter a , then it is evident from Eq. 8.14 that

$$E_a = \frac{dt/t}{da/a} = 1.0$$

when all other parameters are held constant. Similarly the error caused by an uncertainty in the value of γ will be

$$E_\gamma = \frac{dt/t}{d\gamma/\gamma} = 1.0$$

When the value for θ is taken to be the recommended value of $2/3$ and β is set equal to the value fixed by MSC's environmental model (Eq. 8.11), the resulting error in the meteoroid protection layer thickness due to an uncertainty in the value for n is

$$E_n = \frac{dt/t}{dn/n} = - \left(\frac{n\theta}{3n\theta\beta+2} \right) = - 0.15$$

The magnitude of the error for the final two parameters ϕ and θ are a function of the material selected for the protection layer. In order to give an indication of the range of errors that can be expected for various protection materials, the errors were calculated for the three structural materials that were selected in the program: aluminum, beryllium and copper. If the meteoroid particle density is assumed to be fixed at the value recommended by the MSC environmental model (Eq. 8.12), then an uncertainty in the value of ϕ from the recommended value of $1/2$ would cause an error in the protection thickness of

$$E_\phi = \frac{dt/t}{d\phi/\phi} = \phi \ln \left(\frac{\rho_p}{\rho_t} \right)$$

which for each of the three structural materials results in the following errors

$$\begin{aligned}
 E_{\phi} &= -0.85 && \text{aluminum} \\
 E_{\phi} &= -0.65 && \text{beryllium} \\
 E_{\phi} &= -1.44 && \text{copper.}
 \end{aligned}$$

The high density and low modulus of elasticity of copper makes its protection characteristics rather undesirable. For this reason the error of 1.44 indicated for copper probably will never be experienced in practice, and this value should be considered as a limiting case.

An uncertainty in the value of θ from the recommended value of $2/3$ would cause an error in the protection layer thickness equal to

$$E_{\theta} = \frac{dt/t}{d\theta/\theta} = \left[\theta \ln \left(\frac{\bar{V}}{c} \right) - \frac{n\theta}{3n\theta\beta+2} \right]$$

which for each of the three structural materials is:

$$\begin{aligned}
 E_{\theta} &= 0.77 && \text{aluminum} \\
 E_{\theta} &= 0.20 && \text{beryllium} \\
 E_{\theta} &= 1.01 && \text{copper.}
 \end{aligned}$$

The errors calculated in the analysis are summarized in Table 3.

TABLE 3. Ratio of Relative Error in Thickness to Relative Uncertainty in Empirical Constants

Protection Material	Aluminum	Beryllium	Copper
Parameter			
a	1.0	1.0	1.0
γ	1.0	1.0	1.0
ϕ	-0.85	-0.65	-1.44
θ	0.77	0.20	1.01
n	-0.15	-0.15	-0.15

If the error values for copper are excluded, the protection thickness is most sensitive to variations in the parameters a and γ and least sensitive to variations in the parameter n . Even though the protection thickness is least sensitive to the selection of n , it should be noted that the 100% variation between the optimistic and pessimistic value of n is the largest of all of the parameters. Also it should be noted that the signs on the values in Table 3 indicate that an increase in the parameters a , γ and θ result in an increase in the protection layer thickness, while an increase in the values for ϕ and n result in a decrease in the protection layer thickness. This fact can be verified by the choice of the values of each of the parameters listed in Table 2. The values labeled as those which will produce a pessimistic value for the protection thickness are maximum values for a , γ and θ and minimum values for ϕ and n .

To further evaluate the effect the meteoroid protection thickness has on the performance of the fin system, the temperature of the coolant fluid at the exit plane of the flow channel was evaluated first under the "pessimistic" conditions for the meteoroid protection layer, second for the "recommended" conditions and finally for the "optimistic" conditions. The results of these computer runs are shown below.

Case	Protection Layer Thickness-Inches	Normalized Outlet Fluid Temperature T/T_o
Pessimistic	0.377	0.8855
Recommended	0.063	0.8922
Optimistic	0.020	0.8932

Even though the thickness of the meteoroid protection layer varies by nearly a factor of 20, the resulting error in the enthalpy drop is only

$$\frac{0.8932 - 0.8855}{1 - 0.8922} \cdot 100\% = 7.15\%$$

9. The Mass of the System

The system mass is computed, firstly as a convenience for the user and secondly for the purpose of the planned system optimization. The system mass includes

- (i) the mass of the fluid in all tubes

$$M_c = n_t \frac{d^2 \pi}{4} \int_0^L \rho_c dz = n_t \rho_{c,o} \frac{d^2 \pi}{4} L \int_0^1 v d\zeta \quad (9.1)$$

- (ii) the mass of the fins

$$M_f = n_t H L \rho_f (s_r + s_t) \quad (9.2)$$

- (iii) the mass of all tubes

$$M_w = n_t s_w L \cdot \pi (d + s_w) \rho_w \quad (9.3)$$

and

- (iv) the mass of the protection layer

$$M_m = n_t s_m L \rho_m [\pi(d + s_w + s_m) - s_r] \quad (9.4)$$

but it does not include the thermal coating nor the mass of the manifold and the fluid in the manifold. In Eqs. 9.1 through 4 represent

- n_t the number of tubes
- d the tube diameter
- ρ the density
- L the tube length
- H the fin height, distance between fin root and fin tip
- s the thickness

while the subscripts designate ρ and s as follows

- c coolant fluid
- f fin

m meteoroid protection layer
r fin root
t fin tip
w tube wall
o inlet condition.

The integral in Eq. 9.1 is time-dependent and evaluated at the initial conditions.

10. Nondimensional System Parameters

The governing equations in the preceding radiator system analysis are developed in non-dimensional form for the purpose of (i) reducing the number of parameters, (ii) evolving the set of relevant parameters, and (iii) presenting the results in a general form which is applicable to groups of systems rather than an individual system. A summary of parameters is presented here for the detailed analysis discussed in the preceding chapters.

The transient flow field in the coolant channel and the temperature field over the fin can be represented as functions of:

a) the independent variables

$$\text{time} \quad \tau = \frac{t w_o}{L} \quad (10.1)$$

$$\text{axial coordinate} \quad \zeta = \frac{z}{L} \quad (10.2)$$

$$\text{radial coordinate} \quad \eta = \frac{2r}{d} \quad (10.3)$$

$$\begin{array}{l} \text{transverse coordinate} \\ \text{normal to the channel} \\ \text{axis} \end{array} \quad \xi = \frac{x}{H}$$

b) the dependent system variables

$$\text{fin temperature} \quad \theta_f (\xi, \zeta; \tau) = \frac{T_f}{T_o} \quad (10.4)$$

$$\text{channel temperature} \quad \theta_w (\eta, \zeta; \tau) = \frac{T_w}{T_o} \quad (10.5)$$

$$\begin{array}{l} \text{meteoroid protection} \\ \text{layer temperature} \end{array} \quad \theta_m (\eta, \zeta; \tau) = \frac{T_m}{T_o} \quad (10.6)$$

$$\text{coolant fluid temperature} \quad \theta_c (\zeta; \tau) = \frac{T_c}{T_o} \quad (10.7)$$

$$\text{coolant fluid pressure} \quad \pi(\zeta, \tau) = \frac{p}{p_o} \quad (10.8)$$

$$\text{coolant fluid velocity} \quad \omega(\zeta; \tau) = \frac{w}{w_o} \quad (10.9)$$

The solution to the problem will depend on the geometry of the system, the material properties and the definition of operational conditions. There was no attempt made to establish similitude with respect to the material properties because the scaling laws would either be too restrictive to allow for general property variations or too complex (for instance, the concept of corresponding states for gases). Consequently, the ϕ -parameters defined in Eqs. 3.27 through 3.30, in Eq. 4.4 and in Eqs. 5.1, 2 and 6 are omitted from this summary; they constitute temperature and pressure variation of properties. This leaves the following list of parameters, in addition to n , the number of tubes:

c) the geometric parameters

$$\text{fin height-to-length ratio} \quad \bar{H} = \frac{H}{L} \quad (10.10)$$

$$\text{fin profile slope} \quad c = \frac{s_r - s_t}{2H} \quad (10.11)$$

$$\text{fin root thickness} \quad \bar{s}_r = \frac{s_r}{H} \quad (10.12)$$

$$\text{tube diameter-to-length ratio} \quad \delta = \frac{d}{L} \quad (10.13)$$

$$\text{channel wall thickness} \quad \bar{s}_w = \frac{2s_w}{d} \quad (10.14)$$

$$\text{protection layer thickness} \quad \bar{s}_m = \frac{2s_m}{d} \quad (10.15)$$

d) the operational parameters

coolant flow Reynolds number $N_{Re} = \frac{dw_o}{\nu_o}$ (10.16)

Prandtl number
(representing coolant selection) $N_{Pr} = \left(\frac{\mu_c p}{k_{c_o}} \right)$ (10.17)

inlet pressure heat $F_p = \left(\frac{p}{\rho w} \right)_o$ (10.18)

compressibility $\bar{Q}_o = \frac{\pi n \rho d_c^2 p}{4 \sigma T_o^3}$ (10.19)

inlet coolant power flux $F_z = \left(\frac{p}{\rho c_p T} \right)_o$ (10.20)

where n is the number of tubes

incident radiant heat flux $\bar{Q}_{rad} = \frac{\alpha_o q''}{\epsilon_o \sigma T_o^4}$ (10.21)

meteoroid velocity $M_m = \frac{v_m}{c_m}$ (10.22)

protection layer density
(representing selection of
protection layer material) $\phi_\rho = \frac{\rho_{mt}}{\rho_m}$ (10.23)

where ρ_{mt} is the density of the meteoroids.

Similarity for ascent and reentry operations is difficult to establish unless one restricts oneself to similar velocity-altitude profiles which can be represented by the

$$\text{max. Mach number} \quad M_{\text{max}} = (v/c)_{\text{max}} \quad (10.24)$$

and its corresponding (through same altitude)

$$\text{Reynolds number} \quad (N_{\text{Re}})_{\infty} = \frac{\rho_{\infty} v L}{\mu_{\infty}} \quad (10.25)$$

$$\text{Prandtl number} \quad (N_{\text{Pr}})_{\infty} = \frac{\mu_{\infty} c_p}{k_{\infty}} \quad (10.26)$$

$$\begin{aligned} \text{Grashof number} \\ \text{(before launch)} \end{aligned} \quad N_{\text{Gr}} = \frac{g L^3 \beta \Delta T}{\nu^2}$$

This completes the list of non-dimensional groups resulting from the detailed analysis.

D. Extension of the Analysis to Related Systems

11. Non-Symmetrical Heating

The purpose of this section is to describe a segment of the program which is intended to extend the application of the radiator simulation to non-symmetrical flow conditions in adjacent tubes. This program will also account for, in an approximate manner, a radiator panel which does not lie in one plane, or a panel which consists of U-shaped tubes.

In the original simulation of the radiator system, it was assumed that the coolant fluid entering all tubes has identical properties. As a result, the operating conditions and heat loss is determined for a single fin segment between two adjacent tubes and these conditions are assumed to exist for all other fin segments. In reality, this situation will exist only when all tubes are fed by a relatively large manifold whose flow rate and temperature entering each tube is unaffected by the removal of coolant fluid at each succeeding channel entrance.

The actual flow situation could possibly be far from the idealized case which was assumed to exist because it leads to a simplified mathematical model. A manifold of realistic size will lose heat by radiation from its surface and by conduction into the fin elements so that the coolant fluid entering individual flow channels will experience a difference in temperature. Furthermore, unless the manifold is carefully reduced in size after passing each tube inlet, neighboring tubes will not receive identical mass flow rates. Also, two adjacent tubes may be fed by the outlet flow from separate fuel cells which may be operating under different load conditions causing non-symmetrical conditions in adjacent fin panels. In short, a situation where two tubes receive fluid at different inlet conditions is to be expected.

For the purpose of extending the application of the main program to situations discussed above, a series of program units were written and integrated into the main program unit. These programs calculate the location of the adiabatic plane on a fin which separates two tubes having different inlet flow rates and temperatures. The fin height to the adiabatic plane is then used as input to the main program. The calculations with the main program remain unaffected since the mathematical model requires only that the input value given for the fin height is that distance from the tube to the location of the adiabatic plane.

The analysis considered here may also account for, in an approximate fashion, fin elements that do not lie in one plane. If the radiator panel is wrapped around a cylindrical structural component (Fig. 3a) adjacent fin panels will be under the influence of different effective sink temperatures. In this analysis the assumption is made that the regular breaks in the radiator panel occur at the adiabatic plane between the tubes rather than at the tubes themselves (Fig. 3b) which is probably the most reasonable location. If the cylindrical panel is composed of numerous tubes and the curvature is gradual, the difference between the two cases should be negligible.

The program accepts two sink temperatures supplied by the user or it calculates the correct sink temperature from the MRI incident flux data. The analysis of this section assumes steady state, one-dimensional conduction in an untapered fin. The fin may radiate from one or both sides when the fin panel is in one plane. When the panel is curved the fin is assumed to radiate only from the convexed surface. Fluid and fin properties are assumed constant at the inlet conditions. No convection from the fin surface and no radiant blocking of the tubes is considered. The only incident fluxes considered in this analysis are those accounted for in the MRI program; i.e. solar, earth and earth albedo.

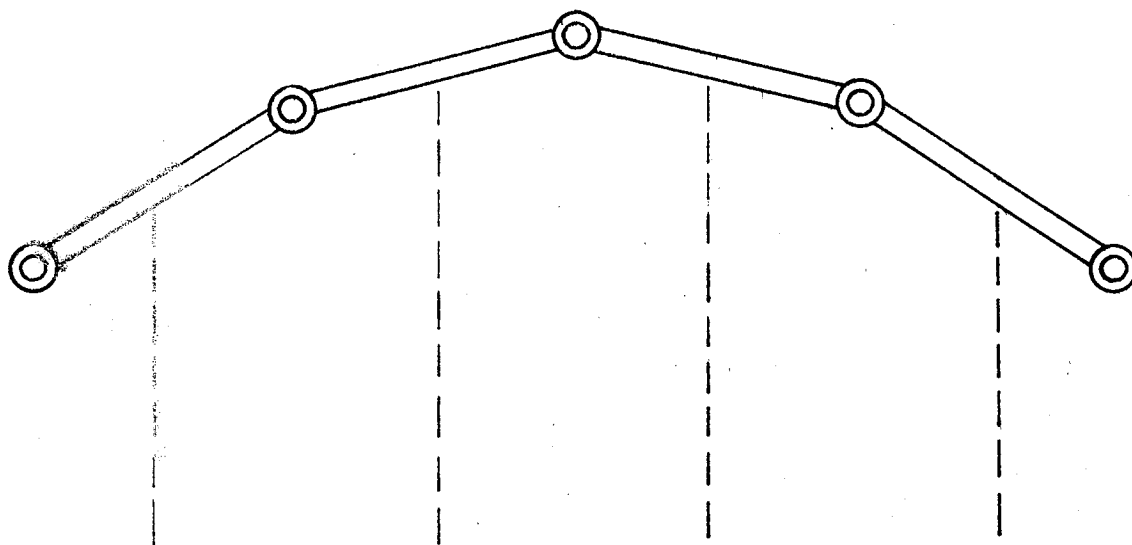
The user is cautioned that the analysis considered here assumes a one dimensional model and as such represents an approximation to the actual operating conditions of the non-symmetrical radiator. This caution is particularly applicable to the panel that contains U-shaped tubes, because this situation can lead to a highly two dimensional condition.

The analysis considers the i th tube of a radiator panel of thickness t , inside tube diameter d , tube length L_i and distance between tubes of $2H$ (Fig. 4). The energy transferred from the i th tube carrying fluid with an inlet temperature of T_{oi} , specific heat of c_p and mass flow rate of \dot{m}_i is

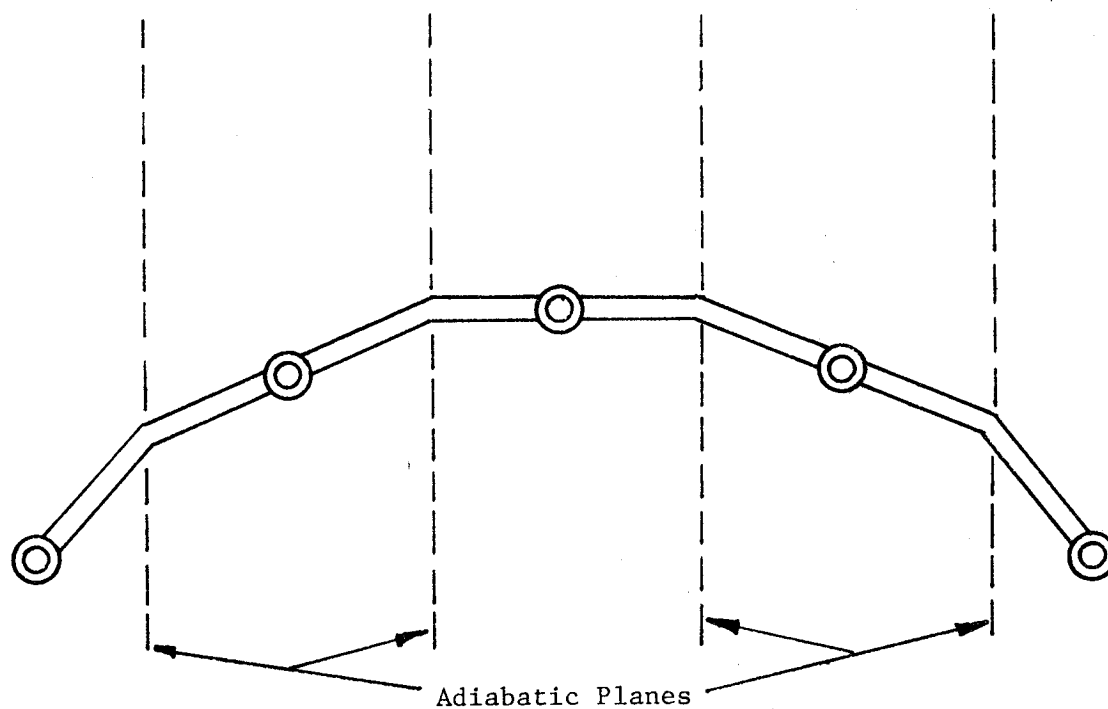
$$q_i = \dot{m}_i c_p (T_{oi} - T_{bi}) (1 - e^{-U_i}) \quad (11.1)$$

The quantity U_i is given by

$$U_i = \frac{\pi d h_i L_i}{\dot{m}_i c_p} \quad (11.2)$$



(a) Fin Segments Inclined At Tube Locations-
Geometry For Physical Model.



(b) Fin Segments Inclined At Location Of Adiabatic
Planes=Geometry For Mathematical Model

Fig. 3

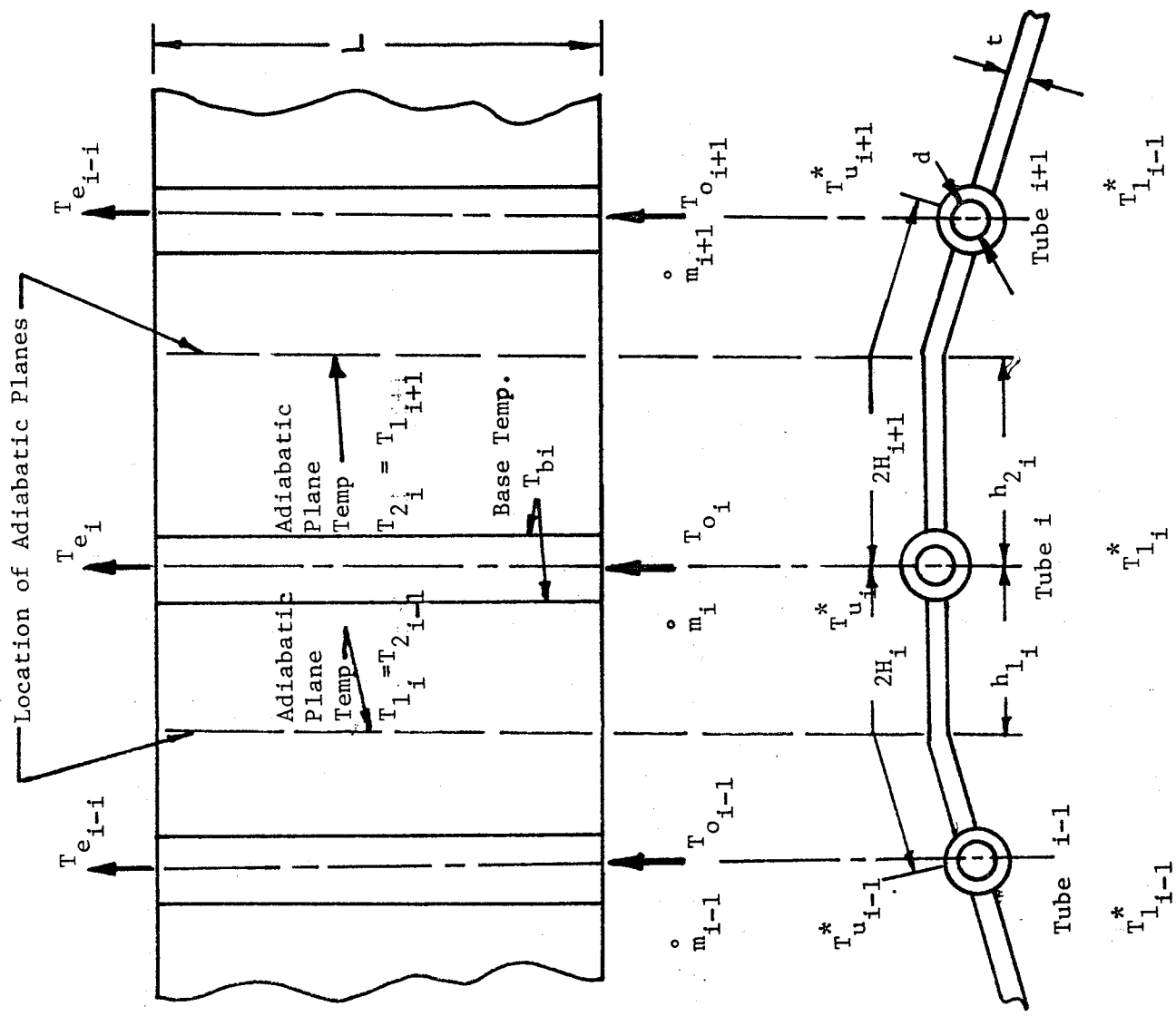


Figure 4. Fin Geometry for Non-Symmetrical Panel

where h_i is the convective heat transfer coefficient of the fluid in the tube and T_{b_i} is the average fluid bulk temperature (also assumed to be the fin root temperature.)

The convective heat transfer coefficient h_i in Eq. 11.1 is evaluated from the Nusselt number which is related to the Reynold and Prandtl numbers by the expressions

$$N_{Nu} = 5 + 0.025 (N_{Re} N_{Pr})^{0.8} \quad \text{for} \quad \begin{cases} N_{Pr} < 0.1 \\ N_{Re} > 2300 \end{cases} \quad (11.3 \text{ a})$$

$$N_{Nu} = 0.023 (N_{Re}^{0.8} N_{Pr}^{0.3}) \quad \text{for} \quad \begin{cases} N_{Pr} > 0.1 \\ N_{Re} > 2300 \end{cases} \quad (11.3 \text{ b})$$

$$N_{Nu} = 3.65 + \frac{0.0668 [N_{Re} N_{Pr} (d/L)]}{1 + 0.045 [N_{Re} N_{Pr} (d/L)]^{2/3}} \quad N_{Re} \leq 2300 \quad (11.3 \text{ c})$$

The heat rejected from the coolant fluid given in Eq. 11.1 under the assumption of steady state and one-dimensional heat transfer can be determined by calculating the net radiant loss from the fin surfaces. If one side of the i th fin surface is radiating to an environment with an effective sink temperature of T_i^* then

$$\begin{aligned} q_i = & \eta_{1i} \epsilon h_{1i} L_i \sigma (T_{bi}^4 - T_i^{*4}) \\ & + \eta_{2i} \epsilon h_{2i} L_i \sigma (T_{bi}^4 - T_i^{*4}) \end{aligned} \quad (11.4)$$

where η_{1i} and η_{2i} are the fin effectivenesses for the fin attached to the left and right of the i th tube, respectively, and h_{1i} and h_{2i} are the distances between the tube centerline and the adiabatic plane for the fin attached to the left and right of the i th tube.

When the fin radiates from both sides, the effective sink temperature will be different for both sides and the net radiative flux will be

$$q_i = 2\eta_{1i} \epsilon h_{1i} L_i \sigma (T_{bi}^4 - T_i^{*4}) + 2\eta_{2i} \epsilon h_{2i} L_i \sigma (T_{bi}^4 - T_i^{*4}) \quad (11.5)$$

where the sink temperature T_i^{*4} becomes

$$T_i^* = \left(\frac{T_{ui}^{*4} + T_{li}^{*4}}{2} \right)^{1/4} \quad (11.6)$$

The subscripts u and l in Eq. 11.6 denote the sink temperatures for the upper and lower surfaces of the fin respectively.

The fin effectiveness in Eqs. 11.4 and 11.5 is a function of the conductance parameter N_c and the ratio of the sink temperature to base temperature T^*/T_b or for the ith tube

$$\eta_{1i} = \eta(N_{cli}, T_i^*/T_{bi}) \quad (11.7)$$

$$\eta_{2i} = \eta(N_{c2i}, T_i^*/T_{bi}) \quad (11.8)$$

The conductance parameter is defined as

$$N_{cli} = \frac{\epsilon \sigma T_{bi}^3 h_{1i}^2}{Kt} \quad \text{and} \quad (11.9)$$

$$N_{c2i} = \frac{\epsilon \sigma T_{bi}^3 h_{2i}^2}{Kt} \quad (11.10)$$

where K is the thermal conductivity of the fin material.

In addition to having a continuous slope in the fin temperature profile at the adiabatic plane, the fin temperature must also be continuous at this plane. For a one dimensional fin the temperature at the adiabatic plane T is a function of the conductance parameter and the ratio of sink temperature to base or

$$T = T(N_c, T^*/T_b) \quad (11.11)$$

As the program searches for the position of the adiabatic plane, the distances between the tube centerline and adiabatic plane is systematically varied until the fin tip temperatures given by Eq. 11.11 for two adjacent tubes are equal. As an example, consider the i th and $i+1$ tube. Using the subscript 1 to denote a fin segment attached to the left of a tube and the subscript 2 to denote the fin segment attached to the right of a tube, the tip temperature profile will be continuous when

$$T_{2i} - T_{1i+1} \longrightarrow 0$$

If the difference in these two tip temperatures is denoted by δ_i , then δ_i becomes a function of T_{2i} and T_{1i+1} . By combining Eq. 11.11 and the definition of N_c these two tip temperatures may be specified by the functional relationships

$$T_{2i} = f(T_{bi}, h_{2i}) \quad \text{and} \quad (11.12)$$

$$T_{1i+1} = f(T_{bi+1}, h_{1i+1}) \quad (11.13)$$

The fin base temperatures of the i th and $i+1$ tube can be determined by Eqs. 11.7 through 11.9 or written functionally

$$T_{bi} = f(h_{1i}, h_{2i}) \quad \text{and} \quad (11.14)$$

$$T_{bi+1} = f(h_{1i+1}, h_{2i+1}) \quad (11.15)$$

If Eqs. 11.12 through 11.15 are combined, the difference in the two temperatures δ_i may be expressed as

$$\delta_i = \delta_i(h_{1i}, h_{2i}, h_{1i+1}, h_{2i+1}) \quad (11.16)$$

But from the geometry of the radiator system

$$h_{1i} = 2H_i - h_{2i-1} \quad \text{and} \quad (11.17)$$

$$h_{1i+1} = 2H_{i+1} - h_{2i} \quad (11.18)$$

where $2H_i$ and $2H_{i+1}$ is the distance between the centerlines of tubes $i-1$ and i and tubes i and $i+1$, respectively.

By combining Eqs. 11.17 and 11.18 with Eq. 11.16, the final functional relationship for the difference in the fin temperatures at the adiabatic plane is given by

$$\delta_i = \delta_i(h_{2i-1}, h_{2i}, h_{2i+1}) \quad (11.19)$$

In other words δ_i can be expressed entirely in terms of the distance from tube centerline to the adiabatic plane for the tube under consideration plus the same distance for tubes on either side.

The approach to the solution for the location for all adiabatic planes is one which gives $\delta_i = 0$ for all i tubes. The program utilizes a Newton iteration to determine an appropriate change in i th adiabatic plane Δh_i . Written in matrix notation, the relationship between Δh_i and the difference in tip temperatures δ_i is

$$[\delta_i] = [P_{ij}][\Delta h_i] \quad (11.20)$$

where the elements of the matrix p_{ij} are given by

$$[P_{ij}] = \frac{\partial \delta_i}{\partial h_j} \quad (11.21)$$

and the elements of the vector Δh_i are given by

$$\Delta h_i = h_i^{k+1} - h_i^k \quad (11.22)$$

where k denotes the k th iteration used to find a set of adiabatic plane locations for all fin elements which result in $\delta_i = 0$ for all i tubes. A mathematical subroutine is used to invert the matrix $[p_{ij}]$ so that the values for all adiabatic planes may be calculated from

$$[\Delta h_i] = [p_{ij}]^{-1} [\delta_i] \quad (11.23)$$

Once the distance to all adiabatic planes have been determined for all tubes which lead to continuous tip temperatures and continuous, zero slopes at the fin tips, the net heat transfer q_i from each fin segment may be determined from Eqs. 11.5 through 11.10. The exit fluid temperature from each tube T_{e_i} may then be determined from

$$q_i = \dot{m} \text{ cp}(T_{e_i} - T_{o_i}) \quad (11.24)$$

Since the main program unit requires only a single distance between the tube centerline and the adiabatic plane, the two distances h_{1i} and h_{2i} must be averaged to yield a single value. The averaging process produces a value \bar{h}_i which results in the same heat transfer for the symmetrical fin. This single value for each tube is calculated by using equation (11.5) resulting in

$$\bar{h}_i = \frac{\eta_{1i} h_{1i} + \eta_{2i} h_{2i}}{\eta_{1i} + \eta_{2i}} \quad (11.25)$$

As previously defined, the subscripts 1 and 2 denote the two halves of the fin attached to both sides of the i th tube. Values for the fin effectiveness are evaluated from Eq. 11.7.

The program considers the case of the radiator panel with U-shaped tubes to be approximated by three sequential parallel tube sections.

The program first calculates the fin base temperature and the distance to the adiabatic plane for the first section of the three tube segments. The heat transferred from the fluid is then calculated from

Eq. 11.1. The outlet fluid temperature from the first tube T_e segment is then calculated from the expression

$$q = \dot{m} c_p (T_e - T_o)$$

The exit fluid temperature simply becomes the inlet fluid temperature to the second tube segment (the base of the U). The same process is repeated for the remaining two tube segments resulting in two more values for the distance to the adiabatic plane. The single value for the distance to the adiabatic plane necessary for entry to the main program unit is determined from an average weighted with respect to the length of each tube segment.

E. Property Fundamentals

The fundamental principles used to prepare the required thermo-physical properties for inclusion into the computer code are exhibited in this chapter while the specific details concerning the materials treated in this program phase are placed into the appendices.

The principles involved are those of macroscopic thermodynamics treated in most elementary texts. The approach of deriving analytic expressions for the required properties is not unique because the starting point is dictated by the availability of experimental data. The result, however, must be of the same form regardless of whether, for instance, the coolant fluid is gaseous or liquid.

The properties of the structural materials are the least problematic ones since they depend on the temperature at most; and the standard polynomial collocation methods are entirely sufficient. Care must be exercised, however, that the collocation imply continuous fourth derivatives for highest integration efficiency or, less desirable, at least continuous representation of the property itself which may exclude piecewise allocation of degrees higher than one.

What is said about the properties of structural materials holds in principle for the description of the atmosphere whose properties depend only on altitude. Even though the optical properties of the thermal coating depend, in general, on wave-length and temperature, the spectral dependence is integrated into the averaged ("gray") properties (see Eqs. 6.5 and 6), and the results are functions of one variable, the temperature. Consequently, there remains but the discussion of the coolant fluid properties which depend strictly on two state variables.

In macroscopic thermodynamics there are required two equations of state for the description of a substance, namely the thermal equation of state $f(\rho, p, T) = 0$ which relates any one of density ρ , pressure p and temperature T to the remaining two, and the caloric equation of state, perhaps in the form of $c_v^0 = f(T)$ where c_v^0 is the zero-pressure specific heat at constant volume. These two equations are sufficient to develop all

of the required thermodynamic functions, namely:

- (i) specific heat at constant pressure $c_p(\rho, T)$
- (ii) isobaric thermal expansion coefficient $\beta(\rho, T)$
- (iii) isothermal bulk modulus $\kappa(\rho, T)$
- (iv) enthalpy $h(\rho, T)$

These functions are discussed in Section 12.

The transport properties, namely the thermal conductivity $k(\rho, T)$ and the dynamic viscosity $\mu(\rho, T)$ are correlated on the basis of residuals as explained in Section 13. The properties of the atmosphere are dealt with in Section 14.

12. Thermodynamic Properties

The first step in developing thermodynamic properties is to secure a thermal equation of state

$$f(p, \rho, T) = 0 \quad (12.1)$$

For almost all pure gases and air, this equation can be found in the literature, either in the form suggested by Benedict-Webb-Rubin (virial expansion) or in that suggested by Beattie-Bridgeman. Both equations are explicit in p ,

$$p = p(\rho, T) \quad (12.2)$$

so that κ is immediately obtained from Eq. 11.2 by implicit differentiation

$$\kappa(\rho, T) = \frac{1}{\rho} \left(\frac{\partial \rho}{\partial p} \right)_T \quad (12.3)$$

which can be evaluated as $\kappa(p, T)$ after inversion of Eq. 11.2 into

$$\rho = \rho(p, T) \quad (12.4)$$

The inversion of Eq. 12.2 is facilitated by computing $(\partial p / \partial \rho)_T$ from Eq. 11.2 and subsequently applying the Newton-Raphson method along the specified isotherm with temperature T in Eq. 12.4

The isobaric thermal expansion coefficient

$$\beta = - \frac{1}{\rho} \left(\frac{\partial \rho}{\partial T} \right)_p$$

is also obtained by implicit differentiation of Eq. 12.2 while keeping the left-hand side constant.

After having collocated the zero-pressure specific heat at constant volume; that is, $c_v^0(T)$ by a power polynomial in T , one obtains first the specific heat at constant volume

$$c_v(\rho, T) = c_v^0(T) - T \int_0^p \left(\frac{\partial^2 p}{\partial T^2} \right)_\rho \frac{d\rho'}{(\rho')^2} \quad (12.5)$$

and then the specific heat at constant pressure

$$c_p(\rho, T) = c_v(\rho, T) + \frac{T\beta^2}{\rho\kappa} \quad (12.6)$$

The derivative in Eq. 12.5 is obtained from Eq. 12.2; and β and κ are both function of ρ or p and T .

Finally the enthalpy h is calculated from its definition

$$h(\rho, T) = \frac{p}{\rho} + u(\rho, T) \quad (12.7)$$

where the internal energy u may be obtained by two successive integrations, the first one along an isotherm (over ρ), and the second one along an isochore (over T):

$$u = u(\rho_0, T_0) + \int_{T_0}^T \int_{\rho_0}^{\rho} c_v(\rho', T') d\rho' dT' + \int_{\rho_0}^{\rho} \left[p - \frac{T\beta}{\kappa} \right] \frac{d\rho'}{(\rho')^2} \quad (12.8)$$

Liquids can be treated, in principle, as gases; except that the equation of state, Eq. 12.1, is rarely available. One may find, with little difficulty the zero-pressure isobaric expansion coefficient $\beta_0 = \beta(T)$, and then represent adequately the isothermal bulk modulus by

$$\kappa(p, T) = a(T) + b(T) p \quad (12.9)$$

Under any circumstances, one must satisfy

$$\left(\frac{\partial \beta}{\partial p} \right)_T + \left(\frac{\partial \kappa}{\partial T} \right)_p = 0 \quad (12.10)$$

which yields, from Eq. 12.9

$$\beta(p,T) = -a'p - \frac{b'}{2} p^2 + c \quad (12.11)$$

where primes indicate differentiation with respect to T , of the polynomials $a(T)$ and $b(T)$ in Eq. 12.9. Equations 12.9 and 11 yield for the density

$$\rho(p,T) = \rho(0,T_0)e^{[a(T)p + \frac{1}{2} b(T)p^2 - \int_{T_0}^T c(T')dT']} \quad (12.12)$$

The specific heats and the enthalpy are to be derived as for gases (see Eqs. 12.6 and 7). Other possibilities are to develop κ from the speed of sound and the ratio of specific heats; but the reader is warned not to imply $\kappa = 0$ or $c_p = c_v$, unless there is sufficient evidence to support these assumptions.

13. Transport Properties

While the thermal conductivity k and the dynamic viscosity μ of liquids may often times be adequately represented by functions of temperature T alone (facilitated by polynomial collocation), these same properties for gases depend on density as well. It is recognized that the difference, or residue

$$\psi_1(\rho) = k(\rho, T) - k^*(T) \quad (13.1)$$

between the thermal conductivity $k(\rho, T)$ and the low-pressure thermal conductivity $k^*(T)$ depends only on the density. Similarly, for the dynamic viscosity

$$\psi_2(\rho) = \mu(\rho, T) - \mu^*(T) . \quad (13.2)$$

Hence k and μ can be represented by the sum of two polynomials, one in ρ and the other in T . The residuals ψ_1 and ψ_2 are published for a number of gases or may be developed from property data (Ref. 19 for N_2 and He).

14. Atmospheric Properties

For the prediction of aerodynamic heat fluxes incident on the radiator system during ascent and reentry (see Section 7) the evaluation of the following atmospheric properties are required:

- Temperature
- Pressure
- Density
- Molecular Weight
- Speed of Sound
- Viscosity
- Thermal Conductivity
- Specific Heat at Constant Pressure
- Enthalpy

The model for these atmospheric properties is presented in two sections. The first covers altitudes from sea-level to 301,000 feet. Within this range the molecular weight is assumed to be constant and the temperature variation with altitude is a sequence of connected line segments. The second section of the model covers altitudes above 301,000 feet where the molecular weight decreases linearly with altitude. For this altitude range the approximate polynomial expressions for density and pressure suggested in Part 4 of Ref. 20 were used. Errors between the values given by the approximate expression and the 1962 Standard Model are less than 5% over the entire range of altitudes.

Atmospheric air is assumed to be an ideal gas for all altitudes. Therefore compressibility effects at low altitudes are neglected. The error in computed densities resulting from the ideal gas assumption may be as high as 0.05% for altitudes below 6 miles, but becomes less than 0.01% above 12 miles (Ref. 20). The air is also assumed to be in hydrostatic equilibrium.

All properties except geopotential altitude, specific heat and enthalpy are evaluated from expressions presented in Refs. 20 and 21. The expression for geopotential altitude was taken from Ref. 22, while specific heat and enthalpy data were taken from Ref. 23.

The model developed for the atmospheric properties is considered to be applied to altitudes up to 100 miles and to latitudes between 30 and 60°N. It is anticipated that atmospheric properties are not needed for altitudes exceeding 100 miles, because the convective heat flux from the fin system will be negligible at this altitude and above.

The properties for the earth's atmosphere are known with increased uncertainty as the altitude increases. In fact, the 1962 Standard Atmosphere (Ref. 21) consists of four regions as follows:

0 - 20 km	Standard
20 - 32 km	Proposed Standard
32 - 90 km	Tentative
90 - 700 km	Speculative

Any uncertainty in the atmospheric properties will naturally be reflected as an error in the convective heat flux on the shuttle vehicle. Fortunately during the ascent phase of the shuttle operation the convective flux from the radiator system is fairly small compared to the radiative flux by the time the shuttle has approached altitudes for which the atmospheric properties are considered to be "speculative"; on the other hand during re-entry, significant convective fluxes are known to exist at altitudes above 90 km. As a result every effort should be made to revise the existing atmospheric property model at high altitudes as new data become available.

The atmospheric model is based on several primary constants. The sea-level pressure, temperature, molecular weight, density and acceleration of gravity and the universal gas constant were assigned the fixed values of

$$\begin{aligned}
 P_o &= 2116.22 \text{ lbf/ft}^2 \\
 T_o &= 518.67 \text{ R} \\
 M_o &= 28.9644 \\
 \rho_o &= 0.07647 \text{ lbm/ft}^3 \\
 g_o &= 32.1741 \text{ ft/sec}^2 \\
 R^* &= 1545.31 \text{ ft lbf/lb mole R}
 \end{aligned}$$

Properties for Altitudes Less than 301,000 feet.

a. Geopotential Altitude - H

The state variables for air are expressed in terms of the single variable, the geopotential altitude

$$H = \int_0^Z \frac{g(z)}{g_0} dz =$$

$$Z - 1.573126 \times 10^{-7} Z^2 + 2.4656553 \times 10^{-14} Z^3$$

$$- 3.8667054 \times 10^{-21} Z^4 + 6.0621354 \times 10^{-28} Z^5$$

$$- 9.5013649 \times 10^{-35} Z^6 \quad (14.1)$$

where Z is the geometric altitude in meters, g_0 is the acceleration of gravity at sea-level and $g(Z)$ denotes the local acceleration of gravity. See Ref. 22 for details.

b. Temperature - T

The general expression of the temperature as a function of geopotential altitude is

$$T = T_b + L(H - H_b) \quad (14.2)$$

T_b and H_b are the endpoints of straight-line segments representing $T(H)$ and are listed, together with $L(H)$ in the following table.

c. Molecular Weight - M

The molecular weight is constant at a value of 28.9644.

d. Pressure - P

Within a region where the temperature varies linearly, the ideal equation of state and the hydrostatic yield the following expressions for

H_b (km)	L (K/km)	T_b (K)
0		288.15
	- 6.5	
11		216.65
	0.0	
20		216.65
	1.0	
32		228.65
	2.8	
47		270.65
	0.0	
52		270.65
	-2.0	
61		252.65
	-4.0	
79		180.65
	0.0	
90		180.65

TABLE 4. Lapse Rate and Base Temperatures for
Atmospheric Model

pressure:

$$\frac{P}{P_b} = \left[\frac{T_b}{T_b + \frac{g_o M_o}{R^* L} (H - H_b)} \right]^{1/2} \quad (L \neq 0) \quad (14.3)$$

$$\frac{P}{P_b} = \exp \left[- \frac{g_o M_o (H - H_b)}{R^* T_b} \right] \quad (L = 0) \quad (14.4)$$

$$\begin{aligned} \text{i.e. } 11 &\leq H \leq 20 \text{ km} \\ 47 &\leq H \leq 52 \text{ km} \\ 79 &\leq H \leq 90 \text{ km} \end{aligned}$$

The subscript "o" denotes a quantity evaluated at sea-level and the subscript "b" denotes a quantity evaluated at the base of one of the straight line segments of the atmospheric model.

c. Density - ρ

The density may be calculated from the ideal equation of state once the temperature and pressure have been evaluated.

$$\rho = \frac{MP}{R^* T} \quad (14.5)$$

f. Speed of Sound - c

The speed of sound was evaluated from the expression

$$c = \left[\gamma \frac{R^* T}{M} \right]^{1/2} \quad (14.6)$$

For altitudes less than 301,000 feet the ratio of specific heats is taken to have a fixed value of 1.40.

g. Viscosity - μ

The dynamic viscosity was evaluated from the expression

$$\mu = \frac{\beta T^{3/2}}{T + S} \quad (14.7)$$

where

$$\beta = 1.458 \times 10^{-6} \frac{\text{kg}}{\text{sec m(K)}^{1/2}}$$

and

$$S = 110.4 \text{ K}$$

h. Specific Heat at Constant Pressure c_p and Enthalpy i

Values for c_p and i between the temperatures of 100 R and 6400 R were taken from the standard Gas Tables (Ref. 23) and placed in the program in tabular form. A value of c_p and i at any temperature intermediate to a pair of tabular values was determined by an interpolation routine (see Section III 4).

Properties for Altitudes Greater than 301,000 Feet

a. Pressure - P

The pressure for altitudes between 301,000 and 528,000 feet is based on the polynomial approximation given in Part IV of Ref. 20. The pressure is written in terms of the sea-level pressure P_o in the form

$$P = P_o \left\{ \sum_{n=0}^{11} [A_n Z^n]^{-4} \right\} \quad (14.8)$$

where Z is the geometric altitude and values for A_n appear in Table 4.1 of Ref. 20.

b. Density - ρ

The density is written in terms of a similar polynomial

$$\rho = \rho_o \left\{ \sum_{n=0}^{11} [B_n Z^n]^{-4} \right\} \quad (14.9)$$

where values of B_n appear in Table 4.1 of Ref. 20.

c. Molecular Weight - M

The molecular weight is assumed to vary linearly with altitude Z (see Fig. I.2.7 in Ref. 21). The resulting expression for M is

$$M = 28.9644 - 0.030949 (Z - 90)$$

where Z is in km.

d. Temperature - T

The temperature is calculated from the values for pressure, density and molecular weight indicated above from the ideal equation of state

$$T = \frac{PM}{\rho R^*}$$

e. Speed of Sound - c

For altitudes greater than 301,000 feet the equation for the speed of sound is the same one as used for the lower altitudes, but the ratio of the specific heats is no longer assumed to be equal to 1.40. The ratio of the specific heats varies with the molecular weight according to the expression

$$\gamma = \frac{c_p}{c_p - R^*/M}$$

The remaining properties are calculated using identical expressions to those outlined for altitudes less than 301,000 feet.

III. NUMERICAL TECHNIQUES

1. Introduction

The analysis carried out in Chapter II lead, as far as the mathematical problem formulation is concerned, to three initial value problems and one matrix manipulation. The three initial-value problems are to establish

- (1) the initial conditions for the coolant fluid, defined by Eqs. 3.42 through 3.45,
- (ii) the dynamics of the coolant flow, defined by Eqs. 3.40 through 42 and 44,
- (iii) the temperature field throughout the system, defined by Eqs. 2.18 through 2.22 for the fin, Eqs. 3.39 and 46 for the coolant, Eqs. 4.6, 7 and 8 for the channel wall, Eqs. 4.7, 5.3 and 5 for the protection layer, or Eq. 4.11 replacing Eqs. 2.19, 4.6, 7 and 8 and 5.3 and 5 in the case where Eq. 4.9 is satisfied. These equations must be supplemented by the specification of the initial, non-dimensional temperature everywhere in the system.

Each initial-value problem is solved by a fourth-order Runge-Kutta-Simpson integration discussed in Section III-2.

The radiosity equation, Eq. 6.17 requires the matrix manipulation, namely either the solution of a system of linear algebraic equations, or a matrix inversion whenever the optical properties of the thermal control coating are considered temperature independent. Either task is accomplished by elementary row operations which transform, in a single process, the augmented coefficient matrix into a row-reduced echelon matrix. The reader is referred for this transformation to standard texts on linear algebra (Ref. 9).

Additional mathematical operations are programmed as subprograms which may be generally applied and which are discussed in Sections III-3 through III-7 in this order: an evaluation of polynomials in one variable, an Aitken interpolation, first and second differentiation, definite integration and integration with variable upper integration limit for functions of equally spaced arguments, and solution to system of linear algebraic equations.

2. The Runge-Kutta-Simpson Integration

Two types of initial-value problems are to be solved in this program. The first type includes Item (i) and (ii) mentioned in the Introduction, namely the fluid dynamics exclusive of the transient fluid temperature field, and involves ordinary, first-order differential equations, linear in the derivatives with respect to the axial distance z , that is Eqs. 3.42, 43 and 44. The equations are solved explicitly for these derivatives so as to take on the general form of Eq. 2.1:

$$\frac{dy_i}{dx} = f_i(x, y_1, y_2, \dots, y_n) \quad (2.1)$$

$$y_i(0) = a_i, \quad i = 1, 2, \dots, N \quad (2.2)$$

Equation 2.2 constitutes the appropriate initial conditions. The other type of initial-values problem, mentioned as item (iii) in the Introduction, involves partial differential equations which are linear and of the first order in the time-derivatives; moreover, all equations, Eqs. 2.18, 3.46, 4.8 and 5.3, are explicit in the time derivatives. Having subdivided the radiator system into intervals, equally spaced in each appropriate domain (fluid, wall, fin, etc.), and then written the different equations corresponding to each one of the resulting N interior nodal points, one may discretize the spatial derivatives occurring on the right-hand sides of the partial differential equations. The result is a set of ordinary differential equations, with time as the independent variable but of a form which is identical to Eq. 2.1. Equation 2.2 is given by the initial temperature distribution; a uniform temperature was chosen for the first start of the integration ($a_i = a$; $i = 1, 2, \dots, N$), subsequent integrations during optimization runs are expected to start from the previously computed steady-state temperature distributions. The boundary conditions may be satisfied in three different ways. Either, the temperatures are computed directly from the finite-difference equation representing the boundary conditions at the end of every time step, or secondly, the boundary conditions may be included into the system of Eqs. 2.1 after differentiation

with respect to time, or lastly, an equation of the form of Eqs. 2.1 may be derived directly from a control volume bounded at one side by the boundary of interest. All three possibilities have been utilized.

Discretization introduces obviously a truncation error; all spatial derivatives are represented consistently with a truncation error proportional to the square of the local spatial interval (see Sect. III 5) but higher order terms may be included anytime by modifying a single program unit each for the first and second derivatives.

The system of Eqs. 2.1 and 2.2 is solved by a fourth-order Runge-Kutta integration, that is if the f_i in Eqs. 2.1 have continuous fourth-order derivatives, the time-related accuracy of the integration is of order four (Refs. 26 and 27). Under much weaker conditions, namely uniform Lipschitz continuity, Ref. 26, the accuracy is still first-order and stability is secured. It may be noted that the Lipschitz continuity is also the prerequisite for uniqueness of the solution to Eqs. 2.1.

An existing single-precision, floating-point Runge-Kutta-Simpson subprogram, SUBROUTINE RKS, written by R. Schubert at the Aerospace Corporation was used. Its fixed-step integration mode was employed for the integration of the fluid flow variables along the channel axis, while the transient temperature field was integrated with variable time steps, chosen automatically so as to keep the "truncation error" per time step below a specified limit. The absolute and relative errors A_i and R_i are specified, by the user, for each variable y_i , and after every Runge-Kutta integration step a Simpson integration is carried out over the same interval and with the intermediate derivatives as used in the former integration. From the difference D_i between the two integrations is calculated the "truncation error" measure

$$E_m = \max E_i = \left| \frac{D_i}{A_i + R_i |y_i|} \right|, \quad i = 1, \dots, N \quad (2.3)$$

and if $0.75 < E_m$ then the time step DEL is divided by $\sqrt[5]{10}$ and the step is repeated, if $0.075 < E_m \leq 0.75$ then DEL is multiplied by $\sqrt[5]{10}$ for the

subsequent step.

All variables y_i are set equal to their initial values in the program which calls RKS. During the integration RKS interacts directly with two other subroutines, namely DERIV and CNTRL, whose names are the first elements of the argument list in the call statement. The first subroutine, DERIV, serves to compute all N derivatives dy_i/dx in accordance with Eqs. 2.1. The second subroutine, CNTRL, controls the output during integration and the termination of integration. Output of current values of all variables along with important system parameters is provided under two different integration modes: general transient system simulation, $MSTOR = 0$ in NAMELIST/RUNOPT/, produces output in arbitrarily chosen, fixed time steps, DTWRTE, up to the final time TEND, both specified in NAMELIST/RUNOPT/ and in hours; the second mode serves to compute the steady-state conditions and is invoked by setting $MSTOR = 1$ and by specifying the number LIMWRT of time intervals DTWRTE at which output is desired.

The integration under the second mode ($MSTOR = 1$) is terminated as soon as the expected truncation error due to program termination is less than five times the specified relative error per time step, RLIMIT, that is R_i in Eq. 2.3. The largest truncation error associated with the j -th time step is anticipated on the basis of Eqs. 1.1 and 2 in Section II as follows

$$\delta_j = \max_i \delta_{i,j} = \max_i \left\{ \Delta_j \tau \frac{\dot{y}_{i,j}}{\ln \frac{\dot{y}_{i,j} - 1}{\dot{y}_{i,j}}} \right\}, \quad i = 1, 2, \dots, N \quad (2.4)$$

The maximum is taken from all N modal points, $\Delta_j \tau$ is the current integration step size with index j , and \dot{y}_i stands for the dy_i/dx in Eqs. 2.1.

The argument list of RKS (and RKSF) is as follows:

- | | | |
|------|--------------------------------------|--|
| (i) | DERIV, name of derivative subroutine | } declared as EXTERNAL
in calling program |
| (ii) | CNTRL, name of control subroutine | |

- (iii) Y , array name*, containing the y_i 's in Eqs. 2.2 **
- (iv) DY, array name*, containing the dy_i/dx in Eqs. 2.1
- (v) A , array name*, containing the A_i 's in Eq. 2.3 **
- (vi) R , array name*, containing the R_i 's in Eq. 2.3 **
- (vii) T , the independent variable X in Eqs. 2.1 **
- (viii) DEL, the integration step**, DEL \neq 0
- (ix) N , (integer) the number of equations**
- (x) IFVD = 0: variable step size**, see Eq. 2.3
= 1: fixed step size equal to DEL
- (xi) IBKP = 0: adjust step size at most once before repeat,**
= 1: adjust in accordance to Eq. 2.3
- (xii) NTRY = 1: continue integration**, normal start
= 2: return from RKS
= 3: repeat last step with new DEL
= 4: restart
- (xiii) IERR = 0, normal integration
= -1 indicates singularity when IFVD = 0
= +1 indicates denominator vanishes in Eq. 2.3 at some time during integration.
- (xiv) through (xx) are array names* with which the user need not be concerned except YS that contains the y's in 2.1 at the previous times step: DELY, PD, SD, YS, YST, DYST, YSIMP.

} to be changed
in
CNTRL

The SUBROUTINE DERIV communicates with RKS only via its argument list which contains, in this order, Y, DY, and T, as specified above under iii, iv, and vii. Here, the current values of Y and T are supplied to DERIV, and the corresponding values of DY returned by DERIV to RKS.

The SUBROUTINE CNTRL communicates with RKS also via its argument list. It contains Y, DY, DEL, T, NTRY, IFVD as specified above under iii, iv, viii, vii, xii and x, respectively. From the array Y are available for output all the results of integration. The time step may be modified to reach a specific time value; and by specifying NTRY one controls the integration process from

* Declared in calling program as array with dimension size equal to the number of differential equations.

** To be specified prior to the calling statement.

variable to fixed step size during the integration by resetting IFVD.

This completes the discussion of the integration of both ordinary and partial differential equations as they occur in the analysis developed in Chapter II. The discussion is deemed sufficient to enable the user to apply the RKS routine to other problems as well.

3. The Evaluation of Polynomials

All polynomials

$$z = a_0 + a_1x + a_2x^2 + \dots + a_Nx^N \quad (3.1)$$

are carried out in a function subprogram based on the simple, efficient recurrence relation

$$\begin{aligned} z_0 &= a_N \\ z_{i+1} &= x \cdot z_i + a_{i+1} \\ i &= 0, 1, \dots, N-1 \end{aligned} \quad (3.2)$$

$$z = z_N$$

The coefficients a , $i = 0, 1, \dots, N$ must be placed, in the calling program, into an array of dimension $(N + 1)$, N is an arbitrary positive integer.

The procedure is coded as a function subprogram called $P\emptyset LY(N, A, X)$, where X is the argument x in Eq. 3.1, A is the array containing $M = N + 1$ elements starting with $A(1) = a_0$.

4. Aitken Interpolation

Experimental data and supporting computer results which are not represented by analytic expressions are interpolated by Aitkens interpolation technique (Ref. 27). An $(n + 1)$ -point Lagrangian interpolation is reduced to a sequence of $1/2 n (n + 1)$ linear interpolations. The interval spacing is arbitrary; and any number $M > n$ of ordered pairs (x_i, y_i) can be supplied in the calling program. The n points of interpolation are spaced equally about the point x of interpolation. It should be noted, however that unless $n = N$ or $n = 2$ the result $y(x)$ is not continuous in general. Care must also be taken that all nodes x_1, x_2, \dots are distinct.

The procedure is coded as a function subprogram called $YINT(X, Y, M, N, P)$, where X and Y are the names of arrays that have the same dimension M and contain the ordered pairs (x_i, y_i) , $i = 1, 2, \dots, M$ such that $x_1 < x_2 < \dots < x_M$. The number n of points used for the interpolation is specified as N , and the value of x at which to interpolate is supplied as P . Note that $2 \leq N \leq M$ must be satisfied.

5. Numerical Differentiation

The first and second derivative of tabulated functions of equally spaced arguments is carried out in SUBROUTINE DDX(Y,DY,DX,N) and in SUBROUTINE D2DX2(Y,D2Y,DX,N), respectively. Each subroutine requires that two arrays be declared in a DIMENSION statement in the calling program, to have at least N elements; one array for the set of ordinates $Y \rightarrow y_i$ supplied by the calling program, the other array for the return of the results, that is $DY \rightarrow dy_i/dx$ or $D2Y \rightarrow d^2y_i/dx^2$. The argument interval Δx and the number of ordinates y_i are to be specified as DX and N, respectively. However, in order that terms of order Δx be retained including at the endpoints of the domain, N must be no less than 3 for DDX and 4 for D2DX2. The truncation error is of order $y'''(\Delta x)^2$ and $y^{IV}(\Delta x)^2$, respectively, for DDX and D2DX2.

6. Numerical Integration

The definite integral

$$F = \int_{X_1}^{X_N} y(x_i) dx, \quad 1 \leq i \leq N; \quad N \geq 2$$

and the indefinite integral

$$G_j = \int_{X_1}^{X_j} y(x_i) dx + G(x_1)$$

$$1 \leq i \leq N; \quad 1 < j \leq N; \quad N > 3$$

of a tabulated function y_i of an equally spaced argument, x_1 , $x_1 + \Delta x$, $x_1 + 2\Delta x, \dots, x_1 + (N-1)\Delta x$ is carried out by a modified Simpson integration in the `FUNCTION DEFINT(Y,DX,N)` Subprogram and in the `SUBROUTINE FINT(Y,YO,DX,N,F)`, respectively.

For `DEFINT` the ordinates y_i are to be placed in the array `Y` whose dimension of no less than N elements must be declared in the calling program. The argument interval and the number of ordinates are specified as `DX` and `N`, respectively.

For `FINT` there are two array declarations necessary in the calling program, both for at least N elements; one for the integrand $Y \rightarrow y_i$ and the other for the integral $F \rightarrow G_i$. The integration constant $G(x_1)$, the argument interval and the number of ordinates are to be supplied as `YO`, `DX` and `N`, respectively.

The truncation error of composite Simpson integration is

$$\frac{x_1 - x_N}{180} (\Delta x)^4 y^{(iv)}(\xi) \quad \text{with} \quad x_1 \leq (\xi) \leq x_N.$$

7. Solution to Systems of Linear Algebraic Equations

Systems of linear algebraic equations are solved by the Gauss-Jordan elimination process. The same technique is used to invert matrices.

Consider the system of n linear algebraic equations

$$\sum_{j=1}^n A_{ij} X_j = y_i .$$

The solution is obtained by performing that sequence of elementary row operations on the augmented coefficient matrix

$$\left(\begin{array}{cccccc} A_{11} & A_{12} & . & . & . & A_{1n} & y_1 \\ A_{21} & & & & & . & y_2 \\ . & & & & & . & . \\ . & & & & & . & . \\ . & & & & & . & . \\ A_{n1} & & & & & A_{nn} & y_n \end{array} \right)$$

which leads to the row-reduced echelon matrix

$$\left(\begin{array}{cccccc} 1 & 0 & . & . & . & 0 & x_1 \\ 0 & 1 & & & & . & x_2 \\ . & & . & & 0 & . & . \\ . & & & . & & . & . \\ . & & & . & & . & . \\ . & & & & 0 & . & . \\ 0 & & & & & 0 & 1 & x_n \end{array} \right)$$

Elementary row operations are defined by

- (i) multiplication of a row by the scalar $c \neq 0$
- (ii) replacement of the r -th row by the r -th row plus c times the s -th row; $c \neq 0$, $r \neq s$; $r, s \leq n$
- (iii) interchange of any two rows.

The augmented coefficient matrix consists of the coefficient matrix A_{ij} in the first n columns and the known column vector y_i in its last, $(n+1)$ -st column.

The row-reduced echelon matrix has the properties that

- (i) the first non-zero element in each non-zero row is 1,
- (ii) every zero-row occurs below every non-zero row,
- (iii) if the first r rows, $i = 1, 2, \dots, r$ have their non-zero entry in column k_i then the k_i 's satisfy $k_1 < k_2 < \dots < k_r$.

In our specific case, the row-reduced echelon matrix has the identity matrix in place of the coefficient matrix.

When a matrix is inverted then the augmented coefficient matrix consists of the $n \times n$ coefficient matrix in its first n columns and the $n \times n$ identity matrix in the second n columns, $j = n+1, n+2, \dots, 2n$. The process indicated above leads $n \times n$ identity matrix in the first n columns and the inverted coefficient matrix in the second n columns, from $j = n+1$ through $j = 2n$.

The particular elementary row operations required are

- (i) division of the i -th row by A_{ii} ,
- (ii) subsequent multiplication of the resulting i -th row by the element A_{ki} of the k -th row,
- (iii) and subsequent replacement of the k -th row by the difference between the k -th row and the i -th row.

This process has to be repeated, essentially, for each row $i = 1, \dots, n$.

IV RECOMMENDATIONS AND CONCLUSIONS

The analysis described in this report has been successful in simulating the transient heat transfer characteristics of a radiator system under operational conditions expected in flight. The analysis serves as a basis for a rigorous computer program that has been systematically sub-divided into modular subprograms. The modular concept facilitates repeated simulation runs with different structural materials, meteoroid protection material, coolant fluids, and thermal control coatings.

The program predicts the net system heat rejection, the fin, tube and fluid temperature profiles, fluid pressure field as well as the meteoroid protection layer thickness and mass of the entire system. Optimization of the system performance may be achieved through enumeration of the parameter sets.

The program has been thoroughly checked and run for a large number of different simulation cases. A sample representation of these cases may be found in reference [29]. These sample runs have aided in the design of the radiator system during ascent, reentry, transient orbital and steady state orbital conditions. As a result of these computer runs it is recommended that an unprotected radiator not be used during reentry phases of the shuttle operation, because during reentry the aerodynamic heating has been found to exceed the ability of the radiator to reject heat. Also experience gained from the sample runs has shown that the rigorous analysis should not be used for parameter studies of the heat rejection system until a satisfactory optimum domain has been identified by the use of the Simplified Analysis [30]. Displays of typical results are presented in that report.

APPENDIX A

STRUCTURAL MATERIAL PROPERTIES

The thermodynamic and mechanical properties of all materials which make up the radiator system are summarized in Appendices A through C.

Appendix A contains properties for the three structural materials: copper, aluminum and beryllium. Copper and aluminum are intended to be used primarily as fin and tube material, while beryllium was selected for a meteoroid protection material. Four properties are evaluated for each material: specific heat at constant pressure, thermal conductivity, modulus of elasticity, while $(1/k) (dk/dT)$ is computed by differentiating the thermal conductivity relationship with respect to temperature.

Appendix B contains properties for four coolant fluids: helium, Dow Corning 200 Silicon oil, the liquid metal NaK, and two 3-M Company fluorochemical liquids FC-43 and FC-75. Six properties are evaluated for each coolant fluid: isobaric thermal expansion coefficient, isothermal compressibility, specific heat at constant pressure, enthalpy, thermal conductivity and dynamic viscosity. In addition, two equations of state are included for each fluid, one explicitly in density and one explicit in pressure, while the property $(1/k) (dk/dT)$ is computed by differentiating the thermal conductivity relationship with respect to temperature.

Appendix C contains the total hemispherical emittance and two auxiliary radiative properties used in the program for the surface coating Z-93.

All property relationships listed in these Appendices are presented in analytical form obtained by fitting a power polynomial through the data points. The data points listed in the tables are taken from the reference entered before each table. Numerical techniques used for the curve fitting process are explained in Section III.

The polynomial expression for each property has been compared with the referenced data and within the listed temperature range has been found to deviate by no more than the percentage error indicated.

I. COPPER

1. Specific Heat

Reference: Touloukian, Y. S., "Thermophysical Properties of High Temperature Solid Materials," Thermophysical Properties Research Center, Purdue University, Vol. 1, 1967, pp. 456-7.

Data Points:

T	C _p
600 R	0.0920 Btu/(lbm R)
1000	0.0975
2000	0.1112

Polynomial Fit:

Temperature Range: 400 to 2000 R

Equation:

$$C_p = (0.08375 + 1.375 \times 10^{-5} TR^{-1}) \times 32.174 \text{ Btu/(slug R)} \quad (\text{A.1})$$

Maximum Error: There was no difference between the computed value and the input data within the accuracy of the computer.

2. Thermal Conductivity

Reference: Touloukian, Y. S., "Thermophysical Properties of High Temperature Solid Materials," Thermophysical Properties Research Center, Purdue University, Vol. 1, 1967, pp. 458-9.

Data Points:

T	k
600 R	228.369 Btu/(hr ft R)
800	225.708
1000	222.805
1200	219.418
1400	215.306

Polynomial Fit:

Temperature Range: 500 to 1800 R

Equation:

$$k = (228.369 - 2.62067 \theta - 0.04033 \theta^3) \text{ Btu/(hr ft R)} \quad (\text{A.2})$$

where

$$\theta = \frac{T - 600.0\text{R}}{200.0\text{R}} \quad (\text{A.3})$$

Maximum Error: 0.87%

3. Temperature Variation of Thermal Conductivity

Eq. A.2 was differentiated with respect to temperature to yield

$$\frac{1}{k} \frac{dk}{dT} = \frac{1}{200} \frac{(-2.62067 - 0.121 \theta^2)}{(228.369 - 2.62067 \theta - 0.04033 \theta^3)} \text{ R}^{-1} \quad (\text{A.4})$$

4. Modulus Elasticity:

Reference: "Material Manual," TRW Equipment Laboratories, February 1966, Report No. ER-6756, Contract No. NAS 9-4884, Fig. 50.

Data Points:

t	Y
0 F	$16.55 \times 10^6 \text{ lbf/in}^2$
400	14.35
800	9.65
1200	3.82

Polynomial Fit:

Temperature Range: 500 to 1600 R

Equation:

$$Y = (16.55 - 0.4933 \theta - 1.935 \theta^2 + 0.2283 \theta^3) \times 1.44 \times 10^8 \text{ (lb f/ft}^2\text{)} \quad (\text{A.5})$$

where

$$\theta = \frac{T - 459.67 \text{ R}}{200 \text{ R}} \quad (\text{A.6})$$

Maximum Error: 0.44%

II. ALUMINUM 7075

1. Specific Heat

Reference: Touloukian, Y. S., "Thermophysical Properties of High Temperature Solid Materials," Thermophysical Properties Research Center, Purdue University, Vol. 2-11, 1967, pp. 810-11.

Data Points:

T	c_p
400 R	0.182 Btu/(lbm R)
600	0.209
800	0.226
1000	0.244
1200	0.270

Polynomial Fit:

Temperature Range: 300 to 1200 R

Equation:

$$c_p = (0.182 + 0.03616 \theta - 0.011417 \theta^2 + 0.00233 \theta^3 - 0.000083 \theta^4) \quad (A.7)$$

X 32.174 Btu/(slug R)

where

$$\theta = \frac{T - 400 \text{ R}}{200 \text{ R}} \quad (A.8)$$

Maximum Error: 0.34%

2. Thermal Conductivity

Reference: Touloukian, Y. S., "Thermophysical Properties of High Temperature Solid Materials," Thermophysical Properties Research Center, Purdue University, Vol. 2-11, pp. 812-13.

Data Points:

T	k
400 R	88.50 Btu/(hr ft R)
600	100.395
800	105.96
1000	104.024
1200	99.18

Polynomial Fit:

Temperature Range: 300 to 1200 R

Equation:

$$k = (88.5 + 13.0665 \theta + 0.33275 \theta^2 - 1.758 \theta^3 + 0.25375 \theta^4)$$

Btu/(hr ft R)

(A.9)

where

$$\theta = \frac{T - 400 \text{ R}}{200 \text{ R}}$$

(A.10)

Maximum Error: 0.96%

3. Temperature Variation of Thermal Conductivity

Equation A.9 was differentiated with respect to temperature to yield

$$\frac{1}{k} \frac{dk}{dT} = \quad (A.11)$$

$$\frac{1}{200} \frac{(13.0665 + 0.6655 \theta - 5.25 \theta^2 + 1.015 \theta^3)}{(88.5 + 13.0665 \theta + 0.33275 \theta^2 - 1.758 \theta^3 + 0.25375 \theta^4)} R^{-1}$$

4. Modulus of Elasticity

Reference: "Material Manual," TRW Equipment Laboratories, February 1966, Report ER-6756, NAS 9-4884, Fig. 50.

Data Points:

t	Y
0 F	$10.71 \times 10^6 \text{ lbf/in}^2$
200	9.90
400	8.50
600	6.15

Polynomial Fit:

Temperature Range: 500 to 1200 R

Equation:

$$Y = (10.71 - 0.63 \theta - 0.115 \theta^2 - 0.06 \theta^3) \times 1.44 \times 10^8 \text{ lbf/ft}^2 \quad (A.12)$$

where

$$\theta = \frac{T - 459.67}{200} \frac{R}{R} \quad (\text{A.13})$$

Maximum Error: 0.38%

III. BERYLLIUM (1/2 - 3% Be O)

1. Specific Heat

Reference: Touloukian, Y. S., "Thermophysical Properties of High Temperature Solid Materials," Thermophysical Properties Research Center, Purdue University, Vol. 6-11, 1967, pp. 753-4.

Data Points:

T	c_p
800 R	0.536 Btu/(lbm R)
1000	0.585
1200	0.622
1400	0.652
1600	0.680

Polynomial Fit:

Temperature Range: 400 to 1700 R

Equation:

$$c_p = (0.536 + 0.05667 \theta - 0.0085 \theta^2 + 0.00083 \theta^3) \quad (\text{A.14})$$

$$\times 32.174 \text{ Btu/(slug R)}$$

where

$$\theta = \frac{T - 800 \text{ R}}{200 \text{ R}} \quad (\text{A.15})$$

Maximum Error: 0.88%

2. Thermal Conductivity

Reference: Touloukian, Y. S., "Thermophysical Properties of High Temperature Solid Materials," Thermophysical Properties Research Center, Purdue University, Vol. 6-11, 1967, pp. 757-9.

Data Points:

T	k
400 R	108.863 Btu/(hr ft R)
600	98.944
800	89.751
1000	80.80
1200	72.091

Polynomial Fit:

Temperature Range: 400 to 1700 R

Equation:

$$k = (108.863 - 10.5643 \theta + 0.82683 \theta^2 - 0.20167 \theta^3 + 0.020167 \theta^4) \text{ Btu/(hr ft R)} \quad (\text{A.16})$$

where

$$\theta = \frac{T - 400 \text{ R}}{200 \text{ R}} \quad (\text{A.17})$$

Maximum Error: 0.90%

3. Temperature Variation of Thermal Conductivity

Equation A.15 was differentiated with respect to temperature to yield

$$\frac{1}{k} \frac{dk}{dT} =$$

(A.18)

$$\frac{1}{200} \frac{(-10.5643 + 1.65367 \theta - 0.60501 \theta^2 + 0.080668 \theta^3)}{(108.863 - 10.5643 \theta + 0.826830 \theta^2 - 0.20167 \theta^3 + 0.020167 \theta^4)} R^{-1}$$

4. Modulus of Elasticity

Reference: "Material Manual," TRW Equipment Laboratories, February 1966, Report ER-6756, Contract No. NAS 9-4884, Fig. 51.

Data Points:

t	Y
0 F	44.36 x 10 ⁶ lbf/in ²
400	40.41
800	33.95
1200	21.80

Polynomial Fit:

Temperature Range: 500 to 1700 R

Equation:

$$Y = (44.36 - 3.755 \theta + 0.335 \theta^2 - 0.53 \theta^3) \times 1.44 \times 10^8 \text{ lbf/ft}^2 \quad (\text{A.19})$$

where

$$\theta = \frac{T - 459.67 \text{ R}}{400 \text{ R}} \quad (\text{A.20})$$

Maximum Error: 0.28%

APPENDIX B
COOLANT FLUID PROPERTIES

I. HELIUM

1. Equation of State Explicit in Pressure

Reference: Akin, S. W., Trans. ASME, Vol. 72, p. 751, 1950.

This reference was used for all Helium properties and for brevity it is not repeated as the reference for the properties listed below.

Equation: The National Bureau of Standards has published a Benedict-Webb-Rubin equation for helium; this equation was found to be valid only up to the specified pressure limit of 3000 lbf/in². Preference was therefore given to the following Beattie-Bridgeman equation:

$$p = \rho^2 [RT(1 - \alpha) \left(\frac{1}{\rho} + B_1 \right) - A] \quad (\text{B.1})$$

where $\alpha = \frac{C}{T^3} \rho$

$$A = A_1(1 - a \rho)$$

The values of the constants in Eq. B.1, in MKSA units, are:

$$\begin{aligned} R &= 2.07702 \times 10^3 \text{ Nm/kgk} \\ A_1 &= 1.369595 \times 10^2 \text{ Nm}^4/\text{kg}^2 \\ B_1 &= 3.5002295 \times 10^{-3} \text{ m}^3/\text{kg} \\ C &= 1.0000658 \times 10^1 \text{ km}^3/\text{kg} \\ a &= 1.496103 \times 10^{-2} \text{ m}^3/\text{kg} \end{aligned}$$

Temperature Range: 160 to 860 R

Pressure Range: 2116 to 360000 lbf/ft²

Maximum Error: 0.095%

2. Equation of State Explicit in Density

Since the equation of state is needed explicit in density, Eq. B.1 was solved using Newton-Raphson iteration method along an isotherm to give

$$\rho_{i+1} = \rho_i - \frac{p - p(\rho_i)}{(\partial p / \partial \rho)_T} \quad (\text{B.2})$$

Using Eq. B.1, one obtains

$$\left(\frac{\partial p}{\partial \rho}\right)_T = RT + 2(RB_1T - A_1 - \frac{CR}{T^2})\rho + 3(A_1a - \frac{CRB_1}{T^2})\rho^2 \quad (\text{B.3})$$

3. Isobaric Thermal Expansion Coefficient

The isobaric thermal expansion coefficient is defined by the equation

$$\beta = - \frac{1}{\rho} \left(\frac{\partial \rho}{\partial T}\right)_p \quad (\text{B.4})$$

Since the equation of state (Eq. B.1) is explicit in the pressure, one can write β as:

$$\beta = \frac{1}{\rho} \frac{(\partial p / \partial T)_\rho}{(\partial p / \partial \rho)_T} \quad (\text{B.5})$$

or

$$\beta = \frac{R[\rho + (B_1 + \frac{2C}{T^3})\rho^2 + \frac{2CB_1}{T^3}\rho^3]}{\rho[RT + 2\rho(RB_1T - A_1 - \frac{CR}{T^2}) + 3\rho^2(A_1a - \frac{CRB_1}{T^2})]} \quad (\text{B.6})$$

4. Isothermal Compressibility

The isothermal compressibility is defined by the equation

$$\kappa = \frac{1}{\rho} \left(\frac{\partial \rho}{\partial p} \right)_T \quad (\text{B.7})$$

Making use of Eq. B.3, the isothermal compressibility can be written as

$$\kappa = 1/\rho \left[RT + 2\rho(RB_1T - A_1 - \frac{CR}{T^2}) + 3\rho^2(A_1a - \frac{CRB_1}{T^2}) \right] \quad (\text{B.8})$$

5. Specific Heat at Constant Pressure:

Equation: Experimental and quantum statistical data for helium show that at zero-pressure, the specific heat at constant volume is independent of temperature

$$c_v^0 = \frac{3}{2} R \quad (\text{B.9})$$

Using Maxwell's equations, the following expression is obtained

$$c_v = c_v^0 - T \int_{\rho_0}^{\rho} \left(\frac{\partial^2 p}{\partial T^2} \right)_{\rho} \frac{d\rho'}{(\rho')^2} \quad (\text{B.10})$$

From the equation of state, (Eq. B.1) the integration is carried out in closed form to give

$$c_v = R \left[\frac{3}{2} + 6a \left(1 + \frac{\rho}{2} B_1 \right) \right] \quad (\text{B.11})$$

The relation between specific heat at constant pressure and that at constant volume is given by:

$$c_p = c_v + \frac{T\beta^2}{\rho\kappa} \quad (\text{B.12})$$

Temperature Range: 180 to 900 R

Pressure Range: 2116 to 216000 lbf/ft

Maximum Error: 0.58% for cp

6. Enthalpy

The variation of internal energy with both temperature and density is

$$du = c_v dT + \left[p - T \left(\frac{\partial p}{\partial T} \right)_\rho \right] \frac{d\rho}{\rho^2} .$$

Substitution of c_v from Eq. B.11 and equation of state data from Eq. B.1 followed by integration along an isochore and an isotherm, one obtains

$$u = u_o + R \left[\frac{3}{2} (T - T_o) + 3 \rho C \left(1 + \frac{B_1}{2} \right) \left(\frac{1}{T_o^2} - \frac{1}{T^2} \right) \right] + \left(\frac{3 R C}{T^2} + A_1 \right)$$

$$(\rho_o - \rho) + \frac{1}{2} \left(\frac{3 C R B_1}{T^2} - A_1 \right) (\rho_o^2 - \rho^2)$$

where $u_o = 3.992 \times 10^4$ j/kg

$T_o = 10.938889$ K

$\rho_o = 4.669193$ kg/m³

with T in K and u in j/kg.

The enthalpy may then be determined from the equation

$$h = u + \frac{p}{\rho}$$

7. Thermal Conductivity

Data Points:

T	k
160 R	0.0404 Btu/(hr ft R)
360	0.0676
560	0.090
760	0.1094

Polynomial Fit:

Temperature Range: 160 to 860 R

Equation:

$$k = (0.0404 + 0.0302 \theta - 0.0033 \theta^2 + 0.0003 \theta^3) \text{ Btu/(hr ft R)} \quad (\text{B.13})$$

where

$$\theta = \frac{T - 160 \text{ R}}{200 \text{ R}}$$

Maximum Error: 0.54%

8. Temperature Variation of Thermal Conductivity

Eq. B. 13 was differentiated with respect to temperature to yield

$$\frac{1}{k} \frac{dk}{dT} = \frac{1}{200} \frac{(0.0302 - 0.0066 \theta + 0.0009 \theta^2)}{(0.0404 + 0.0302 \theta - 0.0033 \theta^2 + 0.0003 \theta^3)} \frac{1}{R} \quad (\text{B.14})$$

9. Dynamic Viscosity

Equation: Viscosity correlations are usually based on the concept of residual viscosity:

$$\psi_1(\rho) = \mu(\rho, T) - \mu^*(T) \quad (\text{B.15})$$

where

ψ_1 is the residual viscosity (function of density alone).

μ^* is the dynamic viscosity at atmospheric pressure.

For helium, the dynamic viscosity is given by:

$$\mu = \mu^* = (2.58394 \times 10^{-5} T/^{\circ}\text{R})^{0.647} \text{ slug/(ft hr)} \quad (\text{B.16})$$

Temperature Range: 160 to 660 R

Maximum Error: 0.29%.

II. SILICON OIL

The following properties are for Dow Corning 200 Silicon Oil (1 Centistoke at 77 F).

1. Isothermal Compressibility

Reference: Gunst, S. B., "Density-Pressure Relationships for Two Low-Viscosity Dimethyl Siloxanes," Trans. ASME 72, May 1950, pp. 401-7.

Data Points: Variation of κ with temperature at 0 psig and 500 psig are given below:

t	κ_o	κ^o_{500}
100 F	$12.35 \times 10^{-6} \text{ in}^2/\text{lbf}$	$11.60 \times 10^{-6} \text{ in}^2/\text{lbf}$
150	16.05	14.94
200	20.45	18.82
250	26.25	23.86
300	36.55	31.88

Polynomial Fit:

Temperature Range: 560 to 760 R

Pressure Range: 2116 to 74116 lbf/ft²

Equation: The variation of κ_o with temperature at 0 psig is given by

$$\kappa_o = (12.35 + 2.9833 \theta + 1.1 \theta^2 - 0.48333 \theta^3 + 0.1 \theta^4) \times 10^{-6} \text{ in}^2/\text{lbf} \quad (\text{B.17})$$

$$\text{where} \quad \theta = \frac{T - 559.67 \text{ R}}{50 \text{ R}} \quad (\text{B.17a})$$

κ is assumed to vary linearly on the above range of pressure, hence

$$\kappa = a + b p \quad (\text{B.18})$$

where

$$a = \kappa_o$$

(B.18a)

$$b = \left. \frac{\partial \kappa}{\partial p} \right|_T \approx \frac{\kappa_{500} - \kappa_o}{500 \text{ psi}}$$

and p is the pressure in psig and κ is in in^2/lbf

Fitting a power polynomial through $\left(\frac{\partial \kappa}{\partial p} \right)_T$ with the same values for temperature as indicated in the table results in the equation

$$b = (-1.5 - 0.0133 \theta - 1.18 \theta^2 + 0.57333 \theta^3 - 0.1 \theta^4) \times 10^{-9} \quad (\text{B.19})$$

in^4/lbf^2

where θ is given in Eq. B.17a.

Maximum Error: There was no difference between the computed and the input data within the accuracy of the computation.

2. Equation of State Explicit in Density

Reference: Gunst, S. B., "Density-Pressure Relationships for Two Low-Viscosity Dimethyl Siloxanes, "Trans. ASME, May 1950, pp. 401-7.

Data Points: Values for the variation of density with temperature at 0 psig are given below:

t	ρ_o
150 F	0.7767 gm/cm ³
200	0.7479
250	0.7188
300	0.6900

Polynomial Fit:

Temperature Range: 540 to 760 R

Pressure Range: 2116 to 146116 lbf/ft²

Equation:

$$\rho_o = (0.7767 - 0.0288 \theta) \times 1.94 \text{ slug/ft}^3 \quad (\text{B.20})$$

where

$$\theta = \frac{T - 609.67 \text{ R}}{50 \text{ R}} \quad (\text{B.20a})$$

The variation of density with pressure is given by

$$dz = \frac{d\rho}{\rho} = -\beta dT + \kappa dp \quad (\text{B.21})$$

Integration along the isotherm $T_o = 609.67 \text{ R}$ and from $p' = 0 \text{ psig}$ to $p' = p$, using Eq. B.18 results in

$$z(p, T_o) = a(T_o)p + b(T_o) \frac{p^2}{2}$$

Integration along the isobar p , from $T' = T_o$, to $T' = T$, using Eq. B.25, yields

$$z(p, T) - z(p, T_o) = p \int_{T_o}^T a'(T') dT' + \frac{p^2}{2} \int_{T_o}^T b'(T') dT' - \int_{T_o}^T c(T') dT'$$

which after simplification reduces to

$$\rho = \rho_o e^{ap + \frac{1}{2} b p^2} \quad (\text{B.22})$$

where values for a and b are given in Eq. B.18a.

Maximum Error: 0.128%

3. Equation of State Explicit in Pressure

Since the equation of state is needed explicit in pressure, Eq. B.22 was rearranged to yield

$$p = \frac{1}{b} \left[-a + \sqrt{a^2 + 2b \ln \frac{\rho}{\rho_o}} \right] \quad (\text{B.23})$$

4. Isobaric Thermal Expansion Coefficient

The zero-pressure isobaric thermal expansion coefficient can be written as:

$$\beta_o = \frac{1}{\rho_o} \left(\frac{\partial \rho_o}{\partial T} \right)_p$$

where ρ_o is given by Eq. B.20.

or

$$\beta_o = \frac{0.0288}{50(0.7767 - 0.0288 \theta)} \frac{1}{R} \quad (\text{B.24})$$

where θ is given by Eq. B.20a.

Making use of Eq. B.21, together with the principle of an exact differential, one may write

$$\left(\frac{\partial \beta}{\partial p} \right)_T = - \left(\frac{\partial \kappa}{\partial T} \right)_p$$

From Eq. B.18, the variation of β with both pressure and temperature is given by

$$\beta = \beta_o - a' p - \frac{b'^2}{2} p^2 \quad (\text{B.25})$$

where the prime superscript indicates differentiation with respect to temperature. The expressions for a and b as a function of temperature are given in Eqs. B.17 and 19, respectively.

5. Specific Heat at Constant Pressure

Reference: Dow Corning, Bulletin 05-145, February 1966.

Data Points: The available data for the variation of zero pressure specific heat at constant pressure for 2 centistokes are:

t	c_p^0	
80 F	0.448	Btu/(lbm F)
160	0.454	
240	0.463	
320	0.476	
400	0.491	

Polynomial Fit:

Temperature Range: 540 to 860 R

Pressure Range: 2116 to 74116 lbf/ft²

Equation: The above data for 2 centistokes silicon oil were multiplied by the ratio of c_p^0 for 1 centistoke to 2 centistokes at 77°F, to give the following expression for the zero-pressure specific heat at constant pressure for 1 centistoke silicon oil

$$c_p^0 = (0.46 + 0.00471 \theta + 0.00141 \theta^2 + 0.000043 \theta^3) \times 32.174 \text{ Btu/(slug R)} \quad (\text{B.26})$$

where

$$\theta = \frac{T - 539.67 \text{ R}}{80 \text{ R}} \quad (\text{B.26a})$$

The variation of c_p with pressure is given by

$$c_p = c_p^0 - T \int_{p_0}^p \left(\frac{\partial^2}{\partial T^2} \right) \left(\frac{1}{\rho} \right) dp' \quad (\text{B.27})$$

Since the exponent in Eq. B.22 is small, the equation for the density, when expanded in a power series, may be truncated after the second

term in the expansion. Applying Eq. B.27 to the two-term expression for density as a function of pressure and temperature by integrating along an isotherm T from $p' = 0$ psig to $p' = p$, results in the expression for

$$c_p = c_p^o - \frac{TI}{\rho_o} \quad (\text{B.28})$$

where

$$I = z_1 p + z_2 p^2 + z_3 p^3 + z_4 p^4 + z_5 p^5$$

and

$$z_1 = 2 \left(\frac{\rho_o'}{\rho_o} \right)^2$$

$$z_2 = \frac{1}{2} \left[\left(2 \frac{\rho_o'}{\rho_o} a' - a'' \right) - a z_1 \right]$$

$$z_3 = \frac{1}{3} \left[a'^2 - \frac{b''}{2} + \frac{\rho_o'}{\rho_o} b' \right] - a \left(2 \frac{\rho_o'}{\rho_o} a' - a'' \right) + \frac{1}{2} (a^2 - b) z_1$$

$$z_4 = \frac{1}{4} \left[a' b' - a \left(a'^2 - \frac{b''}{2} + \frac{\rho_o'}{\rho_o} a' \right) + \frac{1}{2} (a^2 - b) \left(2 \frac{\rho_o'}{\rho_o} a' - a'' \right) + \frac{1}{2} a b z_1 \right]$$

$$z_5 = \frac{1}{10} \left[\frac{b'^2}{2} - 2a a' b' + (a^2 - b) \left(a'^2 - \frac{b''}{2} + \frac{\rho_o' b'}{\rho_o} \right) \right.$$

$$\left. + a b \left(2 \frac{\rho_o'}{\rho_o} a' - a'' \right) + \frac{1}{2} b^2 z_1 \right]$$

where the prime superscript indicates differentiation with respect to temperature. The symbol a represents the zero pressure isothermal compressibility defined in equation B.17 and b is defined by equation B.19.

Maximum Error: For zero pressure specific heat at constant pressure the maximum error was 0.065%. For higher pressures no experimental data were available for comparison. However, the

expression for enthalpy was numerically differentiated with respect to temperature at constant pressure and compared with the computed values of specific heat at constant pressure. The comparison showed no difference within the accuracy of the computation.

6. Enthalpy

The variation of enthalpy with both pressure and temperature is given by:

$$dh = c_p^o dT + \frac{1}{\rho} [1 - T\theta] dp$$

This expression was integrated along the isobar $p = 0$ psig from $T' = 539.65$ R to $T' = T$, and then along an isotherm T from $p' = 0$ psig to $p = p$, to give

$$\begin{aligned} h = & \{ 80(0.46 + 0.00471 \theta + 0.00141 \theta^2 + 0.000043 \theta^3) \\ & + \frac{1}{\rho_o \cdot 337.37} \left[-\frac{1}{20} b b' T p^5 - \frac{1}{8} (a b' + a' b) T p^4 \right. \\ & + \frac{1}{6} (T(b' - a a') - b(1 + T \frac{\rho_o'}{\rho_o})) p^3 + \frac{1}{2} (a' T - a (1 \\ & \left. + T \frac{\rho_o'}{\rho_o})) p^2 + (1 + T \frac{\rho_o'}{\rho_o}) p \right] \times 32.174 \} \text{ Btu/slug} \quad (\text{B.29}) \end{aligned}$$

where θ is given by Eq. B.26a
 T is temperature in R
 a is given by Eq. B.17 in in^2/lbf
 ρ_o is given by Eq. B.20 in slug/ft^3
 b is given by Eq. B.19 in in^4/lbf^2
 p is pressure in lbf/in^2
 and primes denote differentiation with temperature.

7. Dynamic Viscosity

Reference: Dow Corning, Bulletin 05-153, July 1966.

Data Points:

t	v	
0 F	1.98	centistokes
100	0.874	
200	0.56	
300	0.41	

Polynomial Fit:

Temperature range: 460 to 760 R

Equation:

$$\ln v = (0.683 - 1.0845 \theta + 0.3065 \theta^2 - 0.04 \theta^3) \quad (\text{B.30})$$

$$\text{where } \theta = \frac{T - 459.67 \text{ R}}{100.0 \text{ R}}$$

where v is in centistokes and the dynamic viscosity is given by

$$\mu = v \rho \quad (\text{B.31})$$

Maximum Error: 0.77%

8. Thermal Conductivity

Reference: Dow Corning, Bulletin 05-145, February 1966.

Data Points: The available data for the variation of thermal conductivity with temperature for 2 centistokes are:

t	k	
- 100 F	0.0674	Btu/(hr ft F)
100	0.0626	
300	0.0578	

Polynomial Fit:

Temperature Range: 360 to 860 R

Equation: The procedure that was used for specific heat at constant pressure was followed to get an expression for the variation of thermal conductivity with temperature for 1 centistoke silicon oil. The resulting expression for the thermal conductivity is given by

$$k = (7.0052 - 2.2105 \times 10^{-3} T/R) \times 10^{-2} \text{ Btu/(hr ft R)} \quad (\text{B.32})$$

Maximum Error: There was no difference between the computed and the input data within the accuracy of the computation.

9. Temperature Variation of Thermal Conductivity

Eq. B.32 was differentiated with respect to temperature to yield

$$\frac{1}{k} \frac{dk}{dT} = \frac{- 2.2105 \times 10^{-3}}{7.0052 - 2.2105 \times 10^{-3} T/^{\circ}\text{R}} \quad 1/R \quad (\text{B.33})$$

III NAK - (78.6% K)

The following physical properties of NaK(78.6 wt% K) were extracted from the latest version of the "Liquid Metals Handbook, Sodium and NaK Supplement" (to be published). Some typical properties of NaK are:

Melting Point: 92 F

Boiling Point: 1445 F

Surface Tension: 0.00739 lbf/ft at Melting point

Since all property values were taken from this single reference, the reference is omitted in each section below.

1. Equation of State Explicit in Density

Data Points: Values for the variation of density with temperature at zero pressure are given by

t	ρ_o
200 F	53.21 lbm/ft ³
500	50.68
800	48.15
1100	45.62
1400	43.09

Polynomial Fit:

Temperature Range: 660 to 1860 R

Equation:

$$\rho_o = (58.773064 - 0.008433 T/R)/32.174 \text{ slug/ft}^3 \quad (\text{B.34})$$

Since the isothermal compressibility for NaK is assumed to be independent of pressure, Eq. B22 reduces to

$$\rho = \rho_o e^{kp} \quad (\text{B.35})$$

where p is the gage pressure. Since the exponent is small, the power series expansion for Eq. B.35 may be truncated after the second term and the variation of density with both pressure and temperature is given by

$$\rho = \rho_o (1 + \kappa p) \quad (\text{B.36})$$

An expression for κ is given later in this section.

Maximum Error: At zero pressure, there was no difference between the computed and the input data, within the accuracy of the computation. For higher pressures there were no experimental data available for comparison.

2. Equation of State Explicit in Pressure

Since the equation of state is needed explicit in pressure, Eq. B.36 was rearranged to yield

$$p = \frac{1}{\kappa} \left(\frac{\rho}{\rho_o} - 1 \right) \quad (\text{B.37})$$

3. Isobaric Thermal Expansion Coefficient

The isobaric thermal expansion coefficient is defined in Eq. B.4. From Eq. B.34, the zero pressure isobaric thermal expansion coefficient is given by:

$$\beta_o = \frac{0.008433}{(58.773064 - 0.008433TR^{-1})} \frac{1}{R} \quad (\text{B.38})$$

Due to the lack of experimental data, the isobaric thermal expansion coefficient was assumed to be independent of pressure.

4. Isothermal Compressibility

In view of the experimental difficulties associated with the measurement of isothermal compressibility at elevated temperatures, such data are not generally available for liquid metals. However, the well-known relationship between velocity of sound c , density ρ , and isentropic compressibility κ_s is

$$\kappa_s = \frac{1}{\rho c^2} \quad (\text{B.39})$$

which makes an alternative approach to the problem possible, if velocities of sound can be measured. Under these circumstances the isothermal compressibility may be obtained from the relation

$$\kappa = \gamma \kappa_s \quad (\text{B.40})$$

where

$$\gamma = \frac{c_p}{c_v}$$

The relation between c_p and c_v is given by

$$c_p - c_v = \frac{T\beta^2}{\rho\kappa} \quad (\text{B.41})$$

From Eqs. B.40 and B.41, one gets

$$\kappa = \kappa_s + \frac{T\beta^2}{\rho c^2}$$

or

$$\kappa_o = \left\{ \frac{1}{\rho} \left[\frac{1}{c^2} + \frac{T\beta^2}{c^2 p} \right] \right\}_{T_o, P_o} \quad (\text{B.42})$$

Due to the lack of experimental data Eq. B.42 was evaluated at the absolute pressure p_o of one atmosphere and the temperature of $T_o = 1260$ R.

at $T_o = 1260$ R

$$\rho_o = 48.15 \text{ lbm/ft}^3$$

$$c_o = 7544 \text{ ft/sec}$$

$$\beta_o = 1.75149 \times 10^{-4} \text{ 1/R}$$

$$C_{p,o} = 0.2091 \text{ Btu/(lbm R)}$$

5. Specific Heat at Constant Pressure

Data Points: For zero-pressure specific heat at constant pressure are given by:

t	c_p^o
200 F	0.2255 Btu/(lbm F)
500	0.1239
800	0.2093
1100	0.2091
1400	0.2120

Polynomial Fit:

Temperature Range: 660 to 1860 R

Equation:

$$c_p^o = (0.2255 - 0.016292 \theta + 0.00539 \theta^2 - 0.000758 \theta^3 +$$

$$0.000054 \theta^4) \times 32.174 \text{ Btu/(slug R)}$$

(B.44)

where

$$\theta = \frac{T - 659.67 \text{ R}}{300 \text{ R}} \quad (\text{B.44a})$$

The variation of c_p with pressure is given by

$$c_p = c_p^o - T \int_{p_o}^p \frac{\partial^2}{\partial T^2} \left(\frac{1}{\rho} \right)_p dp'$$

Integrating along the isotherm T from $p = 0$ psig to $p' = p$, using Eqs. B.36 and B.38 results in

$$c_p = c_p^o - \frac{2T\beta_o^2}{\rho_o \kappa} \ln (1 + \kappa p) \quad (\text{B.45})$$

Maximum Error: At zero pressure, the maximum error was 0.075%.

6. Enthalpy

The variation of enthalpy with both pressure and temperature is given by

$$dh = c_p dT + \frac{1}{\rho} [1 - T\beta] dp$$

The enthalpy was arbitrarily chosen to be zero near the melting point, or $T = 469.67^\circ \text{R}$. The above expression was integrated along an isobar $p = 0$ psig from $T' = 469.67^\circ \text{R}$ to $T' = T$, and then along an isotherm T from $p' = 0$ psig to $p' = p$, to give

$$h = \left[300 \left(0.2255 \theta - 0.016292 \frac{\theta^2}{2} + 0.00539 \frac{\theta^3}{3} - 0.000758 \frac{\theta^4}{4} + 0.000054 \frac{\theta^5}{5} \right) + \frac{1 - T\beta}{\rho_o \kappa} \ln (1 + \kappa p) \times \frac{1}{778.26} \right] 32.174 \text{ Btu/slug} \quad (\text{B.46})$$

where ρ and ρ_o are in lbm/ft^3 , κ is in $\text{ft}^2/\text{lb f T}_o$ in R, θ is given in Eq. B.44a, β is in R^{-1} and p is gage pressure in lb f/ft^2 .

7. Thermal Conductivity

Data Points:

t	k
200 F	13.36 Btu/(hr ft F)
500	14.57
800	15.18
1100	15.03
1400	14.13

Polynomial Fit:

Temperature Range: 660 to 1860 R

Equation:

$$k = (13.36 + 1.414167 \theta - 0.142083 \theta^2 - 0.069167 \theta^3 + 0.007083 \theta^4) \text{ Btu/(hr ft R)} \quad (\text{B.47})$$

where

$$\theta = \frac{T - 659.67 \text{ R}}{300 \text{ R}}$$

Maximum Error: 0.2%

8. Temperature Variation of Thermal Conductivity:

Eq. B.47 was differentiated with respect to temperature to yield

$$\frac{1}{k} \frac{dk}{dT} = \frac{1}{300} \frac{(1.414167 - 0.284166\theta - 0.207501\theta^2 + 0.028332\theta^3)}{(13.36 + 1.414167\theta - 0.142083\theta^2 - 0.069167\theta^3 + 0.007083\theta^4)} \frac{1}{R} \quad (\text{B.48})$$

9. Dynamic Viscosity

Data Points:

t	μ
200 F	1.1316 lbm/(ft hr)
500	0.746
800	0.534
1100	0.411
1400	0.340

Polynomial Fit:

Temperature Range: 660 to 1860 R

Equation:

$$\mu = (1.316 - 0.896667 \theta + 0.419833 \theta^2 - 0.102833 \theta^3 + 0.009667 \theta^4)/32.174 \quad \text{slug/(ft hr)} \quad (\text{B.49})$$

where

$$\theta = \frac{T - 659.67\text{R}}{300\text{R}}$$

Maximum Error: 1.2%

IV. FC-75 INERT FLUOROCHEMICAL LIQUID

The thermodynamic and transport properties of FC-75 fluid are extracted from "3M Brand Inert Fluorochemical Liquids, 3M Company, Chemical Division, 1965."

Due to the lack of experimental data, all properties were evaluated at atmospheric pressure and were assumed to be pressure independent.

At one atmosphere some typical properties are:

Nominal Boiling Point: 216 F
 Pour Point: - 135 F
 Surface Tension, at 77F: 15 dynes/cm

1. Equation of State

Data Points:

t	ρ	
- 50 F	120.7	lbm/ft ³
70	110.5	
190	100.3	

Polynomial Fit:

Temperature Range: - 80 to 216 F

Equation:

$$\rho = (155.522 - 0.085 T R^{-1}) \times 32.174 \text{ slug/ft}^3 \quad (\text{B.50})$$

Maximum Error: There was no difference between the computed and input data, within the accuracy of computation.

2. Isobaric Thermal Expansion Coefficient

Using the definition of the isobaric thermal expansion coefficient, Eq. B.4, and Eq. B.50, one obtains

$$\beta = \frac{0.085}{155.522 - 0.085 T R^{-1}} \frac{1}{R} \quad (\text{B.51})$$

3. Isothermal Compressibility

Since the equation of state (Eq. B.50) was assumed to be pressure independent, the isothermal compressibility defined by Eq. B.7 was assigned the value of zero

$$\kappa \equiv 0$$

4. Specific Heat at Constant Pressure

Data Points: The variation of the zero pressure specific heat at constant pressure is given by:

t	c_p^0	
80° F	0.2464	Btu/(lbm F)
140	0.2610	
200	0.2756	

Polynomial Fit:

Temperature Range: 70 to 210 F

Equation:

$$c_p^0 = (0.115082 + 2.4333 \times 10^{-4} T R^{-1}) \times 32.174$$

Btu/(slug R)

(B.52)

The variation of c_p with pressure is given by Eq. B.27. With ρ independent of pressure, Eq. B.27 was integrated along an isotherm T from $p' = 0$ psig to $p' = p$ resulting in:

$$c_p = c_p^o - \frac{2\beta^2 T}{\rho} p \quad (B.53)$$

A check on the magnitude of the terms in Eq. B.53, using typical running conditions, showed that the term $2\beta^2 TP/\rho$ was only 0.00064% of c_p . Therefore, c_p was taken to be a function of temperature alone, namely

$$c_p = c_p^o \quad (B.54)$$

Maximum Error: 0.025%

5. Enthalpy

The variation of enthalpy with both pressure and temperature is given by

$$dh = c_p^o dT + \frac{1}{\rho} (1 - T\beta) dp \quad (B.55)$$

This expression was integrated along the isobar $p = 0$ psig from $T' = T = 324.67$ R to $T' = T$, and then along an isotherm T from $p' = 0$ psig to $p' = p$ to give

$$h = [0.115082 (T - T_o) + \frac{1}{2} \times 2.4333 \times 10^{-4} \quad (B.56)$$

$$(T^2 - T_o^2)] \times 32.174 + \frac{p}{778.26 \rho} (1 - T\beta) \text{ Btu/slug}$$

where ρ is in slug/ft³, p is gage pressure in lbf/ft², T is in R and β is in R⁻¹.

A check of the magnitude of the terms in Eq. B.56, using typical running conditions, showed that the last term which accounts for the pressure variation is only 0.00087% of h . Hence the enthalpy was taken to be a function of temperature alone, or

$$h = [0.115082 (T - T_0) + \frac{1}{2} \times 2.4333 \times 10^{-4} (T^2 - T_0^2)] \times 32.174 \text{ Btu/slug} \quad (\text{B.57})$$

Maximum Error: No data for enthalpy at atmospheric pressure were available for comparison. However, when the value of c_p (Eq. B.52) was compared with the result of differentiation of h with respect to temperature, there was no difference within the accuracy of the computation.

6. Thermal Conductivity

Data Points:

t	k
- 50 F	0.08745 Btu/(hr ft F)
50	0.0809
150	0.0744

Polynomial Fit:

Temperature Range: -100 to 216 F

Equation:

$$k = 0.114181 - 6.53 \times 10^{-3} T R^{-1} \text{ Btu/(hr ft F)} \quad (\text{B.58})$$

Maximum Error: 0.044%

7. Dynamic Viscosity

Data Points: The variation of kinematic viscosity with temperature is given by:

t	v	
- 50 F	5.15	centistokes
10	1.74	
70	0.84	
130	0.50	

Polynomial Fit:

Temperature Range: - 80 to 190 F

Equation:

$$v = e (1.639 - 1.312933 \theta + 0.25265 \theta^2 - 0.02471667 \theta^3) \text{ centistokes} \quad (\text{B.59})$$

where

$$\theta = \frac{T - 409.67 \text{ R}}{60 \text{ R}}$$

The dynamic viscosity is given by

$$\mu = v\rho \quad (\text{B.60})$$

Maximum Error: 0.82%

V. FC-43 INERT FLUROCHEMICAL LIQUID

The thermodynamic and transport properties of the FC-43 are extracted from "3M Brand Inert Fluorochemical Liquids, 3M Company, Chemical Division, 1965."

Due to the lack of experimental data, all properties were evaluated at atmospheric pressure and were assumed to be pressure independent.

At one atmosphere some typical properties are:

Nominal Boiling Point:	345 F
Pour Point:	- 58 F
Surface Tension at 77F:	16 dynes/cm

1. Equation of State

Data Points:

t	ρ	
- 20 F	123.6	lbm/ft ³
130	112.15	
280	100.75	

Polynomial Fit:

Temperature Range: - 50 to 340 F

Equation:

$$\rho = (157.0883 - 0.076167 T R^{-1}) \times 32.174 \text{ slug/ft}^3 \quad (\text{B.61})$$

Maximum Error: There was no difference between the computed and input data, within the accuracy of computation.

2. Isobaric Thermal Expansion Coefficient

Using the definition of the isobaric thermal expansion coefficient, Eq. B.4, and Eq. B.61, one obtains

$$\beta = \frac{0.076167}{157.0883 - 0.076167 T R^{-1}} \frac{1}{R} \quad (\text{B.62})$$

3. Isothermal Compressibility

Since the equation of state (Eq. B.61) was assumed to be pressure independent, the isothermal compressibility defined by Eq. B.7 was assigned the value of zero.

$$\kappa \equiv 0$$

4. Specific Heat at Constant Pressure

Data Points: The variation of zero pressure specific heat at constant pressure is given by:

t	c_p^o
40 F	0.25 Btu/(lbm F)
77	0.27

Polynomial Fit:

Temperature Range: 40 to 77 F

Equation:

$$c_p^o = (-0.020092 + 5.4054 \times 10^{-4} T R^{-1}) \times 32.174$$

Btu/(slug R)

(B.63)

A similar procedure to that used in the case of FC-75 (See Section B IV 4) has shown that to a close approximation c_p is pressure independent, or

$$c_p = c_p^o \quad (B.64)$$

Maximum Error: There was no difference between the computed and input data within the accuracy of computation.

5. Enthalpy

The variation of enthalpy with both pressure and temperature is given by Eq. B.55. Integration of this equation in a procedure similar to that followed for the coolant fluid FC-75 yields

$$h = [-0.020092 (T - T_o) + \frac{1}{2} \times 5.4054 \times 10^{-4} (T^2 - T_o^2)] \times \\ 32.174 + \frac{P}{778.26\rho} (1 - T\beta) \text{ Btu/slug} \quad (B.65)$$

where $T_o = 401.67 \text{ R}$, ρ is in slug/ft³, T is in R, β is in R⁻¹, and p is gage pressure in lbf/ft².

A check of the magnitude of the terms in Eq. B.64, using typical running conditions, showed that the last term which accounts for the pressure variation is only 0.00084% of h . Therefore the enthalpy was taken to be a function of temperature alone or

$$h = [-0.020092 (T - T_o) + \frac{1}{2} \times 5.4054 \times 10^{-4} (T^2 - T_o^2)] \times \\ 32.174 \text{ Btu/slug} \quad (B.66)$$

Maximum Error: No data for enthalpy at atmospheric pressure were available for comparison. However, when the value of c_p (Eq. B.63) was compared with the result of differentiation of h with respect to temperature, there was no difference within the accuracy of the computations.

6. Thermal Conductivity

Data Points:

t	k
- 50 F	0.0512 Btu/(hr ft F)
50	0.0487
150	0.0462

Polynomial Fit:

Temperature Range: - 58 to 250 F

Equation:

$$k = 0.061442 - 2.5 \times 10^{-5} T R^{-1} \text{ Btu/(hr ft F)} \quad (\text{B.67})$$

Maximum Error: 0.11%

7. Dynamic Viscosity

Data Points: The variation of kinematic viscosity with temperature is given by:

t	ν
- 20 F	15.80 centistokes
70	2.84
160	0.855
250	0.35

Polynomial Fit:

Temperature Range: - 80 to 320 F

Equation:

$$\nu = e (2.76 - 2.043483 \theta + 0.362 \theta^2 - 0.034717 \theta^3) \text{ centistokes} \quad (\text{B.68})$$

where

$$\theta = \frac{T - 439.67 \text{ R}}{90 \text{ R}}$$

The dynamic viscosity is given by

$$\mu = \nu \rho \quad (\text{B.69})$$

Maximum Error: 1.0%

APPENDIX C

Optical Properties

Three optical properties are required in the radiative analysis discussed in Chapter 6, namely the total hemispherical emittance

$$\epsilon(T) = \frac{1}{E_b(T)} \int_0^{\infty} \epsilon_{\lambda}(T) E_{b,\lambda}(T) d\lambda \quad (C.1)$$

and the two auxiliary functions (see Eqs. 6.10 and 6.11)

$$XX(T_1, T_2) = \frac{1}{E_b(T_2)} \int_0^{\infty} \epsilon_{\lambda}(T_1) \epsilon_{\lambda}(T_2) E_{b,\lambda}(T_2) d\lambda \quad (C.2)$$

$$XXX(T_1, T_2, T_3) = \frac{1}{E_b(T_3)} \int_0^{\infty} \epsilon_{\lambda}(T_1) \epsilon_{\lambda}(T_2) \epsilon_{\lambda}(T_3) E_{b,\lambda}(T_3) d\lambda \quad (C.3)$$

In view of the temperature independence of the spectral emittance for dielectrics, the two functions XX and XXX are functions of a single temperature, the temperature of the surface element represented by the last subscript on the left-hand sides of Eqs. 6.10 and 6.11:

$$XX(T) = \frac{1}{E_b(T)} \int_0^{\infty} \epsilon_{\lambda}^2 E_{b,\lambda}(T) d\lambda \quad (C.4)$$

$$XXX(T) = \frac{1}{E_b(T)} \int_0^{\infty} \epsilon_{\lambda}^3 E_{b,\lambda}(T) d\lambda \quad (C.5)$$

I. SURFACE COATING Z-93

The functions C.1, C.4 and C.5 of the previous section are evaluated for the zinc oxide/potassium silicate coating Z-93 on the basis of spectral reflectance data measured by IITRI and published in the NASA Contractor Report No. 1420, titled Emissivity Coatings for Low-Temperature Space Radiators, by G. R. Cunningham, J. R. Grammer, and F. J. Smith, Lockheed Aircraft Corp., Sunnyvale, Calif., Sept. 1969, pp. 66 through 81.

The evaluated functions defined through Eqs. C.1, 4 and 5 are collocated by power polynomials of this form

$$f(T) = \sum_{i=0}^N a_i T^i \quad (C.6)$$

For the total hemispherical emittance, a fourth degree power polynomial was found to be satisfactory with

$$\begin{aligned} a_0 &= 0.8990103 \\ a_1 &= -0.1400633 \times 10^{-3} \\ a_2 &= 0.387900 \times 10^{-6} \\ a_3 &= -0.3937509 \times 10^{-9} \\ a_4 &= 0.1015627 \times 10^{-12} \end{aligned}$$

For the auxiliary functions XX and XXX the coefficients are

XX	XXX
$a_0 = 0.7804112$	0.6538383
$a_1 = -0.5527205 \times 10^{-4}$	0.1144374×10^{-3}
$a_2 = 0.2530228 \times 10^{-6}$	$-0.2432286 \times 10^{-7}$
$a_3 = -0.3229181 \times 10^{-9}$	$-0.1437500 \times 10^{-9}$
$a_4 = 0.8854202 \times 10^{-13}$	$0.4947915 \times 10^{-13}$

APPENDIX D

I. The Fin-To-Tube Shape Factor

A closed-form integration for the view factor of the fin with respect to the tube was carried out by Mr. Yao. This view factor occurs in Eqs. 6.15 and 6.16. Only the final results are given here.

The reader should recognize that some of the symbols defined below (Eqs. D.1 through 6) apply only here.

Let (x_f, y_f, z_f) designate the position of the center of an area element A_f on the fin and z_m the same on the tube. Let r_e , s_t and s_r represent, respectively, the outer tube radius, the fin tip and the fin root thickness, and let the fin height be given as H .

Then, with

$$\rho = x_f^2 + y_f^2 \quad (D.1)$$

$$\beta = \arctan \frac{y_f}{x_f} \quad (D.2)$$

$$\alpha = \arctan \frac{s_r - s_t}{2r_e} \quad (D.3)$$

$$\phi = \arctan \frac{s_r}{2r_e} \quad (D.4)$$

$$a = \rho^2 + r_e^2 + (z_f - z_m)^2 \quad (D.5)$$

$$\phi^* = \arcsin \frac{r_e}{\rho} \quad (D.6)$$

one obtains first

$$Z_1 = \ln \frac{a-2r_e \rho \cos(\phi^*-\beta)}{a-2r_e \rho \cos(\phi-\beta)} + \frac{a-2r_e^2 \cos(\alpha+\beta)}{a-2r_e \rho \cos(\phi^*-\beta)} - \frac{a-2r_e^2 \cos(\alpha+\beta)}{a-2r_e \rho \cos(\phi-\beta)} \quad (D.7)$$

$$Z_2 = \frac{8r_e^2 \rho^2 (z_t - z_m)^2 + 4\rho^2 r_e^2 a - a^3}{2(a^2 - 4r_e^2 \rho^2)^{3/2}} \quad (D.8)$$

$$Z_3 = \arcsin \frac{2r_e \rho - a \cos(\phi^*-\beta)}{a-2r_e \rho \cos(\phi^*-\beta)} - \arcsin \frac{2r_e \rho - a \cos(\phi-\beta)}{a-2r_e \rho \cos(\phi-\beta)} \quad (D.9)$$

$$Z_4 = \frac{2a(z_f - z_m)^2 - a^2 + 4r_e^2 \rho^2}{a^2 - 4r_e^2 \rho^2} \quad (D.10)$$

$$Z_5 = \frac{r_e \rho \sin(\phi^*-\beta)}{a-2r_e \rho \cos(\phi^*-\beta)} - \frac{r_e \rho \sin(\phi-\beta)}{a-2r_e \rho \cos(\phi-\beta)} \quad (D.11)$$

The final result is

$$SS = \Delta A_1 \Delta z \left[\frac{-Z_1}{4\pi\rho} + \frac{\sin(\alpha+\beta)}{2\pi\rho} \frac{\phi^*-\phi}{2} + Z_2 Z_3 Z_4 Z_5 \right] \quad (D.12)$$

This expression contains all the geometric relations that are required for fin-channel radiative interaction. It needs to be evaluated only once for every fin element.

The values of SS given by Eq. D-12 vary greatly depending on the fin and tube elements under consideration. Typically the shape factor between tube element and adjacent fin element is three to five orders of magnitudes larger than the shape factor between tube element and the next closest fin

element. If this large variation in shape factor is allowed to remain, unrealistic oscillations in the fin radiosity will occur and sizeable truncation errors will result when the radiant fluxes are integrated across the fin surface.

To eliminate these truncation errors the local shape factor for the root fin element is replaced by a mean value between two adjacent elements which have the same Z location. The mean value for the shape factor between a tube element and its adjacent fin element is calculated from

$$SS = \left[\frac{1 - \sin \gamma}{\pi} \right] \left[\phi_o + \frac{\sin 2\phi_o}{2} \right] \quad (D.13)$$

rather than Eq. D.12.

Expressions for γ and ϕ_o are:

$$\gamma = \tan^{-1} \left[\frac{Z_m - Z_f}{X_f} \right]$$

$$\frac{r_e [\cos \phi_o + \tan \phi_o \sin \phi_o] - y_f}{r_e + X_f} - \tan \phi_o = 0$$

II. Tube to Tube Shape Factor

The simplified analysis has indicated that optimum dimensions of the radiator system will result in close tube spacing. Therefore for the case of an optiminually designed system, the radiant interaction between adjacent tubes must be taken into account. This section summarizes the results of the shape factor between two fin elements. The procedure used is Hottel's crossed string method which is valid for infinitely long elements that are generated by a straight line moving parallel to itself. The finite length of the tube elements to accounted for by multiplying Hottel's result by a weighting factor.

From Hottel's crossed string method (see Fig. 5) the shape factor between two infinitely long tubes is:

$$F_{1-2} = \left[\frac{1}{\pi/2 - \phi} \right] \left\{ \gamma + \left[\left(\frac{t}{R_2} \right)^2 + \left(\frac{2L}{R_2} - \cos \phi \right)^2 - 1 \right]^{1/2} - \left(\frac{2L}{R_2} - \cos \phi \right) \right\} \quad (D.14)$$

where

$$\phi = \sin^{-1} \left(\frac{t}{R_2} \right)$$

t = one half the fin thickness at its root.

R_2 = outside radius of the tube

L = one-half the distance between tube centers

$$\gamma = \frac{\pi}{2} - (\theta_1 + \phi_1)$$

$$\phi_1 = \tan^{-1} \left(\frac{t}{2L - R_2 \cos \phi} \right)$$

$$\theta_1 = \cos^{-1} \left(\frac{R_2 \sin \phi_1}{t} \right)$$

The weighting factor for two tube elements of width ΔZ located at Z_1, Z_2 (see Fig. 5) is

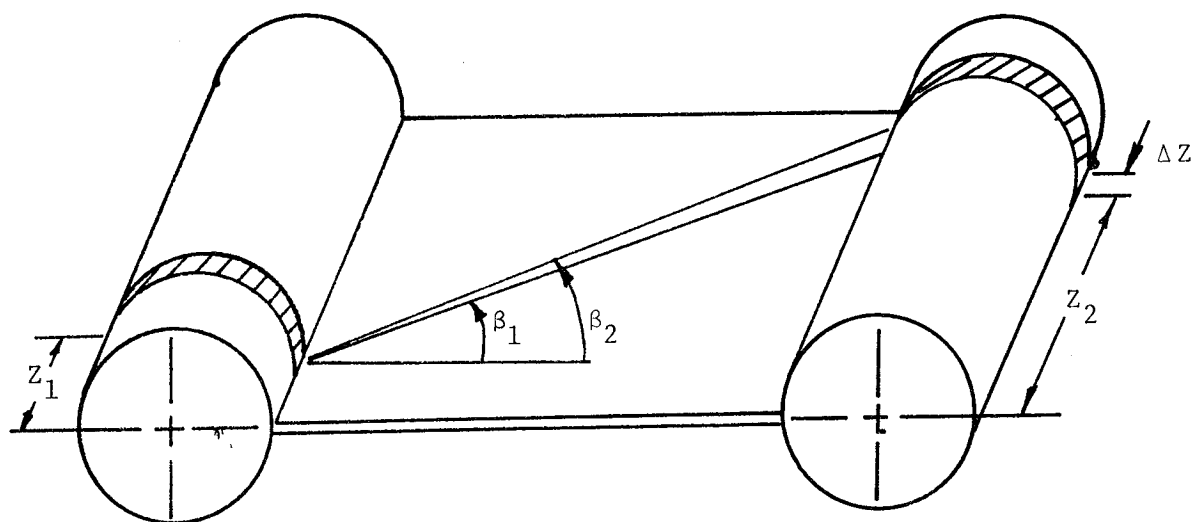
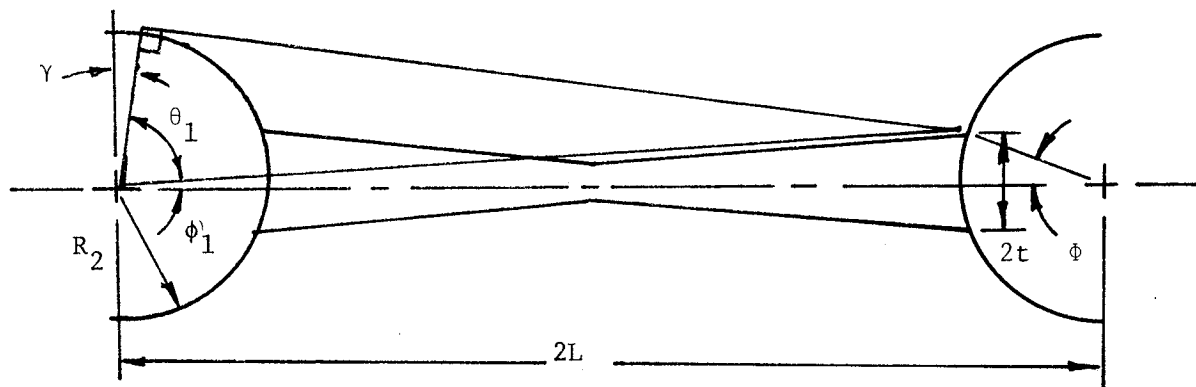


Fig. 5 Shape Factor Between Adjacent Tubes

$$WF = \int_{\beta_1}^{\beta_2} \cos^2 \beta d\beta = \frac{1}{2} (\beta_2 - \beta_1) + \frac{1}{4} (\sin 2\beta_2 - \sin 2\beta_1) \quad (D.15)$$

where

$$\beta_1 = \tan^{-1} \left[\frac{Z_2 - \Delta Z/2 - Z_1}{2(L-R_2)} \right]$$

$$\beta_2 = \tan^{-1} \left[\frac{Z_2 + \Delta Z/2 - Z_1}{2(L-R_2)} \right]$$

The shape factor between tube element is now

$$SS_{1-2} = \frac{WF}{\pi/2} F_{1-2} \quad (D.16)$$

where the value for F_{1-2} is given by Eq. D.14.

BIBLIOGRAPHY

1. Schiller, Vortr. a.d. Geb. der Aerodynamik und verwandten Gebieten, Aachen, 1929.
2. Nikuradse, Forschungsheft No. 256, VDI
3. Techo, R., Tickner, R. R. and James, R. E., J. Applied Mech. Vol. 87, p. 443, June, 1965.
4. El-Wakil, M. M., Nuclear Power Engineering, McGraw-Hill, 1962, p. 255.
5. Hausen, H. Z. VDI, Beihefte Verfahrenstechnik, 1943, p. 91.
6. Kreith, F., Principles of Heat Transfer, 2nd. ed., p. 128.
7. Hottel, H. C. and Sarofim, A. F. Radiative Transfer, McGraw-Hill, 1967.
8. Armaly, B. F. and Tien, C. L., A Note on the Radiative Exchange Among Nongray Surfaces, Tran. ASME, Vol. 92, Series C, No. 1, Feb. 1970, p. 178.
9. Guard, F. L. and Schultz, H. D., Space Shuttle Aerodynamic Heating Considerations, ASME Paper No. 70-HT/SpT-16, June, 1970.
10. Eckert, E.R.G., Survey on Heat Transfer at High Speeds, WADC Technical Report 54-70 USAF Wright-Patterson AFB, April, 1954.
11. Shapiro, A. H., The Dynamics and Thermodynamics of Compressible Fluid Flow, Vol. II., Ronald Press, New York, 1953.
12. Milton, J. F. and Schramm, W. B., Space Shuttle Vehicle Concept and Technology Requirements ASME Paper No. 70-HT/SpT-21, June, 1970.
13. Wallace, R. R., Jr.; Vinson, J. R. and Kornhauser, M., Effects of Hypervelocity Particles on Shielded Structures, American Rocket Society Paper 1683-61, 1961.
14. Rodriguez, D., Meteoroid Shielding for Space Vehicles, Aerospace Engineering Vol. 19, No. 12, December, 1960.
15. Radiator Design for Space Vehicles, Publication MS-AP-0069, Garrett Corp., Airesearch Mfg. Co., Los Angeles, Calif.
16. Cosby, W. A. and Lyle, R. G., The Meteoroid Environment and Its Effects on Materials and Equipment, NASA SP-78, 1965.
17. Wright, C. C., Thermal Analysis and Meteoroid Protection of Space Radiators, Air Force Report No. SSD-TR-66-98, June, 1966.

18. NASA Space Vehicle Design Criterion [Environment] Meteoroid Environment Model - 1969 [Near Earth to Lunar Surface] NASA SP-8013, March 1969.
19. Wulff, W. and Schipma, Design Guide for Pressurized Gas Systems, Task 7, NASA Contract No. NAS7-388, IITRI Report No. C6070-20, 1967.
20. U. S. Standard Atmosphere Supplements, 1966 U. S. Government Printing Office, Washington, D. C., 1966.
21. U. S. Standard Atmosphere, 1962, U. S. Government Printing Office, Washington, D. C., December, 1962.
22. Minzner, R.A., Champion, K. S. W. and Pond, H. L., The ARDC Model Atmosphere, 1959 AFCRC-TR-59-267, Air Force Cambridge Res. Center, August, 1959.
23. Keenan, J. H., and Kaye, J., Gas Tables, John Wiley and Sons, New York, 1945.
24. Champion, K. S. W. and Minzner, R. A., Proposed Revision of U. S. Standard Atmosphere 90 to 700 km., AFCRL-62-802, Air Force Cambridge Res. Labs., July, 1962.
25. Kopal, Z., Numerical Analysis, John Wiley and Sons, p. 195.
26. Keller, B. K., Numerical Methods for Two-Point Boundary-Value Problems.
27. Todd, Survey of Numerical Analysis, McGraw-Hill, 1962, p. 39.
28. Lieblein, Seymour "Analysis of Temperature Distribution and Radiant Heat Transfer Along a Rectangular Fin of Constant Thickness." NASA Technical Note D-196, Nov. 1959.
29. Black, W. Z. and Wulff, W., "Space Radiator Simulation--Manual for Computer Code," Final Report, Contract No. NAS9-10415, Georgia Institute of Technology, Atlanta, Georgia, April 1972.
30. Wulff, W., "Simplified Analysis and Optimization of Space Base and Space Shuttle Heat Rejection Systems," Final Report, Contract No. NASA-10415, Georgia Institute of Technology, Atlanta, Georgia, April 1972.

